

# Incorporating an IceTop veto for cascade events

Hadis Bagherpour

A thesis submitted to the University of Canterbury  
in fulfilment of the requirements for the degree  
of Doctor of Philosophy.

School of Physical and chemical Sciences  
Department of Physics  
February 2019

First I thank my supervisors: Dr. Jenni Adams and Dr. Mark Aartsen. Both were always willing to give their time and knowledge and go above and beyond whenever I needed their support.

A special heartfelt thanks to my husband. Without the support of him I would definitely be lost. Thanks to my parents and my brother for always being there for me.

# Contents

<b>1</b>	<b>Introduction</b>	<b>1</b>
1.1	Cosmic rays . . . . .	2
1.1.1	Acceleration of Cosmic Rays . . . . .	4
1.1.2	Sources of Cosmic Rays . . . . .	5
1.1.3	Galactic Sources . . . . .	6
1.1.4	Extragalactic Sources . . . . .	6
1.1.5	Cosmic Ray Air Showers . . . . .	8
1.2	Neutrinos and Neutrino Astronomy . . . . .	8
1.2.1	Neutrino Fundamental Properties . . . . .	8
1.2.2	Neutrino Astronomy . . . . .	10
1.2.3	Atmospheric neutrinos . . . . .	14
1.2.4	Neutrino spectra . . . . .	15
<b>2</b>	<b>The IceCube Neutrino Observatory</b>	<b>17</b>
2.1	IceCube Detector Components . . . . .	17
2.2	Neutrino Detection Principle . . . . .	20
2.3	Neutrino search techniques . . . . .	21
2.4	Simulation . . . . .	25
2.5	Event Reconstruction . . . . .	27
2.6	Ice . . . . .	29
2.6.1	Dust layer veto region . . . . .	29
2.7	IceCube astrophysical neutrino results . . . . .	30
2.8	Extensions to the IceCube array . . . . .	32
<b>3</b>	<b>IceTop and its Veto Potential</b>	<b>34</b>
3.1	IceTop Array Introduction . . . . .	34
3.1.1	IceTop Science . . . . .	35

3.2	IceTop as a Veto . . . . .	36
3.3	Other IceTop Veto Work . . . . .	38
3.4	Simulation of Cosmic Ray Air Showers on IceTop . . . . .	39
3.4.1	Comparison of parameterisation code with data . . . . .	42
3.5	Scope of IceTop as a veto . . . . .	47
3.6	Relationship between in-ice event energy estimates and primary particle energy . . . . .	49
<b>4</b>	<b>Incorporating an IceTop veto into a Cascade Analysis</b>	<b>53</b>
4.1	Initial Cascade Filtering Levels . . . . .	54
4.1.1	Containment criterion . . . . .	55
4.2	Contained Event Selection . . . . .	56
4.3	Uncontained Event Selection . . . . .	58
4.4	IceTop Veto and the Contained Sample . . . . .	61
4.5	IceTop Veto and the Uncontained Sample . . . . .	68
<b>5</b>	<b>Investigations into a Suitable Time Interval to define Correlated Hits</b>	<b>74</b>
5.1	Calculation of the front impact time on IceTop . . . . .	75
5.2	Time window considerations . . . . .	77
5.2.1	Natural spread . . . . .	77
5.2.2	Angular resolution of the cascades . . . . .	78
5.2.3	Unwanted removal of signals . . . . .	83
5.3	Chapter summary . . . . .	84
<b>6</b>	<b>Incorporating the time dependent IceTop veto on the uncontained cascade sample</b>	<b>89</b>
6.1	IceTop veto with a time window on simulated background . . . . .	90
6.2	IceTop veto with a time window on a subset of experimental data . . . . .	93
6.3	Potential Improvement of the IceTop Veto . . . . .	96
<b>7</b>	<b>Discussion and Conclusion</b>	<b>102</b>

# List of Figures

1.1	Measured energy spectrum of cosmic ray by various experiments	3
1.2	Acceleration at a moving cloud. . . . .	5
1.3	Shock front acceleration mechanism. Figure adapted from [1].	5
1.4	Maximum achievable energy by charged particles estimated by Hillas . . . . .	7
1.5	Charged-Current and Neutral-Current neutrino interaction. This plot is taken from [2]. . . . .	9
1.6	The resonant antineutrino electron scattering (Glashow resonance. The figure was taken from [3].) . . . . .	10
1.7	The cosmic horizon for $\gamma$ ray astronomy. . . . .	11
1.8	Fluxes of neutrinos. . . . .	16
2.1	A schematic view of IceCube Neutrino Observatory. . . . .	18
2.2	The IceCube Digital Optical Module (DOM). . . . .	20
2.3	Light patterns of a shower caused by neutrino interactions in IceCube. . . . .	22
2.4	Light patterns of a track caused by muon neutrino interactions in IceCube. . . . .	22
2.5	Optical attenuation length at 400 nm as a function of vertical depth. The figure adapted from [4] . . . . .	30
2.6	Extension of current IceTop . . . . .	33
3.1	IceTop veto strategy for the IceCube observatory . . . . .	37
3.2	Radius of Air Shower Events . . . . .	43
3.3	Distribution of Number of hit IceTop tanks for Experimental and Simulation Data. . . . .	44
3.4	Median number of hit tanks over a range of MuEx and radius for Experimental and Simulation Data (Muon hits only) . . .	45

3.5	Median number of hit tanks over a range of MuEx and radius for Experimental and Simulation Data (Muon and electron hits)	45
3.6	The probability of getting one or more muon hits.	48
3.7	Vetoing event fraction of IceTop and extended array	49
3.8	Credo and primary cosmic ray particle energy relationship.	51
3.9	MUEX and primary energy relationship.	51
4.1	IceCube layers in Horizontal plane	56
4.2	Energy distribution after preliminary_L4 cut and after adding Veto cut.	63
4.3	Energy distribution after containment cut and after adding Veto cut.	64
4.4	Energy distribution after containment and earliestLayer cuts and after adding Veto cut.	65
4.5	Energy distribution after containment and maxDomChargeOM cuts and then adding Veto cut.	66
4.6	Signals before and after adding MaxDomChargeOm position to the preL4 cuts	67
4.7	Signal distribution against SPE variable.	70
4.8	Event rates as a function of zenith angle for contained cascade analysis with IceTop veto.	71
4.9	Event rates as a function of energy for uncontained cascade analysis with IceTop veto.	72
4.10	Event rates as a function of energy for uncontained cascade analysis with IceTop veto.	73
5.1	Schematic of an event detected coincidentally in IceCube-InIce and IceTop	76
5.2	Residual time	78
5.3	Comparison between cosmic ray shower axis and the reconstructed direction using MnopodFit	80
5.4	Comparison between cosmic ray shower axis and the reconstructed direction using SPEFit	81
5.5	Cosine of the angular difference between the cosmic ray shower axis and the reconstructed direction found using MonopodFit, with fine binning.	83

5.6	Cosine of the angular difference between the cosmic ray shower axis and the reconstructed direction found using SPEFit, with fine binning. . . . .	84
5.7	Different possible shower planes on the surface array. . . . .	86
5.8	Different hit times on tanks. . . . .	87
6.1	Veto potential on CORSIKA level 5 events. . . . .	90
6.2	Veto potential on CORSIKA level 5 events after relaxing SPE criteria. . . . .	91
6.3	Rate of CORSIKA events as a function of energy before and after a cut on IceTop hits within a specific time window. . . . .	93
6.4	Rate of CORSIKA events as a function of energy at L5 and after taking out cuts when timewindow was obtained around the vertex based on vertical proxy for the shower. . . . .	94
6.5	Rate of CORSIKA events as a function of energy that remained after taking out cuts when timewindow based on monopod reconstruction was used. . . . .	95
6.6	Event rate for experimental data, as a function of energy, at Level 5 and after applying an IceTop veto with a time window based on the SPEFit reconstruction. . . . .	96
6.7	Event rate for experimental data, as a function of energy, at Level 5 and after applying an IceTop veto with a time window based on the vertical proxy. . . . .	97
6.8	Event rate for experimental data, as a function of energy, at Level 5 and after applying an IceTop veto with a time window based on the Monopod reconstruction. . . . .	98
6.9	Hits on IceTop with their original times. . . . .	99
6.10	Hits on IceTop with their original times. . . . .	100
6.11	Scatter plot of zenith versus angle between true and reconstructed directions for simulated cosmic ray events at L5 without an SPE cut. . . . .	100
6.12	Event rates as a function of energy for uncontained cascade analysis with IceTop veto requiring three hits. . . . .	101

# List of Tables

4.1	Summary of Level4 selection criteria . . . . .	57
4.2	Summary of Level5 selection criteria . . . . .	62
4.3	Background reduction with IceTop and extended IceTop array	68
4.4	Signal reduction with different cut criteria . . . . .	69
5.1	Spread in IceTop tank arrival times arising from a parcel of cosmic ray incident directions distributed over $21^\circ$ . . . . .	82
5.2	Spread in IceTop tank arrival times arising from a parcel of cosmic ray incident directions distributed over $12^\circ$ . . . . .	82
5.3	Number of unbiased Icetop hits in various size time windows – run date 2013.05.05 . . . . .	85
5.4	Number of unbiased Icetop hits in various size time windows – run date 2013.12.31 . . . . .	85
5.5	Number of unbiased Icetop hits in various size time windows – run date 2014.12.31 . . . . .	88



## Abstract

The IceCube observatory, at the South Pole, includes an array of optical sensors deployed between 1450 and 2450 m below the surface and a surface array of cosmic ray detectors. The deep array, IceCube-InIce, is the world's largest neutrino detector and consists of over 5000 optical sensors which detect the optical Cherenkov light emitted by the charged particles produced when neutrinos interact in the ice. Neutrinos are unique astronomical messenger particles as they can travel across the Universe without interference or being absorbed by matter. In contrast to charged particles, whose trajectories are affected by magnetic fields, neutrinos' trajectories can be used to point back to their sources to aid the identification of particle acceleration sites.

Although the main aim of IceCube-InIce is to search for astrophysical neutrinos, the majority of events recorded are background events originating from the interaction of cosmic rays in the Earth's atmosphere. In this thesis, the use of the IceTop surface array as a veto to identify background events is investigated. The focus of this thesis is the study of the implementation of an IceTop veto within an IceCube-InIce cascade analysis. A cascade analysis focuses on selecting IceCube-InIce events where the neutrino interaction has resulted in a shower or cascade of secondary particles rather than a long-range particle. The resulting pattern of light detected across the optical sensors appears globular rather than elongated and track-like. There are two variations of cascade analyses; contained and uncontained analyses. Contained cascade analyses concentrate on events where the central point of the light pattern is well-contained within the IceCube-InIce array while the uncontained analyses focus on the remaining events.

In this thesis it is shown that there is potential for an IceTop veto to be used in a way that allows other filter criteria to be relaxed in an uncontained cascade analysis in order to aid signal retention and for the veto to be used to remove additional high-energy background events. In order to link hits in the IceTop array with events in IceCube-InIce it is necessary to determine a time window within which hits will IceTop hits will be associated with IceCube-InIce event. The various factors which affect the choice of the time window length were investigated and it was found that the most limiting factor is the poor direction reconstruction of cascade events. A time window of 2000 ns

was chosen and the performance of the IceTop veto with this time window was studied for simulated background events. In addition, the IceTop veto was applied to a sample of data events.

# Chapter 1

## Introduction

In this research project new techniques for detecting neutrinos with the IceCube neutrino detector are investigated. IceCube, installed at the South Pole, was constructed with the goal to detect astrophysical neutrinos, motivated by the fact that neutrinos, being neutral and weakly interacting, are unique cosmic messengers. In particular it is hoped that neutrinos will be able to identify the origin of the highest energy cosmic rays. Cosmic rays themselves do not point back to their sources as they are electrically charged and deflected by magnetic fields.

Neutrinos are observed via the optical detection of secondary particles which are produced in neutrino interactions inside the Antarctic ice. Two basic event topologies can be distinguished: track-like patterns of light which originate when a long-range particle is produced and spherical light patterns which originate when a cascade or shower of particles is produced. This research is concerned with the second case which is referred to as the cascade channel.

The majority of events recorded by IceCube are not the events that are sought, but background events. The background events have their origin in cosmic ray interactions in the Earth's atmosphere with the data collected by the IceCube detector dominated by atmospheric muons. In this thesis we investigate how the IceTop air shower array might be used to remove background events. IceTop is a cosmic ray air shower detector which is located directly above the IceCube neutrino detector.

The thesis is organized as follows: Chapter one gives an introduction to cosmic rays and their connection to neutrinos. Chapter two gives an overview of the IceCube experiment and discusses the principle of neutrino detection via charged secondaries in more detail, the interaction of high energy particles in the ice and the light propagation in the ice is explained. Based on these mechanisms, the different event topologies created by muons and neutrino interactions are introduced. The IceTop detector is introduced and its potential as a veto is explained in Chapter three. Incorporating an IceTop veto on contained and uncontained cascade samples is investigated in Chapter four. In Chapter five a suitable time-window to use for the IceTop data to define correlated hits is discussed. Analysis is tested on burn sample in Chapter six and finally a discussion of the project and outlook are given in Chapter seven.

## 1.1 Cosmic rays

Cosmic rays are charged particles that travel through the interstellar medium to Earth with velocities close to the speed of light. The discovery of an increasing ionization of the air with increasing altitude by Victor Hess in 1912 revealed a component of ionizing radiation which originated from outer space [1].

At lower energies cosmic rays are mostly protons, but there are also electrons, helium and heavier nuclei. The composition changes with energy. Measurements indicate the dominance of heavier elements at EeV energies [5]. Cosmic rays are observed over a wide energy spectrum up to  $3 \times 10^{20}$  eV. The cosmic-ray energy spectrum exhibits a power-law relation of  $\frac{dN}{dE} \propto E^{-\gamma}$ . It shows three features: ‘the knee’ at an energy of  $\sim 3$  PeV; ‘the second knee’ at energies of about 100 PeV; and ‘the ankle’ at  $\sim 3$  EeV where the slope of the spectrum changes. The slope steepens after the knee and steepens further after the second knee but above the ankle the spectrum hardens again. These features are believed to be related to changes in the sources and composition of cosmic rays with extra-galactic sources likely to be dominant for energies above the ankle. Determining the cosmic ray chemical composition and the spectral distribution of the various nuclear species is currently an active research area.

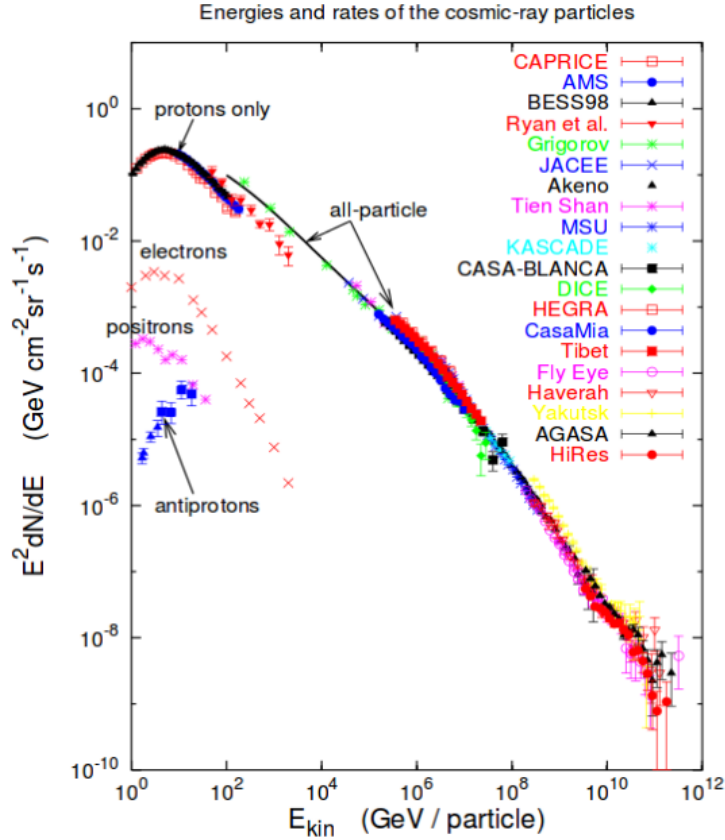


Figure 1.1: Different measurements of the cosmic ray flux over a wide energy range. The figure is taken from [6].

The cosmic ray spectrum does not appear to extend beyond  $10^{20}$  eV which can be explained by the GZK effect. The letters GZK refer to the surnames of Kenneth Greisen, Vadim Kuzmin and Georgiy Zatsepin who predicted that cosmic rays with energies over  $5 \times 10^{19}$  eV would interact readily with the relic thermal radiation photons suppressing the observed cosmic ray spectrum above this energy.

A model with three cosmic ray sources has been suggested by Gaisser [7]. These three sources are a low-energy galactic component, mainly ejected by supernova remnants, a higher energetic galactic component and an extra-galactic component, both of yet unknown origin. The model could be derived from fits to data collected by the balloon-borne cosmic ray experiments

CREAM [8] and ATIC2 [9]. The data were extrapolated to higher energies because the direct measurements reach only up to energies of about 100 TeV. In this model H, He, CNO, Mg-Si, Mn-Fe are the most abundant nuclei in the Universe [10] which describe the cosmic ray composition. Features in the spectrum are related to the rigidity dependent limit to the highest energy a particular source can accelerate cosmic rays. This limit is related to the gyroradius of the cosmic rays and will be discussed further in section 1.1.2.

### 1.1.1 Acceleration of Cosmic Rays

The origin of cosmic rays and the mechanism by which particles are accelerated to such high energies have been the subject of much research. The generic mechanism currently accepted for the acceleration is known as Fermi acceleration [11], of which a brief description is given below. More details with a full derivation of the various relationships is given in [1]. In Fermi's second-order scenario, charged particles are reflected by the magnetic fields from randomly moving plasma clouds. By staying for a characteristic time in the acceleration region, charged particles gain energy by several reflections from these clouds. When a particle enters a cloud, momentum is transferred from the cloud to the particle with the assumption that the clouds' momentum is unchanged in the collision process with the charged particles. A schematic illustration of this process is given in fig. 1.2. It can be shown that the energy spectrum which results is a power law in the energy as observed. However the energy gain by the charged particles in collisions with random clouds can be shown to be second order in  $u/c$  where  $u$  is the cloud speed. This is not considered to be efficient enough to account for the observed cosmic ray energies, especially as charged particles that gain small energies quickly lose energy through ionization. Therefore, the initial acceleration process must be fast enough to compensate this energy loss. For this reason and when the time scales are taken into account, second-order Fermi acceleration is not considered to be the acceleration mechanism responsible for cosmic rays with a more efficient process required.

In the Fermi first-order scenario the charged particles pass back and forward through a shock front which with a first order dependence on  $u/c$  is more efficient and allows the acceleration of particles to higher energies. A shock is formed by particles in a plasma which move with speeds larger than the

speed of sound. Each time a particle moves through the shock front it gains some energy in this proposed acceleration mechanism so that the particle with energy  $E_0$  acquires energy  $\zeta E_0$  after one encounter and in a number of subsequent encounters  $n$  has a net gain in energy  $E_2 = E_0(1 + \zeta)^n$ . The probability of a particle remaining in the acceleration region decreases as the number of crossings increase. This means that fewer particles are accelerated to higher energies. Taking the energy-dependent probability of escape into account it can be determined that the Fermi first order mechanism predicts a power law spectrum with a spectral index of  $-2$  [1]. A schematic figure to indicate the shock front acceleration mechanism is shown in fig. 1.3. The upstream and downstream regions indicated in fig. 1.3 are moving respectively with speeds  $u_1$  and  $u_2$  in the moving coordinate system of the shock. A particle which enters with the energy  $E_1$  is scattered multiple times and leaves the shock front with energy  $E_2$ . Figure adapted from [1].

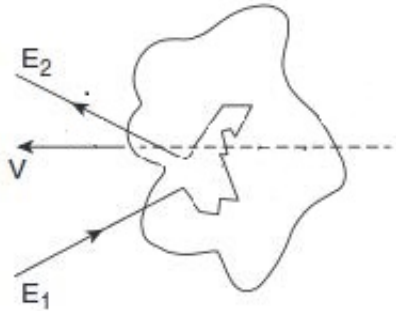


Figure 1.2: Acceleration at a moving cloud.

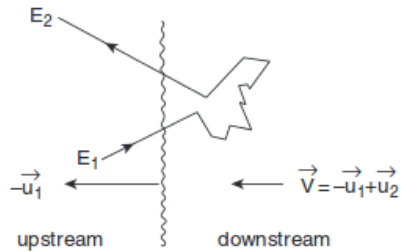


Figure 1.3: Shock front acceleration mechanism. Figure adapted from [1].

### 1.1.2 Sources of Cosmic Rays

To accelerate charged particles to the highest energies, magnetic fields are assumed to provide confinement of the particles in the acceleration region because charged particles will otherwise escape before reaching the highest energies. Such an assumption allows the size of source candidates to be correlated with the strength of the magnetic fields  $B$  by the gyro radius  $r_g$  of the particle with energy  $E_0$  and charge  $Z_e$  in the high energy [12]. The probability of a particle to escape the region where it was being accelerated increases,

if the particle's gyroradius is comparable to the size of the acceleration region. Therefore, the acceleration region has to be larger than the gyroradius of the particle:

$$r_g = \frac{E_0}{|Z_e| \cdot B}. \quad (1.1)$$

As the gyroradius depends on the charge, it can be seen that the energy limit for a given source is dependent on the mass of the cosmic ray. It has been proposed that features in the cosmic ray spectrum can be attributed to a transition between different cosmic ray source classes, as discussed above. The mass dependence of the cut-off means that the transition would be softened from a sharp slope change. The relation between acceleration energy and the size and magnetic field of the acceleration region is illustrated in the Hillas plot in fig. 1.4 taken from [13]. In this plot some source candidates are shown as a function of their magnetic field and size. Each of the source types are briefly discussed below.

### 1.1.3 Galactic Sources

**Supernova remnants (SNR):** The primary origin of the galactic cosmic rays below  $10^{18}$  eV is considered to be supernova remnants. Energy released by supernovae and the energy density observed in cosmic rays at the Earth show that SNR contribute largely to the observed cosmic-ray flux. The FERMI -LAT instrument reported  $\gamma$ -ray observations consistent with the neutral pion decays [14], from the galactic SNRs supporting this hypothesis for hadronic acceleration in SNRs.

### 1.1.4 Extragalactic Sources

A possible source of the highest energetic cosmic rays is the core of active galaxies. These active galactic nuclei (AGN) generate large amounts of electromagnetic radiation. Their energy is assumed to be a result of matter accreting around and falling into supermassive black holes at their centres. Another extragalactic source for the highest energy cosmic rays in nature is Gamma-ray bursts (GRBs) one of the most luminous phenomena known in the Universe. Models of GRB predict the formation of multiple shock regions



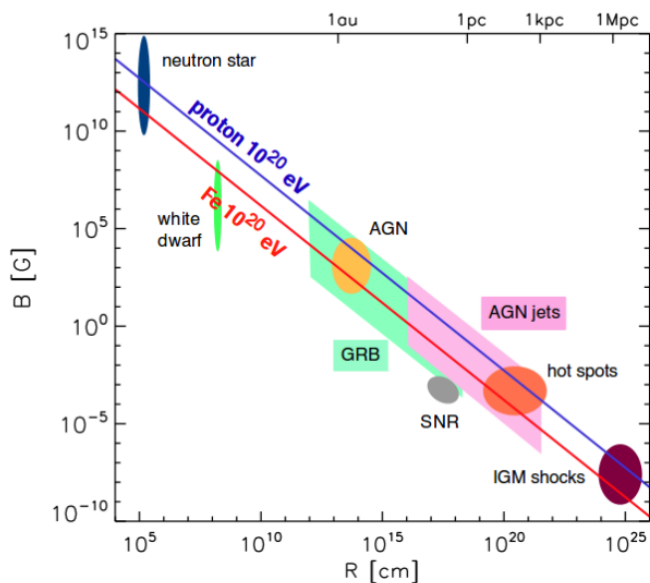


Figure 1.4: The “Hillas plot”: Magnetic field strength of the objects and their extension. The maximum gyro radius of a particle accelerated in this object is its size, therefore a maximum energy which can be reached by particles being accelerated in these objects can be defined. These energies are indicated with the two lines for proton and iron. Sources must be above the upper diagonal line to accelerate protons to more than  $10^{20}$  eV. This plot is taken from [13].

which are potential acceleration sites for cosmic rays. Starburst galaxies, which are galaxies with intense star formation, have enhanced supernova activity and would therefore be expected to be an enhanced source of sub  $10^{18}$  eV cosmic rays through the mechanism mentioned in the previous subsection. It has also been proposed that ultra-high energy cosmic rays may be accelerated in the large-scale terminal shock of the superwind that flows from the starburst engine [15]. Starburst galaxies are particularly relevant in the astrophysical neutrino context as they have been shown to have the conditions to efficiently convert cosmic-rays into pions and neutrinos [16] through the processes described in section 1.2.2.

### 1.1.5 Cosmic Ray Air Showers

An important aspect of studying cosmic rays is an understanding of the shower of particles which is initiated when a cosmic ray interacts in the Earth's atmosphere. These air showers, often called extensive air showers due to their large extent of many kilometres, start with the interaction of a primary cosmic ray particle with a nucleus in the atmosphere. This interaction produces hadrons which can interact or decay depending on their energy and the depth in the atmosphere. Three components of the air shower arise: the hadronic core and electromagnetic and muonic components. The electromagnetic component is fed by photons from decays of the hadronic particles with each high-energy photon generating an electromagnetic sub-shower through alternate pair production and bremsstrahlung. The muonic component is fed by the decays of charged pions and kaons.

The detection of high-energy cosmic rays is through the observation of their extensive air showers as the high-energy particles are too rare to be detected directly with the size range of detectors which can be deployed above the Earth's atmosphere. For example most of the measurements displayed in fig. 1.1, with energies above the knee, are from surface air shower detectors.

An understanding of cosmic ray air showers is needed for astrophysical neutrino detection as the muons and neutrons in the showers are a source of background for searches for astrophysical neutrinos. Using the IceTop surface array to identify this background is the focus of this thesis and simulations used to model the air showers are described in chapter 3.

## 1.2 Neutrinos and Neutrino Astronomy

### 1.2.1 Neutrino Fundamental Properties

The existence of neutrinos was proposed in 1930 by Wolfgang Pauli [17] in order to explain the continuous energy spectrum of electrons emitted in radioactive  $\beta$  decay [18]. However their discovery only happened over twenty years later in an experiment conducted by Frederick Reines and Clyde Cowan in 1953 [19] exploiting the inverse beta decay ( $\bar{\nu}_e + p \rightarrow e^+ + n$ ).

Since its discovery the neutrino has been much studied, and according to our current model for particle physics, there are three flavours of neutrinos, with one neutrino flavour for each of the three charged leptons, electron, muon and tauon. These three neutrino flavour states do not correspond to the neutrino mass eigenstates, and the mixing matrix which relates the flavour and mass states is the subject of great experimental and theoretical interest. The implications of neutrino mixing for the neutrinos of interest in this thesis is discussed in section 1.2.2

All three flavours of neutrinos interact with nucleons (protons and neutrons) via either the charged current or neutral current interaction. This leads to six possibilities for neutrino interactions with nucleons (three flavours times two possible interactions). In a charged current interaction, the exchange of a  $W^\pm$  gauge boson occurs and the charged lepton associated with the neutrino is produced. In a neutral current interaction, the exchange of a  $Z^0$  gauge boson occurs and there is a neutrino in the final state after the interaction. These two interactions are depicted in fig. 1.5.

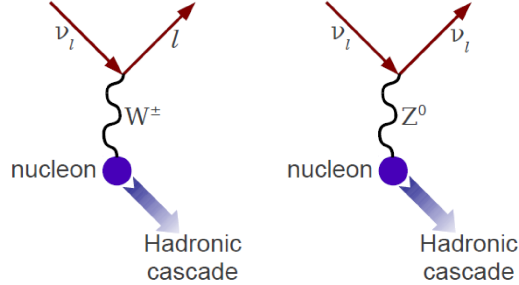


Figure 1.5: Charged-Current and Neutral-Current neutrino interaction. This plot is taken from [2].

In addition to neutrinos interacting with nucleons, electron type antineutrinos have an enhanced probability of interacting with electrons when the center-of-mass energy of the system reaches the mass of the mediating boson. This process which was first pointed out by Glashow and is referred to as the Glashow resonance. For electrons at rest and using the mass of the  $W$  boson  $m_W = 80.4$  GeV, the Glashow resonance can be calculate to occur at a neutrino energy of  $6.3 \times 10^{15}$  eV. The interaction probability for electron

antineutrinos is dramatically enhanced at this energy.

For scattering of neutrinos with nucleons at high energies the cross sections are shown in fig. 1.6. Up to energies of  $\sim 10^{13}$  eV, the cross section grows linearly with the neutrino energy and is larger for neutrinos than for antineutrinos; the latter is a consequence of the opposite helicities of neutrinos and antineutrinos [20]. At higher energies, the energy transferred in the interaction by the intermediate boson can no longer be neglected which leads to a suppression of the cross section and reduces the difference between neutrinos and antineutrinos [20].

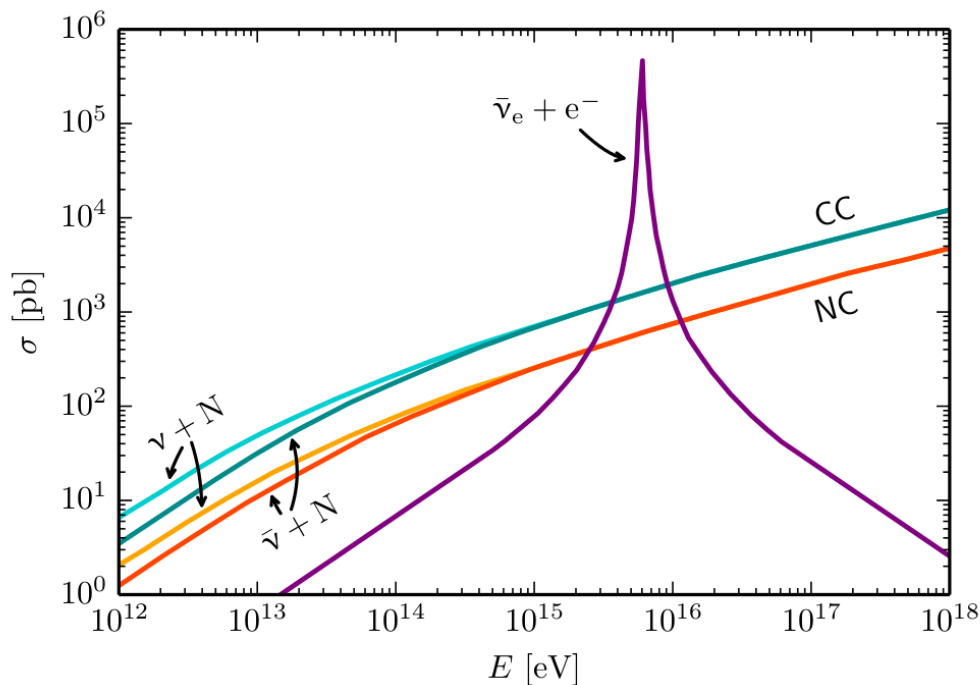


Figure 1.6: The resonant antineutrino electron scattering (Glashow resonance). The figure was taken from [3].)

## 1.2.2 Neutrino Astronomy

Neutrinos are electrically neutral leptons and hence are only affected by the electroweak force and not by the electromagnetic or strong forces. This means

they have an extremely small cross-section or probability to interact with matter. Consequently they can travel to the Earth from their sources and reach the detector without being deflected by magnetic fields or absorbed. This means that neutrinos can escape all but the densest environments and implies that neutrinos can reach the Earth from the farthest edges of the Universe. This distinguishes them from photons, which with increasing energy, are more and more likely to get absorbed in electron pair-production interactions with ambient radiation fields, such as the cosmic microwave background. The gamma-ray horizon, from beyond which photons are unlikely to reach the Earth, is depicted in fig. 1.7.

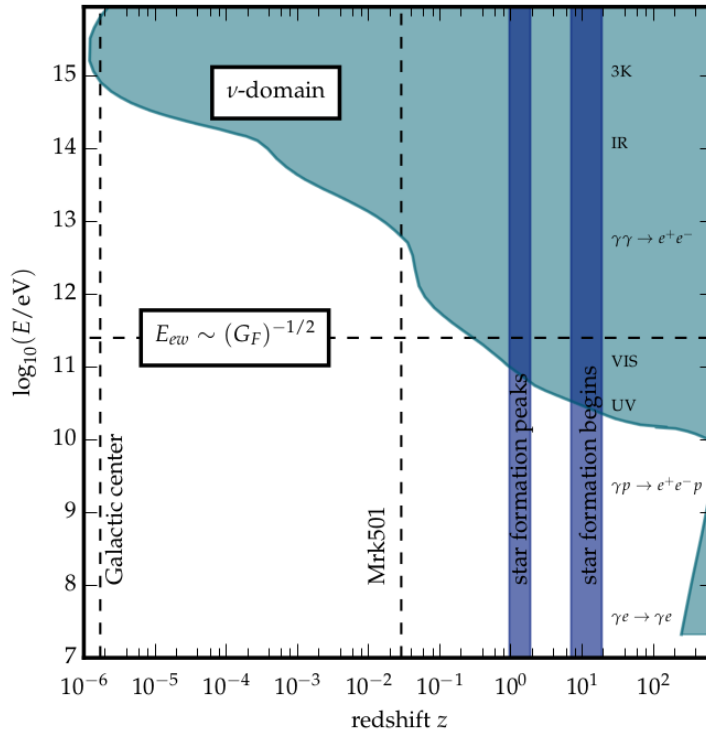


Figure 1.7: The cosmic horizon of high energy  $\gamma$  ray astronomy is limited due to the interaction of  $\gamma$  rays with intergalactic radiation fields. Gamma-ray photons are likely to be absorbed by the radiation fields however there is no corresponding horizon for neutrinos and Gamma-ray measurements are complemented using neutrinos. Figure adapted from [21].

In contrast charged particles, whose trajectories are affected by magnetic fields, cannot point back to their sources. It is therefore unlikely that it will be possible to identify the origin of cosmic rays, or the sites where they are accelerated, using only cosmic-ray observations. However it is expected that neutrinos will be produced at the sites of cosmic ray acceleration [22,23] and these neutrinos could be used to locate the sources of cosmic rays. These neutrinos are referred to as astrophysical neutrinos and their detection and characterisation is a major research goal for the IceCube telescope.

High-energy cosmic rays can produce neutrinos when they interact with target particles or radiation. The properties of the target as well as the primary cosmic ray are two factors that the resultant neutrino flux depend on. In the hadronuclear scenario the accelerated cosmic rays collide with nuclei, producing neutral and charged pions in inelastic scattering processes. In the simplest  $pp$  scenario both nuclei are protons. The basic interaction and decay chain of interactions is:

$$p + X \rightarrow \left[ \begin{array}{cc} \pi^0 & + & X \\ \pi^\pm & + & Y \end{array} \right] \quad (1.2)$$

$X$  represents either a proton or neutron, and  $Y$  another or several other particles.

The charged pions decay to produce neutrinos

$$\pi^+ \rightarrow \mu^+ + \nu_\mu \rightarrow e^+ + \nu_e + \bar{\nu}_\mu + \nu_\mu \quad (1.3)$$

$$\pi^- \rightarrow \mu^- + \bar{\nu}_\mu \rightarrow e^- + \bar{\nu}_e + \nu_\mu + \bar{\nu}_\mu \quad (1.4)$$

The neutral pions immediately decay via

$$\pi^0 \rightarrow \gamma + \gamma \quad (1.5)$$

According to hadronic models, the high-energy gamma-rays are produced by the decay of  $\pi^0$  mesons emerging from the interaction of cosmic rays with ambient matter or radiation. Since neutrinos can only be produced in a hadronic acceleration model, the simultaneous observation of neutrinos from a high-energy gamma-ray source can help to distinguish the acceleration mechanisms. This is because gamma-rays alone do not necessarily mean there is hadronic acceleration as there is another model that explains high

energy gamma-ray fluxes from a variety of objects; the leptonic model. In the leptonic model high-energy radiation is produced by synchrotron and bremsstrahlung emission from high-energy electrons.

Another possible scenario is the so-called  $p\gamma$  or photohadronic scenario. In this case at high energies, protons may interact with ambient photons  $\gamma$  in which the target for the high-energy cosmic rays are photons and the cross section for such interactions is particularly large near the  $\Delta$  resonance, which means the energy of the cosmic rays and of the target photons have to match so that in the center-of-mass system the  $\Delta^+$  can be produced. The dominant decay modes of  $\Delta^+$  contain pions.

$$p + \gamma \rightarrow \Delta^+ \rightarrow \left[ \begin{array}{cc} \pi^0 & + & p \\ \pi^+ & + & n \end{array} \right] \quad (1.6)$$

In this scenario negatively charged pions arise only in the process called multipion production which happens when center-of-mass energy exceeds the rest mass of the pion in inelastic collisions. As an outcome fewer electron antineutrinos are produced compared to the  $pp$  scenario. Thus, measurement of the flux at the Glashow resonance can be used to distinguish between the  $pp$  and the  $p\gamma$  scenario since the cross section for electron antineutrinos is substantially enhanced at the resonance around 6.3 PeV and so with having antineutrinos present in the cosmic neutrino flux, the rate of events is expected to increase. Fewer  $\bar{\nu}_e$  produced in  $p\gamma$  sources compared to  $pp$  sources gives us the idea that an accurate measurement of the cosmic neutrinos rate at the Glashow resonance is sensitive to the neutrino neutrino mechanism [24].

From eq. (1.3) and eq. (1.4) above it can be seen that at the source, the neutrino flavour ratio is  $\nu_e : \nu_\mu : \nu_\tau = 1 : 2 : 0$ . Over cosmic distances neutrino mixing will convert the  $(1 : 2 : 0)$  flavour ratio to  $(0.93 : 1.05 : 1.02) \approx (1 : 1 : 1)$  [25]. Alternative neutrino production models involve neutron decay or take into account muon energy loss and predict source flavour scenarios such as an electron-neutrino-only case  $(1 : 0 : 0)$  or a muon-neutrino-only scenario  $(0 : 1 : 0)$ . Averaged over astronomical distances, neutrino oscillation converts these two production ratio cases into  $(1.6 : 0.6 : 0.8)$  and  $(0.6 : 1.3 : 1.1)$  respectively [25].

### 1.2.3 Atmospheric neutrinos

The hadro-nuclear scenario described above is essentially the same process which occurs when cosmic rays interact in the Earth's atmosphere creating the extensive air showers described above. In this case the neutrinos produced are called atmospheric neutrinos. Atmospheric neutrinos and astrophysical neutrinos are predicted to have different spectra or energy dependence. This is because the cosmic ray spectrum is expected to be altered by energy dependent diffusion to evolve from a power law with an exponent of approximately -2 at the source to a power law with an exponent of -2.7 at Earth. The astrophysical neutrinos are predicted to follow the cosmic ray spectrum at their source.

A distinction is made between the atmospheric neutrinos which result from mesons containing only up, down and strange quarks such as pions or kaons and, neutrinos resulting from mesons containing charm quarks. The former are known as 'conventional' atmospheric neutrinos and the latter as 'prompt' atmospheric neutrinos. The label 'prompt' refers to the fact that these neutrinos would be created high in the atmosphere close to the location of cosmic ray interaction due to the fact that the mesons containing charmed quarks decay more quickly than pions and kaons. Prompt atmospheric neutrinos have not yet been observed. The spectrum of the prompt atmospheric neutrinos is expected to follow the observed cosmic ray spectrum while the conventional atmospheric neutrinos have a softer spectrum due to the energy dependent interactions which can occur in the neutrino parent particles.

Pions and kaons do not always decay, but often interact again with air molecules. The interplay between decay and interaction is governed by the density of the atmosphere and the energy and lifetime of the particle. For a given atmospheric density and particle, the critical energy is defined as the energy at which decay and interaction are equally likely; below, decay prevails, above, interaction is more likely. In the Earth's atmosphere, the critical energy of charged pions is  $\approx 115$  GeV, that of charged kaons is  $\approx 850$  GeV, and that of neutral long-lived kaons is  $\approx 205$  GeV. Because the pions and kaons lose energy when interacting, the energy spectrum of conventional atmospheric neutrinos is steeper ( $E^{-3.7}$ ) than that of the primary cosmic rays ( $E^{-2.7}$ ). The conventional neutrino flux contains electron and muon neutrinos. The power-law index of the prompt neutrino flux component fol-



lows the one of the cosmic ray flux because they decay so quickly ( $\sim 10^{-12}$  s) that they do not interact with the atmosphere. Since charmed mesons are heavier than the tau mass, they can decay into all three neutrino flavors, and therefore they add the atmospheric tau neutrino flux. The prompt neutrinos are expected to become the dominating part of the atmospheric neutrino flux at energies of about 100 TeV.

The spectrum of atmospheric muon and anti-muon neutrinos can be parametrized as function of the neutrino energy  $E_\nu$  and the zenith angle  $\theta$

$$\Phi_\nu(E_\nu) = \frac{\Phi_N(E_\nu)}{Z_{NN}} \cdot \left( \sum_{n=1}^3 \frac{A_i}{1 + B_i \cos(\theta) \frac{E_\nu}{\epsilon_i}} \right) \quad (1.7)$$

Here,  $i$  runs over the decay contributions from pions, kaons and charmed hadrons. The factors  $A_i$  and  $B_i$  are constants. The overall normalization factor is the primary flux of nucleons  $\Phi_N(E_\nu)$  calculated at the neutrino energy  $E_\nu$  and multiplied with the factor  $1/(1 - Z_{NN})$ , which is related to the nucleon attenuation length.

## 1.2.4 Neutrino spectra

The energy dependence of various sources of neutrinos is shown in fig. 1.8. In this figure the electron neutrino and muon neutrino fluxes for conventional atmospheric neutrinos are shown separately as the electron neutrino flux is a factor of two lower than the muon neutrino flux at lower energies and a factor of ten lower at higher energies. The prompt atmospheric flux is predicted to be equal for muon and electron neutrinos. The atmospheric tau neutrino flux is negligible at the relevant energies for this project while as discussed below the astrophysical neutrino flux is expected to be an equal mixture of all three flavours. A benchmark model for astrophysical neutrinos is the featureless  $E^{-2}$  spectrum, although particular astrophysical objects are expected to have spectra which vary from this. For instance, in fig. 1.8 the spectrum from AGN, according to the Stecker model [26] is shown. The GZK neutrino prediction which is also shown in the figure refers to the neutrinos which would be produced when cosmic rays interact with the cosmic microwave background photons through the GZK effect described earlier in this chapter.

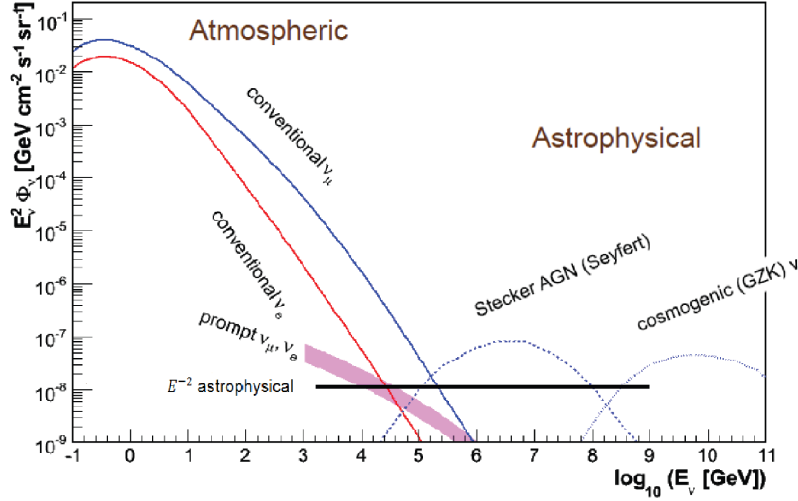


Figure 1.8: The atmospheric neutrino energy spectrum and astrophysical neutrino energy spectrum from Stecker AGN as a particular model for the neutrino flux expected from AGNs and GZK limit (see text for explanation). Figure adapted from [27].

In the generic neutrino production scenario the pions and muons are expected to decay without interacting, and will be the case when the density of the matter around the source is small. In this situation the neutrino spectrum will follow the production spectrum of their parent cosmic rays.

## Chapter 2

# The IceCube Neutrino Observatory

IceCube is a neutrino detector built at the South Pole with the goal of studying high energy neutrinos. It is the world's largest neutrino detector encompassing a cubic kilometre of ice below the surface at the South Pole. In this chapter we describe the main components of the IceCube observatory, the principles of neutrino detection with IceCube, and some of the latest astrophysical neutrino results.

### 2.1 IceCube Detector Components

A schematic view of the IceCube neutrino observatory is shown in fig. 2.1. It is made up of two main components the surface array of detectors called IceTop and the array of optical sensors deployed deep below the surface. This array below the surface is often simply referred to as IceCube. We mainly follow this convention in this thesis, although when we want to make clear the distinction between the array below the surface, and IceTop we will refer to the IceCube-InIce array. IceCube is made up of an array of optical sensors referred to as Digital Optical Modules (DOMs) which detect visible light. The sensors are deployed on vertical cables with a vertical spacing of 17m between sensors. The horizontal spacing between cables is

around 125m. The individual cables have lengths of about 3500 metres, the instrumented part is deployed in depths of around 1450 - 2450 metres, where the hydrostatic pressure leads to a suppression of gas bubbles in the ice. Ice above 1450 m contains too many bubbles, making it much less transparent and therefore less suitable for the experiment. The IceCube components are shown in fig. 2.1. The detector construction started in 2005 and was finished in December 2010. Construction was only possible in the austral summers due to the conditions at the South Pole.

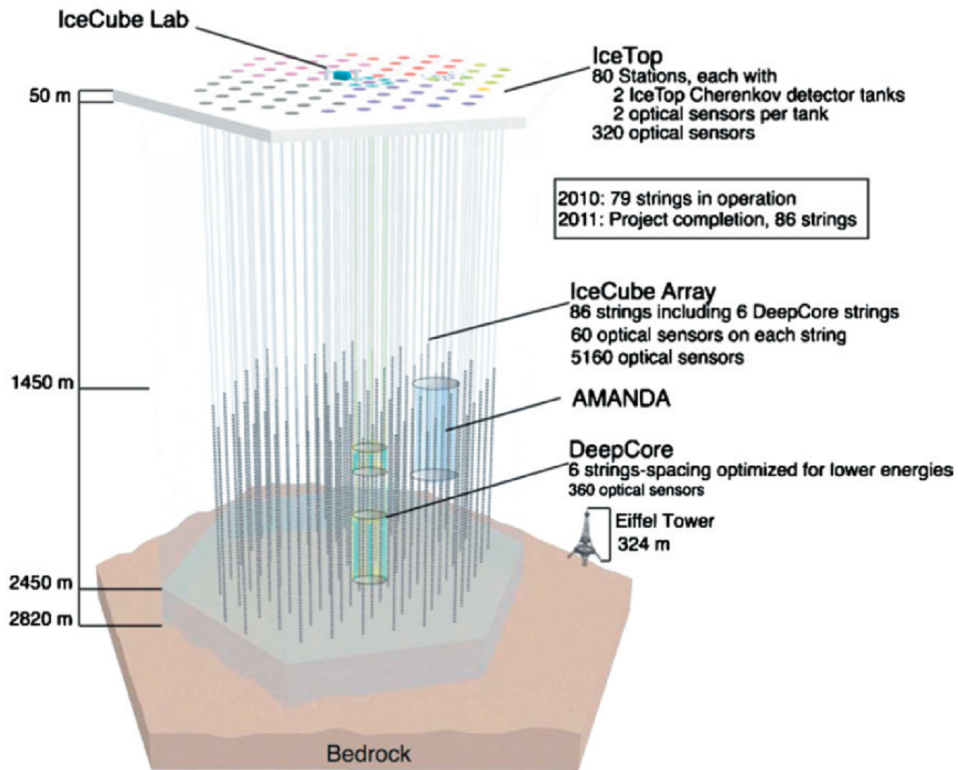


Figure 2.1: A schematic view of IceCube Neutrino Observatory. The vertical lines show 86 IceCube strings with 60 digital optical modules instrumented on each string between the depth of 1450m and 2450m. At the centre of the IceCube detector 8 strings, shown in green colour, are deployed relatively close to optimise for lower energies. This region is called DeepCore.

The design of IceCube is optimized for the primary goal of the discovery of an extraterrestrial or astrophysical neutrino flux. The volume of the detector was chosen so as to be sensitive to the predicted astrophysical neutrino flux which was detected soon after IceCube was completed, as described in section 2.7. The 125m spacing between the cables means that the low energy threshold for neutrino detection in IceCube is  $\sim 1$  TeV.

In order for IceCube to be sensitive to the lower energy neutrinos, with which oscillation effects can be studied, and also neutrinos in the energy range expected from dark matter annihilations, the core of IceCube has been instrumented with a higher density of DOMs. The central 8 strings have a module density 5 times higher than the rest of the detector, with a horizontal distance of 72 m and a vertical distance of 7 m and a location below 2100 m. They form the so-called DeepCore [28] part of the IceCube detector. The PMTs have a 35% higher quantum efficiency than the standard IceCube DOMs, which together with the clearer ice, leads to a much lower energy threshold of 10 GeV in the DeepCore volume.

The IceCube detector is accompanied by a surface detector, IceTop which is designed to measure the cosmic ray spectrum particularly in the energy range where the spectrum is less well understood. It measures the muons produced in particle showers which are generated by cosmic ray interactions with the atmosphere which facilitates the exploration of the cosmic ray composition in the energy range from 100 TeV up to 1 EeV. IceTop will be described in further detail in the next chapter. The use of IceTop as a veto array for detecting neutrinos is the subject of this thesis.

The central component and basic detection unit of IceCube is called a Digital Optical Module and consists of a 25 cm-diameter photomultiplier tube (PMT) and several electronics boards, contained within a pressure resistant 13 mm thick glass sphere of 35.6 cm-diameter. The housing is filled with nitrogen at a pressure of 0.5 atmospheres. The PMT is optically connected to the housing by a transparent gel. It is also enclosed in a  $\mu$ -metal grid, which shields the PMT against the Earth's magnetic field. The PMTs measure the light emitted by neutrino interactions. A DOM which measures light above threshold is said to have received a hit.

The incoming stream of DOM hits are combined into physics events by the data acquisition system (DAQ) which is a software trigger algorithm. Multiple trigger conditions exist. The simplest condition is the simple multiplicity

trigger (SMT). The SMT-8 trigger, for instance, requires 8 local coincidence hits within a time window of  $5 \mu\text{s}$ . A local coincidence hit is one in which a neighbouring DOM has also recorded a hit. The readout window contains all hits that satisfy this condition, as well as the hits in the preceding  $4 \mu\text{s}$  and subsequent  $6 \mu\text{s}$ .

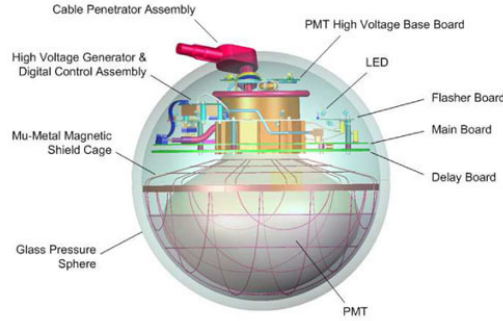


Figure 2.2: The light sensor of IceCube neutrino detector (Digital Optical Module). The Digital Optical Module for the IceCube neutrino detector consists of glass sphere contains the key component such as flasher board, PMT etc.

## 2.2 Neutrino Detection Principle

IceCube detects neutrinos by observing the optical light which is emitted by the products of neutrino interactions in the ice. This optical light is called Cherenkov radiation and occurs when any charged particle travels faster than the local speed of light in a dispersive medium.

Neutrinos are observed via the optical detection of charged secondary particles which are produced in neutrino interactions inside the Antarctic ice. Two basic event topologies can be distinguished: track-like patterns of light which originate when a long-range particle is produced and spherical light patterns which originate when a cascade or shower of particles is produced. This research is concerned with the second case which is referred to as the cascade channel. All neutrino interactions produce a hadronic cascade. This cascade occurs due to the ‘hit’ nucleon splitting into its quark constituents and these quarks subsequently producing a cascade of hadrons in a process

referred to as jet fragmentation. In neutral current interactions the only source of Cherenkov light is from this hadronic cascade. The length of the cascade is no more than five metres and so given the large spacing between IceCube cables appears as a point-like source of light in the detector.

In charged current interactions there will also be Cherenkov light associated with the charged lepton which is produced. Each of the three charged leptons evolve differently in the ice. The outgoing electron from a charged current interaction of an electron neutrino interacts readily and initiates an electromagnetic cascade containing electrons, positrons and photons. So in this case there is Cherenkov light from both the hadronic and electromagnetic cascades. However the two cascades are not able to be resolved separately. The muon from a charge current interaction, on the other hand, can propagate a significant distance and if it has high enough energy it can traverse across the entire IceCube. The muon emits Cherenkov radiation as it travels. A tau from a charged current interaction will travel a short distance before decaying. In most cases the decay products from the tau will initiate an electromagnetic cascade. The distance travelled will depend on the relativistic time dilation related to how energetic the tau is. For tau energies under 1 PeV, the cascade from the tau decay and the initial hadronic cascade will not be able to be resolved.

In fig. 2.3 we can see the light pattern for a short-range cascade which deposits its energy in the detection volume. This will be the type of light pattern produced in five of the six interaction possibilities. While fig. 2.4 shows the track-like signature produced by a long-range muon traversing the detection volume. In both figures the gray dots mark IceCube DOMs. The colour coding illustrates the arrival time of the light at the DOM and the size of the dot scales with the amount of light recorded by the DOM.

## 2.3 Neutrino search techniques

The majority of events recorded by IceCube are not the events we are looking for, but background events. The background events have their origin in cosmic ray interactions in the Earth's atmosphere with the data collected by the IceCube detector dominated by atmospheric muons. When a cosmic ray interacts it initiates a shower of particles. Pions and kaons are created in

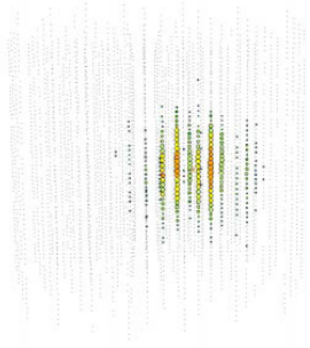


Figure 2.3: Simulation of a cascade in IceCube.

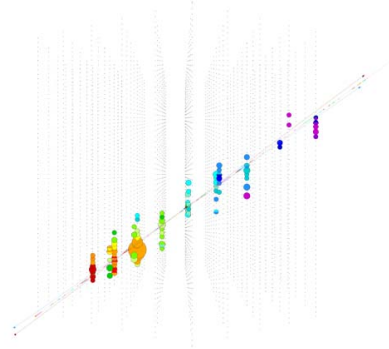


Figure 2.4: Simulation of a long-range muon in IceCube.

these particle showers, which decay into muons and muon neutrinos. While muons decay into neutrinos, too, their long mean lifetime of  $2.2 \mu\text{s}$  prevents them from doing so before reaching the detector if their energy exceeds a few GeV. The vast majority of the triggered events in IceCube are produced by muons created by cosmic rays interacting in the atmosphere above IceCube. The event rate varies seasonally with the atmospheric muon flux from 2.5 kHz to 2.9 kHz, with a median rate of 2.7 kHz. Filtering strategies are used to isolate neutrino events from the dominant background. These strategies are based on data analysis involving various reconstruction tools first operating on the raw data and then on the information derived from the raw data.

The first step of filtering is by a computing system at the South Pole, the so-called online filter which reduces the data volume to a level where the data can be transferred into the North via a satellite with limited bandwidth. The reduced data sample is then sent over satellite directly to the IceCube headquarters in Madison, Wisconsin. The rest of the data is shipped later on tapes. Before the OnlineFilter is applied the event properties are reconstructed in several steps. First, pulses are extracted from the digitized waveforms; by running the so-called FeatureExtractor on the raw data. The raw data coming from the DOMs are called waveforms and contain the measured charge of the PMT as a function of the time. Each pulse is specified by its arrival time and the extracted number of photoelectrons. Based on



these pulses, simple reconstruction algorithms try to infer basic properties of the light-emitting particle, such as its energy, direction, and interaction time and vertex. This information is then used by the filter algorithms to decide whether an event is transmitted or not.

The first stage of filtering at the Pole is done for all analysis types and then different Pole filters create corresponding data samples which can overlap. The different analysis types focus on for example different energy regimes and different event types such as track or cascade. Further analysis is done by applying reconstruction routines and cuts on one or more of these data samples. This thesis is particularly concerned with cascade analyses. Although track events have better direction reconstruction, cascade events have better energy reconstruction, especially in the case of an electron neutrino. The energy of events is deduced from the amount of Cherenkov light. In the case of an electron neutrino all of the incoming neutrino's energy is transferred into the hadronic and electromagnetic cascades which will be contained within the detector and so an accurate measurement of the amount of light produced and hence energy of the neutrino can be made. In contrast a muon passes through the detector and only some of its energy is deposited in the detector volume which means that it is harder to determine the energy of muon neutrinos. Furthermore cascade events are produced by all three neutrino flavours, while tracks are only produced by muon neutrinos; this increases the probability to detect astrophysical neutrinos.

The cascade channel aims to select the events which are cascade-like. For example, the pole filtering for the cascades usually consists of two cuts placed on variables called the line-fit velocity and the tensor of inertia eigenvalue ratio which are described in section 2.5 below, and are based on the properties of cascades having a stationary light source and a more spherical, rather than elongated, distribution of hit DOMs.

A key feature of the atmospheric muon background is that the muons produce Cherenkov light along their path and so will be emitting light as they enter the detector. This is not the case for neutrinos which interact inside the detector volume, where the first light detected will be inside the detector. For this reason, many background rejection techniques are based on selecting events where the first light is seen within the detector volume. However such techniques mean that the detector volume available for neutrino detection is reduced. For this reason it is useful to separate events which are

completely in the detector and the ones which are partially within IceCube. With this motivation the cascade selection is further split into the *contained* and *uncontained* samples. Cascade events for which the reconstructed vertex (position of the neutrino interaction) is beyond the detector, or where the DOM with the largest charge is on one of the outer strings, are known as uncontained events and the rest are contained events. The contained events have a lower proportion of background contamination while including an uncontained sample allows for a greater effective volume for detecting neutrinos. The subsequent filtering steps differ between the uncontained and contained samples.

In contrast to the cascade channel, the track channel selects events such as that displayed in fig. 2.4. This is particularly useful for upward going events which necessarily must be neutrinos rather than cosmic ray muons. Although it is not possible to distinguish atmospheric and astrophysical neutrinos on an event by event basis, it is possible to fit for both components given their different spectral properties<sup>1</sup>.

Although the main aim of this thesis is to investigate how an IceTop veto can be used in a cascade analysis, in one of the studies performed in this thesis it was most useful to use data with a good angular resolution. The most suitable stream of data for this study is the one containing high-energy events. The data stream used is called the Extremely High Energy (EHE) event sample and consists of events which triggered the in-ice detector with a charge at least 1000 photoelectrons (p.e.). Most of these events will be muon background events. The EHE neutrino analyses refine this sample further, notably by requiring events to have at least 25,000 p.e. and 100 hit DOMs, to search for the GZK neutrinos mentioned in chapter 1.

The neutrino filtering strategy which was effective in first identifying astrophysical neutrinos is the High Energy Starting Event (HESE) search. Neutrino candidates were selected by finding events that originated within the detector interior. The HESE criteria for keeping an event was that at least 6000 p.e. had to be recorded in total and fewer than three of its first 250 observed p.e. where the veto region was defined to be the outer parts of the instrumented volume. This event selection rejects 99.999% of the muon background above 6000 p.e. while retaining nearly all neutrino events in-

---

<sup>1</sup>See section 1.2.3 for a discussion of the spectral properties of the astrophysical and atmospheric neutrinos.

interacting within the fiducial volume at energies above a few hundred TeV. This selection is largely independent of neutrino flavour, event topology, or arrival direction. The results obtained from the HESE search are described in section 2.7.

## 2.4 Simulation

Simulation of the IceCube detector is needed to characterise IceCube’s acceptance of neutrino signal, as a function of neutrino energy and direction, and also for use in developing the filtering strategies to remove background events. Monte Carlo techniques are used with the aim of simulating the full range of signal and background particles incident on the detector. The simulation is done in several steps with separate modules treating different aspects. At the beginning, muons or neutrinos are produced with so-called generators. Particles are generated according to a given spectrum in some energy range.

The neutrino event simulation starts with the injection of neutrinos and then simulates the propagation and detection in IceCube. For the simulation of neutrino interactions around the IceCube detector, the IceCube NuGen module is used, which is able to simulate neutrinos and antineutrinos of all flavours in a wide energy range. Its fundamental physics is based on the All Neutrino Interaction Generator (ANIS) [3]. Neutrinos are injected with a parametrized angular and energy distribution (e.g. the conventional atmospheric spectrum or the isotropic astrophysical spectrum), and propagated through the earth. For the density profile of the earth, the Preliminary Earth Model [29] is used. In the next step, the neutrinos are forced to interact in a pre-defined volume around the detector. This makes the simulation process more efficient. This forced interaction is taken into account by an interaction probability weight which the simulated neutrinos based on the energy dependent cross-section for neutrino interaction. Once the weighting is taken into account the distribution of events simulated should follow that expected in data.

After the interaction of the particles in the detector volume is simulated, the secondary particles like muons that are created in that step are propagated. All particle showers generated in interactions of the primary particles or their

secondaries are simulated. The Monte Carlo code PROPOSAL (PRopagator with Optimal Precision and Optimised Speed for All Leptons [30] is used to model the propagation of secondary particles through matter. PROPOSAL is the successor to the Muon Monte Carlo code which was previously the standard within IceCube. PROPOSAL simulates a muons energy losses due to ionization, bremsstrahlung, photo-nuclear interaction and pair production when traveling through matter. It takes into account continuous as well as stochastic energy losses.

In the next step, the Cherenkov photons produced by the muons and particle showers are propagated through the ice, taking into account scattering and absorption. If the Cherenkov photons reach a DOM, the number of photoelectrons produced is calculated. Additional photoelectrons originating from the DOMs noise are added to the simulation. After the determination of the number of photoelectrons in the cathode of the PMT, the DOMs response is simulated as well. If the DOM trigger condition is fulfilled, its data is read out. The fulfillment of the individual DOM trigger condition is checked for all DOMs. Based on that, the detector trigger condition of the full detector is determined. If the event fulfills the detector trigger condition, it is saved and is passed on to the next filter level.

Estimation for the contribution of the penetrating muon background are usually based on Monte-Carlo simulations performed with the air shower simulation code, CORSIKA (COsmic Ray SIMulations for KAscade) [31]. Protons and light nuclei can be selected as the primary particle. From the primary interaction CORSIKA tracks the secondary particles through the atmosphere until they undergo reactions with the air nuclei or, in the case of unstable secondaries, decay. Monte-Carlo methods are used to simulate the possible interaction and decay outcomes according to the appropriate cross-sections and decay properties. All secondary particles are tracked and their arrival times, energies, locations and directions are stored. For IceCube all muons from the shower are passed to the PROPOSAL module for further propagation in the ice and the subsequent steps described above for neutrino-induced muons are similarly applied to the CORSIKA muons. It can happen that two or more atmospheric muons simultaneously move through the detector, trigger it and are recorded in the same event. The rate of coincident muon events is at least about a factor of 10 smaller than the single muon rate.

The main difficulty lies in the simulation of a sufficient number of air showers,

because such a vast number of muons reach the IceCube detector, also signatures that happen very rarely can appear as a background in searches for neutrino events. Sampling such rare cases requires the production of a number of air showers comparable to the number of naturally occurring showers during the data taking period which is not always feasible. Furthermore, the outcome of the simulations depends strongly on the assumed elemental composition of the primary cosmic rays (which is not well known for cosmic rays with PeV energies and cannot be tested under laboratory conditions at such high energies).

## 2.5 Event Reconstruction

Reconstruction in IceCube is an iterative process of determining what combination of hypothesized topology, position, direction, time, and energy gives the best match to the observed hits on the DOMs. The most basic element of a reconstruction is the event hypothesis, that is, a model of the physical event underlying the data. The hypothesis determines which parameters should be used to describe the event; a specific reconstruction is just a way of determining that parameters of the model that best describe the data. A cascade-like event can be described by the location of the neutrino interaction referred to as the cascade vertex ( $x$ ,  $y$ , and  $z$ ), the time of the event ( $t$ ), the orientation of the cascade (polar angles  $\theta$  and  $\phi$ ), and the visible energy of the cascade ( $E$ ).

In addition to the physics parameters describing the physical event, it can be useful to construct other variables from the observed hits which can be used to distinguish signal and background events. For example in this thesis the following variables are used [27].

- **LineFit-velocity:** This variable is a quantity, which differentiates between a cascade event and a muon event on the basis of the different characteristics of the speed of the source of the light pattern observed in the IceCube detector volume. For muon events the source of light moves through the detector at a speed approaching  $c$  which means muon events should have larger values of line-fit velocity. In contrast, the cascade can be thought of as a stationary source of light due to its small spatial extent and time duration. For this reason the cascade

events are supposed to have a line-fit velocity close to zero.

- Tensor of Inertia Eigenvalue Ratio: This variable characterizes the distribution of light of an event along the three principal axes in the detector. Taking the distribution of light to be analogous to a mass distribution the definition of the variable follows the definition of the tensor of inertia of a mass distribution. The eigenvalue ratio is the ratio of the lowest eigenvalue to the sum of all three eigenvalues. For a perfectly spherical event the eigenvalue ratio would be  $1/3$  because all three eigenvalues would be equal, while a track-like event being elongated has an eigenvalue ratio close to zero.
- MUEX: A quantity used by the IceCube collaboration as a proxy for the energy associated with a muon event. The MuEx value is derived from the amount and pattern of detected light under the assumption that the light has been produced by a muon.

Reconstruction routines used are:

- MonopodFit: An advanced reconstruction which is a combination of vertex, time, direction, and energy reconstruction that reliably gives energy and angle information. This method uses a likelihood approach.
- CredoFit: Credo is a likelihood reconstruction algorithm for cascade-like events. Credo describes events with the parameters of  $t, x, y, z, \theta, \phi, E$  with  $E$  being the energy of a particle shower which emits the amount of light observed in the detector.
- SPEFit: likelihood reconstruction for muon tracks to find things that reconstruct approximately as muons. The algorithm is implemented as a direction reconstruction for muon tracks not energy reconstruction. SPEFit, short for single photo electron fit, only consider the very first pulse of each DOM.
- Acer: Atmospheric Cascade Energy Reco which is used to define a high energy branch in the Cascade Level 3 filtering.

## 2.6 Ice

The south polar ice sheet was chosen not only because the quantity of ice far exceeds what could be produced artificially, but also because the quality of the ice is extremely high. Its properties do vary with depth due to the combination of slow deposition over time by snowfall, which contains varying amounts of dust and volcanic ash, and pressure and temperature variations within the ice sheet. These properties must be measured so they can be included accurately in both reconstruction and simulation of data observed in the detector. The main properties of interest are the scattering and absorption of photons. Despite the fact that Antarctic ice belongs to the clearest natural media found on Earth, allowing photons to travel for hundreds of metres before being absorbed, it has relatively large scattering coefficients, meaning that light quickly diffuses in the ice. The scattering and absorption coefficients vary strongly with depth. Foremost, at depths near 2000 m there is a large concentration of dust, which causes far greater absorption (as well as scattering) than in the rest of the ice volume. Additionally, the deepest ice, below the dust layer is extremely pure, with absorption lengths in excess of 100 m, allowing light to be observed from quite distant emitters, while above the dust layer the ice is not quite as clean, and so both scattering and absorption are greater. Several models of the optical properties of the ice have been developed based on measurements of the dust concentration. The models described the ice as a layered structure, with uniform properties within each layer however a complexity which has been revealed by recent studies of the ice is that these layers are tilted [4] and the scattering is anisotropic [32] for example the light is scattered preferably into the flow direction of the Antarctic glacier.

### 2.6.1 Dust layer veto region

In order to understand some of the event characteristics it is important to recognise that the detecting medium (the ice) is not uniform and the layout of the detector varies. This non-uniformity affects the variables which are important for my research. To reduce background some criteria are taken however they can be inefficient in extremely dusty regions of the ice. For example consider a muon that enters the detector in a very dusty region

so that the light by the muon as it enters the detector is absorbed before detection on any DOMs and the first light which is seen is in the central part of the detector. The dustiest ice region, between 2000 and 2100 m in depth with stronger scattering and absorption than in the adjacent ice is called the dust layer. The attenuation length of the ice at the wavelengths where the DOMs are sensitive is shown in the following figure:

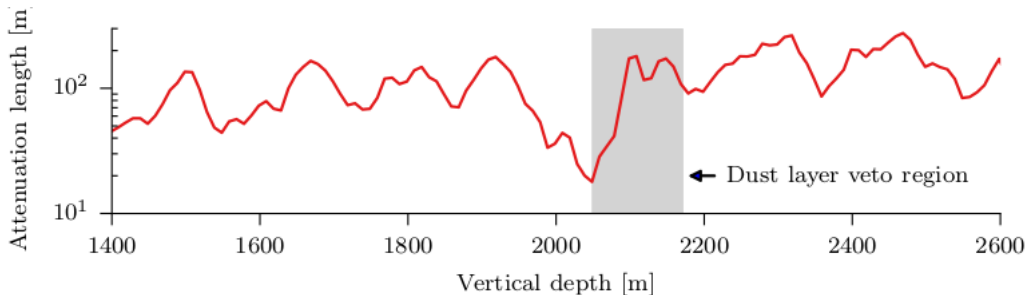


Figure 2.5: Optical attenuation length at 400 nm as a function of vertical depth. The figure adapted from [4]

As indicated in the figure the attenuation length is on average on the order of half the detector string spacing (120 m) or more, making it generally difficult for high energy background events to pass between two strings undetected. The exception is at 2050 m depth at which the attenuation length drops to 20m and inclined background events can sneak between two strings in the outer layer and appear to start at the depth of around 2100 m when the absorption length increases and a previously-undetachable energy deposition rate suddenly becomes detectable. For this reason we need to recognise the dustiest regions of the detector.

## 2.7 IceCube astrophysical neutrino results

In 2013 IceCube announced the first evidence for astrophysical neutrinos [33]. This evidence was found through a filtering search which looked for High Energy Starting Events or HESE as described above. The initial two year search found 28 events and provided evidence for the presence of an astrophysical flux of neutrinos events above the atmospheric background at



$4\sigma$ . This was followed up by an additional year of data. The three-year data set, with a livetime of 988 days, contained a total of 37 neutrino candidate events and a purely atmospheric explanation could be rejected at  $5.7\sigma$  [34]. Most recently 7.5 years of the HESE search has been released with 103 events [35]. In addition, evidence for astrophysical neutrinos has also been seen in searches looking for upward going muon events, cascade events and other analyses similar to the HESE analysis but targeted at lower energy ranges (see [36] for descriptions and results from various IceCube searches).

The spectral index fit of the form  $E^{-\gamma}$  to the astrophysical component of the diffuse neutrino flux varies somewhat between the different searches. For the HESE analysis the best fit is  $\gamma = 2.87 \pm 0.3$  while for the upward going muon events it is  $\gamma = 2.19 \pm 0.1$  [35]. The latest flavour composition from the HESE 7.5 year analysis is  $\nu_e : \nu_\mu : \nu_\tau = 0.35 : 0.45 : 0.2$  [35].

Until recently no association had been found between IceCube neutrino events and known astrophysical objects. However in September 2017, a high-energy neutrino event was found to be consistent in direction with a blazar observed to be in a flaring state [37]. The coincidence in direction of a blazar and a high-energy neutrino is not compelling on its own, as the large number of blazar objects in the sky means that a chance match in direction has a reasonably high probability. However the fact that the blazar was in a flaring state added significance to the association. The details of the high-energy neutrino event were sent in an IceCube alert and the Fermi and MAGIC gamma-ray telescopes following up on this alert found that the blazar TXS 0506-056 was coincident in direction and was undergoing a period of elevated gamma-ray emission. To take advantage of multi-messenger opportunities, IceCube has established a system of real-time alerts that rapidly notify the astronomical community of the direction of astrophysical neutrino candidates [38]. From the start of the programme in April 2016 through to October 2017, 10 public alerts have been issued for high-energy neutrino candidate events with well-reconstructed directions [39]. Chance coincidence of the IceCube170922A event with the flare of TXS 0506+056 is statistically disfavored at the level of  $3\sigma$  in models associating neutrino and  $\gamma$ -ray production [37]. In a subsequent analysis [40], an excess of high-energy neutrino events with respect to atmospheric backgrounds was found at the position of TXS 0506-056 between September 2014 and March 2015. Allowing for time-variable flux, this constitutes  $3.5\sigma$  evidence for neutrino emission from the direction of TXS 0506+056, independent of and prior to the 2017 flar-

ing episode and suggests that blazars are the first identifiable sources of the high-energy astrophysical neutrino flux.

## 2.8 Extensions to the IceCube array

IceTop does not extend beyond the cross-sectional area of the IceCube neutrino sensors which limits the use of IceTop as a veto. IceCube collaboration is currently investigating a new generation IceCube detector, referred to as IceCube-Gen2 with the aim to particularly extend the sensitivity of IceCube to neutrinos from the Southern Hemisphere, where the background from atmospheric muons is most limiting (as muons cannot make it all through the Earth). Extended surface detector might allow to reject a large fraction of the atmospheric background muons as well as neutrinos. It is expected that the large area of the surface array of the new generation will be more efficient than IceTop in detecting the cosmic-ray air showers and vetoing the muons and neutrinos produced in the atmosphere. The techniques investigated in this thesis, will help develop the Gen-2 project.

The unique properties of the Antarctic glacier, revealed by the construction and operation of IceCube, allow the spacing between light sensors to exceed 250 metres in IceCube-Gen2, the ten-cubic-kilometre detector, instead of the current 125 metres. The deployment of sensors in strings with larger spacings will enable the IceCube-Gen2 instrumented volume to rapidly grow at modest costs. IceCube-Gen2 will benefit from the successful designs of the hot water drill systems and the digital optical modules in the original IceCube project. Minimal modifications will target improvements focused on modernization, efficiency, and cost savings. Because of its digital architecture, the next generation facility can be operated without a significant increase in costs. By roughly doubling the instrumentation already deployed, the telescope will achieve a tenfold increase in volume to about 10 cubic kilometres, aiming at an order of magnitude increase in neutrino detection rates. The instrument will provide an unprecedented view of the high-energy Universe, taking neutrino astronomy to new levels of discovery.

## IceVeto extended array

IceCube-Gen2, the second generation detector at South Pole is planned on the same principles as IceCube but with roughly an order of magnitude better sensitivity for achieving key science goals related to the high energy astrophysical neutrino flux. This increase derives primarily from larger area and an enhanced surface veto to increase the significance of astrophysical neutrino events relative to a background of air shower induced muons and neutrinos [41]. The air shower array detector simulated using a code that reads a list of IceVeto detector coordinates is displayed in 2.6.

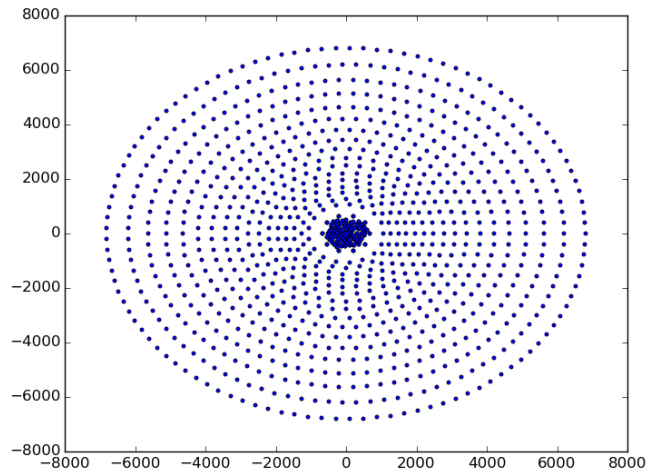


Figure 2.6: The suggested extension of current IceTop air shower array, which is known as IceVeto, this detector array geometry is IceTop plus an array of scintillator panels.

# Chapter 3

## IceTop and its Veto Potential

As introduced earlier, the aim of this thesis is to investigate how an IceTop veto can be used in a cascade analysis to distinguish astrophysical neutrino events from events initiated by atmospheric muons. While the main goal is to implement an IceTop veto within a cascade filtering strategy, in this chapter we present the IceTop veto potential in general terms considering the energy, zenith angle and surface intercept ranges for the incident cosmic rays which would result in sufficient hits on IceTop to allow their related in-ice event to be vetoed. We show that it is difficult to make a prediction for the number of IceTop hits using the in-ice event characteristics which motivates the simple IceTop veto strategy we describe in the remaining chapters of this thesis. The extended array (introduced in section 2.8) is also considered in this chapter and the enhanced veto potential it would enable is determined. In addition, we start this chapter by describing the IceTop detector array and its components and giving an overview of IceTop science results and the work of Tosi, which also employs IceTop as a veto.

### 3.1 IceTop Array Introduction

IceTop is the surface component of IceCube [42]. It consists of 81 detector stations covering an area of  $1 \text{ km}^2$  above IceCube. Stations are located close to IceCube strings. Each IceTop station is composed of two cylindrical ice-

filled tanks separated by 10 m to detect air shower particles using Cherenkov light created in the tanks' ice. The reason for having two tanks per station is to make air shower reconstruction more robust against signal fluctuations and allows a measurement of these fluctuations. The inner radius of a tank is 91 cm and the tank is filled with ice up to a height of 90 cm. To detect Cherenkov light emitted by charged particles in the ice, a tank is equipped with two DOMS (like those described in fig. 3.6d) which are separated by 58 cm and placed at the top of the ice facing downward. The photomultiplier tubes inside the DOMs are operated at two different gains, high-gain DOMs and low-gain DOMs in order to enhance the dynamic range. To increase the light yield at the photomultiplier, the inner surface of the tank is coated with a diffusely reflective white liner made of Zirconium dioxide powder.

### 3.1.1 IceTop Science

The IceTop array enables studies of the energy spectrum of cosmic rays in the energy range of  $10^{14}$  eV to  $10^{18}$  eV and determination of the primary mass composition as a function of energy.

The thickness of the Antarctic glacier means that IceTop is located at an altitude of about 2835 m above sea level. This altitude, equivalent to an average atmospheric depth of  $695 \text{ g/cm}^2$ , is quite close to shower maximum for protons in the energy range of interest of  $10^{14}$  to  $10^{18}$  eV. Shower maximum for protons is about  $550 \text{ g/cm}^2$  at 1 PeV to  $720 \text{ g/cm}^2$  at 1 EeV [1]. An advantage of the detector being located at the shower maximum is that fluctuations of shower density are smaller than at other stages of shower development. This allows IceTop to have good energy resolution which in turn enables features in the cosmic ray energy spectrum to be distinguished.

Cosmic ray studies are made using the IceTop surface array alone and also using information from the in-ice IceCube array in conjunction with the surface detections. Coincident events can provide information about the cosmic ray composition by analysing the ratio of energy of the muons passing into the deep ice and the shower size at the surface.

A recent review of science results can be found in [43]. The cosmic ray spectrum measurements are in good agreement with other experiments and show significant hardening of the spectrum around 20 PeV and the presence of

the second knee above 200 PeV. IceTop composition studies show consistency with other experiments below 100 PeV but above this energy range the IceTop composition is high mass (iron like) while other experiments have found that the composition transitions to proton and lower mass nuclei above 100 PeV.

In addition to the spectrum and composition of cosmic rays, another quantity which is accessible to measurement is the arrival direction. As explained earlier, charged cosmic ray particles are repeatedly scattered in the chaotic interstellar magnetic fields and as a result the distribution of arrival directions is expected to be highly isotropic. This is indeed what is found, however a small anisotropy at the  $10^{-3}$  level has been observed by IceTop and IceCube. Over recent years IceCube has accumulated one of the largest cosmic ray data sets at TeV to PeV energies which has allowed a detailed study of the morphology, energy dependence and time stability of the anisotropy in the southern sky. Before the IceCube measurements high-statistics results in the TeV range were only available in the Northern Hemisphere. These measurements showed that most of the power is in low multipoles there are small scale, few degree anisotropies on the order of  $10^{-5}$  to  $10^{-4}$ . The anisotropy has been measured to be energy dependent with the most prominent anisotropy observed in the IceCube data below 50 TeV. The IceCube results are in general agreement with Northern Hemisphere results. The source of the cosmic ray anisotropy remains unknown. Although a small dipole is predicted from diffusion theory from discrete sources but the observed morphology is more complex than simple diffusion models suggest.

## 3.2 IceTop as a Veto

IceTop can detect particles at the surface from the same air showers associated with in-ice detections of the cosmic ray muons and neutrinos which are background to the search for astrophysical neutrinos. Tagging these background events through their air shower imprint on the IceTop array can be a means to identify and remove the background. A schematic showing the use of IceTop as a veto for identifying background events is shown in fig. 3.1.

Unfortunately the geometrical overlap of IceTop and IceCube is small, which limits the technique but it is still useful to use the information available from IceTop if it gives improvements in sample size or signal purity. The

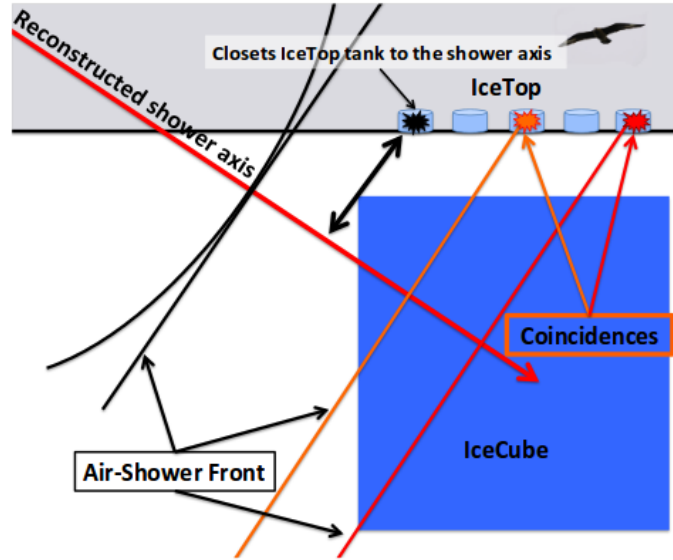


Figure 3.1: IceTop veto strategy for the IceCube observatory. Figure taken from [44].

proposed future extended array mentioned in section 2.8 will have better veto possibilities and strengthens the motivation for investigation into the details of how a surface veto could be implemented.

Further to an overall motivation to increase signal events through incorporating a surface veto, particular motivation is given as a surface veto allows improved access into detecting astrophysical neutrinos which enter IceCube from above, that is from the southern sky. As the cosmic-ray induced background enters the in-ice array from above, analyses remove most, if not all, down going events which will include any astrophysical neutrinos from the southern sky. The fact that the galactic centre is in the southern sky provides additional interest in enhancing the sensitivity for astrophysical neutrinos from this direction. Another motivating factor for improving sensitivity for downward going neutrinos is the fact that at primary energies above hundred of TeV the Earth starts to become opaque to neutrinos due to the increasing cross section for interaction with energy.

It should also be noted that in many cases, filter criteria which are based on identifying cosmic ray muons will not only reduce the rate of muon back-

ground in a sample, but will also reduce the down-going atmospheric neutrino events present. This is because atmospheric neutrinos are accompanied by muons which activate the veto criteria meaning that the atmospheric neutrino events will also be removed from the sample. This effect has been studied for active in-ice vetoes [45–47] and would also need to be quantified for surface vetoes for a full analysis.

### 3.3 Other IceTop Veto Work

Information from IceTop has been used in various IceCube analyses. For example the HESE analyses [33, 34] have looked for accompanying hits in the IceTop array for all of the events which passed the selection criteria, and in the three-year analysis found that two events did have evidence for an accompanying cosmic-ray air shower in IceTop [34].

The most substantial work that is going on to incorporate IceTop into an astrophysical neutrino analysis with IceCube is that of Delia Tosi which is ongoing. The most recent description of Tosi’s analysis approach is given in [48]. Tosi is focused on high energy and very downward going track events where IceTop has optimal veto capabilities and hopes to improve acceptance of down-going muon neutrinos that interact in the volume between IceTop and IceCube. Such a track event is excluded by current analyses like the starting track analysis, and is lost in the background of down-going muons. Tosi’s analysis is based on events which are captured by the EHE filter mentioned in section 2.3. The selection is refined first by selecting only events which are reconstructed within  $32^\circ$  of vertical and have threshold values of track length in the inice part of IceCube and distance of the extrapolated surface intercept of the shower from the perimeter of IceCube. The threshold values are currently set at 800m and 62.5m respectively but have not yet been optimised. Tosi then uses a likelihood method where each event is given a score expressing its likelihood to be signal or background. The likelihood calculation is based on three parameters: the charge measured in each IceTop tank, the residual time (the difference between recorded and expected time) for each IceTop hit and the perpendicular lateral distance from the shower axis of the hit tanks. The perpendicular lateral distance from the shower axis and the expected arrival time of the shower at the tank, are calculated



by extrapolating the muon track to the surface and using a data-derived model for the curvature of the shower front. As mentioned above Tosi's approach is motivated by wanting to capture a particular angular range of track events which are hard to obtain with any other analysis strategy. The analysis described in this thesis, on the other hand, is motivated by wanting to add IceTop information into the existing cascade analysis strategy, aiming to obtain a combination of more signal and better signal purity. The use of traditional cascade variables in our analysis strategy is quite distinct from Tosi's approach which relies mostly on the IceTop information to determine the distinction between signal and background.

The initial plan for the use of IceTop as a veto in the analysis was to take the event information obtained from the sensors in the ice to predict the signal on the surface. The in-ice event information from the light distribution for each event in the detector was to be used to predict the cosmic ray zenith angle, energy and surface intercept of the cosmic ray source. This information was necessary to be used in the simulation code to predict the IceTop response and determine the likelihood that a tank is hit and compare this with the measured hits. However as it is shown in section 3.6 it was not possible to predict the primary cosmic ray energy based on the in ice energy. Another issue with using the cascade selection to predict the properties of the primary was the limited angular resolution of cascade type events which is explained in section 5.2.2. Therefore, this plan was not used in my analysis and just direction and timing information in ice were applied in the analysis.

### **3.4 Simulation of Cosmic Ray Air Showers on IceTop**

In section 2.4 the CORSIKA code, which is used to generate the muon background for the inice component of IceCube, was introduced. There was no joint IceCube-InIce and IceTop CORSIKA simulation which was suitable to be used for the research projects undertaken for this thesis. Instead an alternative code was used to investigate the veto potential of the IceTop array. This code was developed first by Sebastian Euler and later by members of the University of Canterbury IceCube group. It uses parameterisations of the cosmic ray air shower content to estimate the response of a surface detector

array to an air shower. In this section, the code, which will be referred to as the parameterisation code, will be described, along with studies undertaken to assess its suitability. In the remaining sections of this chapter, studies evaluating IceTop and an extended array’s veto capabilities, will be described along with studies to investigate how the code might be implemented into an IceCube neutrino search.

The parameterisation code developed by Sebastian Euler takes as input an incident cosmic ray with a specified atomic number, energy, zenith angle and surface impact point and determines the muon and electron density at user-specified coordinates (usually corresponding to the detector station locations). The muon and electron density are determined using parameterisations of the longitudinal and lateral air shower development. These functions depend on the atmospheric overburden for which an appropriate expression for the South Pole is used. More details of the parameterisation expressions can be found in [49]. The parameterisation expressions are appropriate for a proton primary cosmic ray particle. Primary particles with atomic number greater than 1 are simulated by considering them as a superposition of  $A$  showers each having energy  $E/A$ .

The probability of detecting the air shower particles  $p$  at each detector element is calculated through the product of the effective detector area with the muon and electron density at its location. In most of our use of the code we determine whether an IceTop tank records a hit or not by comparing a randomly generated number with an expression derived from the Poisson fluctuation expression for  $k$  detections. The latter is given by

$$P(k) = \frac{p^k e^{-p}}{k!} \quad (3.1)$$

where  $p$  is the probability mentioned above obtained from the product of the detector area and particle density and the probability of getting at least one detection is given as  $P(1 \text{ or more hits}) = 1 - P(0 \text{ hits}) = 1 - e^{-p}$ . The tank is deemed to have recorded a hit if a random number  $N_{\text{rand}}$ , generated in the interval 0 to 1 satisfies,  $N_{\text{rand}} \leq P(1 \text{ or more hits})$ .

From this description of the parameterisation code one can appreciate the difference between it and CORSIKA; CORSIKA is a Monte-Carlo simulation program where each simulation run from CORSIKA provides a particular realisation of the possible particles arriving at the chosen detector while the

parameterisation code is an average response. By running CORSIKA multiple times a distribution of many possible particle realisations can be built up, including extreme occurrences where for example an unusually high proportion of the initial energy is transferred to a secondary particle. A disadvantage in running CORSIKA is that the individual particle tracking means that the simulation is quite slow to run. In contrast the parameterisation code does not track individual particles but uses the parameterisations mentioned to determine the average density of particles expected at each detector for a cosmic ray of a particular primary energy. One advantage is that the parameterisation code is much quicker to run and also, for the purposes in this thesis project, determining the average expected particle density at the detector stations is more useful compared to a single realisation as would be obtained from a single CORSIKA run.

Euler made a comparison of CORSIKA and the parameterisation code, comparing, for two zenith-angle ranges, the probability as a function of energy for a cosmic ray shower to be vetoed by IceTop. He found very good agreement between the two codes [50]. Below we describe a study that we have undertaken comparing the predictions from the parameterisation code with experimental data.

In most of the studies we have performed in this thesis work we require both IceCube-InIce and IceTop hit information for the events. To obtain this information for the simulated cosmic ray background events we have used a hybrid of CORSIKA and the parameterisation code. Standard IceCube simulation production CORSIKA data sets provide the IceCube-InIce event recordings for muon background. However these production of CORSIKA data sets do not contain any prediction for IceTop hits and to add this information we use the parameterisation code. We use the true primary cosmic ray energy, zenith direction and surface intercept as input to the parameterisation code to predict whether each IceTop tank will register a hit or not for that event. We store separately the IceTop hits due to the muon component of the shower and the electron component of the shower. This is performed with an IceTray module version of the parameterisation code written in C++ by Mark Aartsen.

### 3.4.1 Comparison of parameterisation code with data

In this section we describe a study we have made which compares the parameterisation code prediction for the number of hit IceTop tanks with the number seen in data. We are particularly interested the cosmic ray air shower events which result in hits in IceCube as this is the category of events which we are wanting to veto. For this reason we use data taken with the EHE filter described in section 2.3. The EHE events were chosen rather than cascade filter events as we wanted events with good direction reconstruction. For the simulated prediction we use the hybrid of CORSIKA and the parameterisation code described above, and apply the EHE filter cuts to the simulation data sets. The experimental data was from 2012 with simulation data created using the same detector settings.

This comparison can also be used to get information on how the IceTop veto logic might be applied. One possibility for using the IceTop event information is to take events detected by the IceCube in-ice array, and use the in-ice information to deduce the likely IceTop hits if the candidate event was actually muon background rather than a neutrino event, and compare this prediction with detected IceTop hits.

A number of comparisons between the simulation and data are shown in figs. 3.3 to fig. 3.7. The question we want to address is the accuracy of the number of hit tanks predicted by the parameterisation code for particular characteristics of the primary cosmic ray, for instance energy, zenith angle and surface intercept. As the details of the primary cosmic ray particle are not known for the experimental data we bin both the simulation and experimental data by characteristics which can be derived from their IceCube-InIce event information. We use the MuEx quantity mentioned in section 2.5 as a proxy for the energy of the cosmic ray and use the reconstructed direction of the muon track (reconstructed using the SPE fit routine) to estimate the surface intercept of the air shower<sup>1</sup> Events are binned using their MuEx value and the distance their surface intercept is from the centre of the IceTop array. The latter quantity is referred to as the radius and fig. 3.2 shows the range of radii used in this study in comparison with the IceTop array. Note that given the events are constrained to having passed through IceCube there is some degeneracy between zenith angle and the surface intercept or radius

---

<sup>1</sup>The procedure for deriving the surface intercept is described in chapter 5.

quantity.

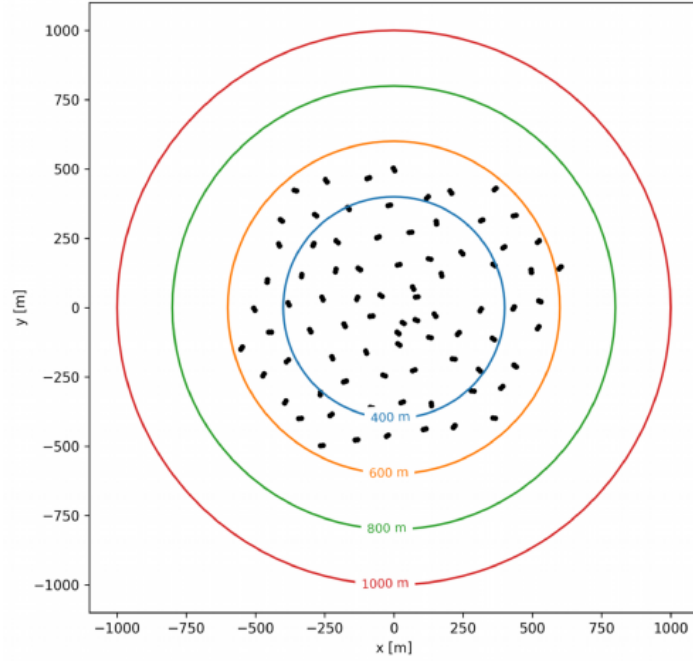


Figure 3.2: Different colour circles show various shower core distances to the centre of the IceTop array. The shower cores themselves are not plotted, but indicate at what range they would appear. Different colour circles show various distances to the centre of the IceTop array. This gives an indication of what shower core distance values can mean in terms of the relative positioning to the IceTop array when the shower core intercepts the surface.

In fig. 3.3 the distribution of the number of hit tanks is shown for events with  $\text{MuEx}$  in the range  $10^{4.5}$  to  $10^5$  and radius in the range 800m to 1000m. In both the left and right panels the orange curve shows the number of hits seen in experimental data, where all hits are counted which fall in a time window of  $(-500\text{ns}, 1500\text{ns})$  window around the reconstructed shower front time. The time window is calculated for each tank individually using the time that the shower front crosses each tank which is based on the reconstructed direction for the air shower (taken as being equal to the reconstructed direction of the muon track in the ice). The blue curves show the number of hit tanks predicted by the parametrisation code; the left panel only includes muon hits and the right panel shows both muon and electron induced hits. These

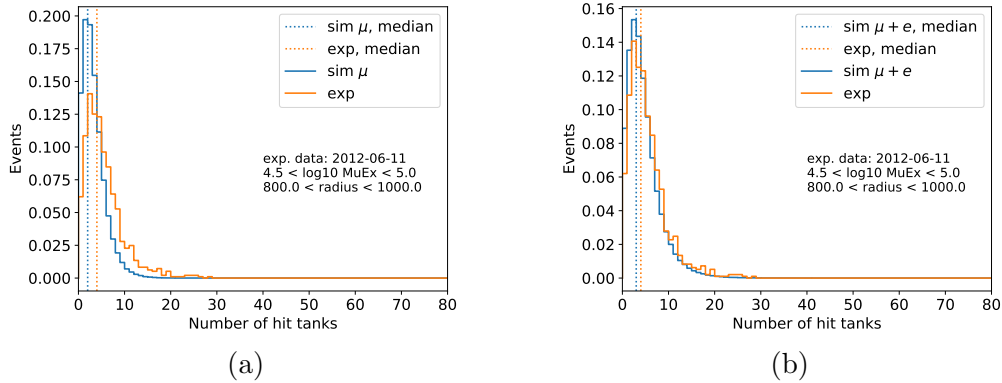


Figure 3.3: In each panel the orange curve is the number of hit tanks in experimental data and the blue curve is the predicted number of IceTop hit tanks from the air shower parametrisation code. Left: Muon hits only and Right: Muon and electron hits. The vertical dashed lines indicate the median points of the distributions.

distributions have been normalised so that the total number of events is 1 and it is therefore the shape of the distributions which is being compared rather than the amplitude. Overall the experimental and simulation distributions look very similar. The experimental data events will also include uncorrelated hits. In chapter 5 we study the background, uncorrelated hit rate in IceTop and see that a randomly chosen 2000ns time window can be expected to have at least one hit tank 40% of the time. Thus we expect to see that the data distribution is shifted somewhat to the right in the plots compared to the simulation data which does not include any uncorrelated hits.

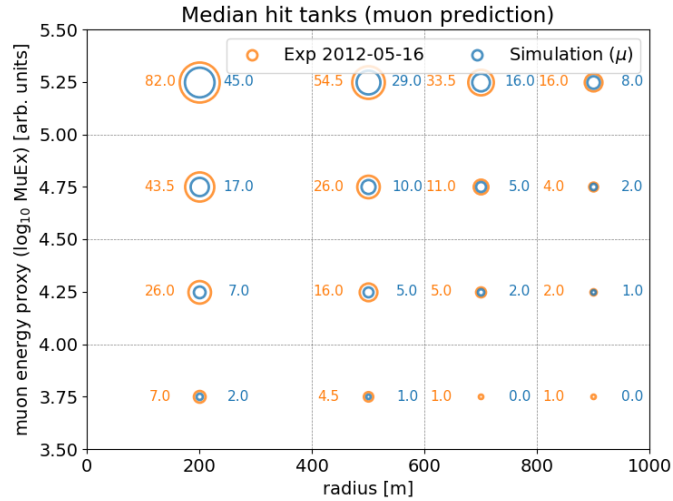


Figure 3.4: Median number of hit tanks over a range of MuEx and radius for experimental (orange) and simulation (blue) data. The area of the circles displayed scales with the median. The simulation prediction includes only muon hits.

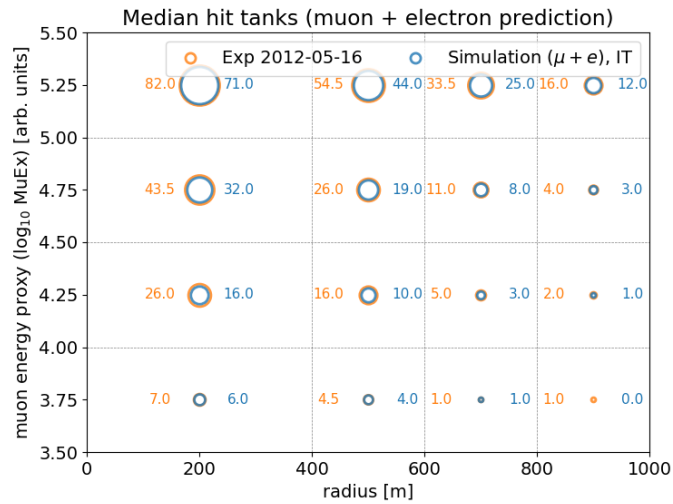


Figure 3.5: Figure similar to fig. 3.4 but with the simulation prediction including both muon and electron hits.

Rather than showing distributions such as that fig. 3.3 in all of the MuEx and radius intervals studied, we show instead in fig. 3.4 and fig. 3.5, the median in each interval allowing a more informative comparison the full range of MuEx and radius studied. The area of the circles scales with the median number of hit tanks for the particular MuEx and radius range indicated on the  $y$  and  $x$  axes respectively. The orange circle areas represent the median numbers in the experimental data and the blue circle areas represent the median numbers for the simulation data. Fig 3.4 show the simulation prediction made with the muon hits only and fig. 3.5 shows the simulation prediction including both both muon and electron hits.

In general terms, one can see in fig. 3.4 and fig. 3.5 that, as expected, the higher energy and smaller radius events have the higher number of hit tanks. This as expected as for the small radius events it is likely that the air shower core, with the greatest density of particles, will impact the IceTop array. fig. 3.4 indicates that if considering only the muon hits in the simulation, that the median number of IceTop hit tanks is underestimated compared to the data. Including the electron hits as in fig. 3.5 improves the agreement between simulation and experimental data. It was anticipated that the electron hits might not contribute as the electromagnetic component of the air shower is more easily attenuated by snow cover on the IceTop tanks<sup>2</sup> and snow attenuation is not included in the parameterisation code. This could be studied further by making a similar comparison study for years later than 2012. The muon hit rate is expected to be reasonably stable and an annual decrease could be modeled to understand better the magnitudes of each hit component. It could also be the case that the parameterisation expressions of the muon density used in the code underestimate the muon component. Several cosmic ray detectors have reported an excess of muons in air showers compared to the expectations from simulations [51–53] and it would be useful to check the muon profiles in the parameterisation code with the most recent IceTop measurements of the muon lateral development function [54]. In any case for our current purpose of preliminary investigations into the use of an IceTop, or extended surface array, veto the general agreement between the code and the data is sufficient. A full IceTop veto implementation, however, would require a careful calibration of simulation estimates with the actual

---

<sup>2</sup>Although the IceTop tanks were installed on the surface, snowfall in the subsequent years means that they are now buried by snow. The IceTop event rate decreases each year which is due to the snow cover



IceTop detection efficiency.

### 3.5 Scope of IceTop as a veto

In this section we describe the results of two studies undertaken to investigate the capability of IceTop to act as a veto for background events in IceCube. The first study was performed by a member of our group, Kiran Munawar, as part of her MSc thesis research [55]. Munawar used the parameterisation code described in the previous section to investigate the number of tanks that were hit as a function of energy, angle of inclined cosmic rays and surface intercept distance (radius quantity in previous section). The results are shown in the heat plots in fig. 3.6. The colour shading indicates the probability that there will be two or more tanks with only the muon density contributing. Each plot is for a different energy primary cosmic ray ranging from  $10^2$  TeV to  $10^5$  TeV, and the probability is shown as a function of zenith angle and surface intercept distance or radius. The basic shapes which can be seen in the plots are a consequence of the geometry required for the shower front to intercept IceTop; for small radii where the surface intercept is within the array boundaries, vertical showers are the most favourable orientation, while the further intercept is from the array boundary the more inclined the shower needs to be for the shower front to impact the array. The plots should be close to symmetrical and the deviations from symmetry indicate a lack of statistics in these plot. It can be seen that for the  $10^2$  TeV shower only the most vertical and close showers have any significant change to be detected, while at  $10^5$  TeV most showers within 2000m of the array centre will be detected by two or more tanks. The probabilities for the intermediate energies link these possibilities with a greater than 70 % probability of two hit tanks for most zenith angles with radii less than 600 at  $10^3$  TeV, while at  $10^4$  TeV this probability is maintained out to radii of 1000m or more.

Fig 3.7 shows the results of a similar study where we have also investigated the potential of the IceVeto extended array introduced in section 2.8. In this study we also investigated the veto efficiency as a function of energy and surface intercept distance or radius but rather than sampling uniformly in these variable spaces we have considered CORSIKA simulations of air shower background events which have been detected in IceCube and examine the

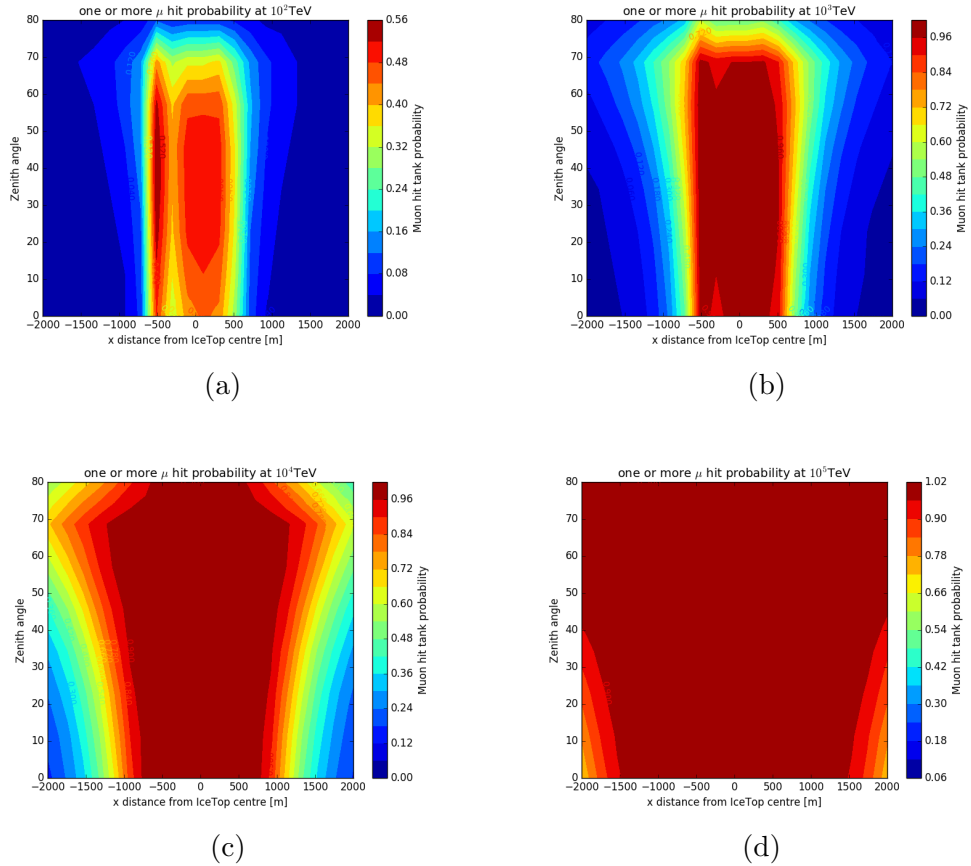


Figure 3.6: Numbers on the colour bar show the probability of getting one or more muon hits. Colours show the change in probability from high (red) to low (blue).

proportion of these events which would be vetoed. The veto condition in this study was two hit tanks with muon and electron densities both included in the hit tank assessment.  $3.2 \text{ m}^2$  panels were assumed for the extended array. The results are shown as a function of the MuEx and radius quantities. While there is not a direct relation between MuEx and the primary cosmic ray particle energy, referring to our study described in the next section and the results displayed in fig. 3.9 it can be seen that the MuEx range in fig. 3.7 relates typically to primary energies in the range  $10^2 \text{ TeV}$  to  $10^5 \text{ TeV}$ . The area of the circles in fig. 3.7 scales with the veto efficiency for the extended array shown in red and the existing IceTop array in blue. Once again it can

be seen that, as expected, high-energy, close showers have the best efficiency to be vetoed and at the highest energies investigated the extended array had nearly 50 % efficiency out to 10000 m where IceTop’s veto efficiency is only 25 % . The extended array also extends significantly the veto efficiency for lower energy events with 30 % efficiency still possible in the  $10^3$  TeV primary energy range (  $\text{MuEx} \sim 10^4$  ) out to radii of 4000m.

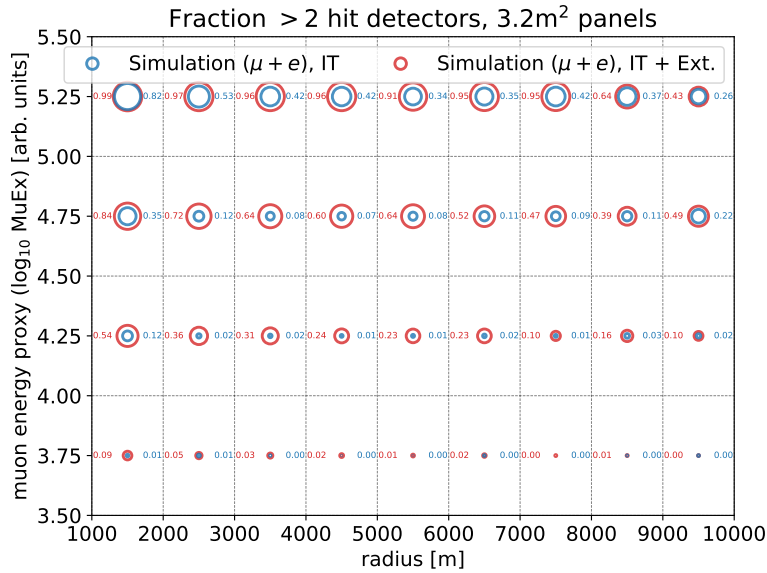


Figure 3.7: Vetoing event fraction, condition: 2 hit detectors. Blue IceTop veto only. Red IceTop + IceVeto extended array.

In the next chapter we investigate the potential for the IceTop veto to enhance background rejection in a cascade analysis where many background events have already been removed through the cascade filter strategy.

### 3.6 Relationship between in-ice event energy estimates and primary particle energy

In the last section of this chapter we investigate the relationship between primary cosmic ray energy and the energy quantities which can be derived

from the in-ice event information. These studies were performed as part of our investigation into possible approaches for implementing the IceTop veto.

One possibility is to use the parameterisation code to determine the likelihood that IceTop tanks are hit for a given event observed in IceCube and to compare this with the observed tank hit number. In order to do this we would need all the inputs that are needed for the parameterisation code. That is the cosmic ray primary energy, surface intercept and direction and these parameters would need to be estimated from the event's characteristics in the ice. The energy of the primary cosmic ray is the quantity which will suffer from the large variability due to the quantum nature of the air showers given that the same cosmic ray energy can result in many different possibilities for the air shower and in-ice muon energies. This is coupled with the uncertainties involved in determining the energy of the muons from the amount and pattern of Cherenkov light detected.

We can characterise the variability using CORSIKA background simulation events. For a given primary particle energy the distribution of variables such as MuEx or other reconstructed quantities depends on the filter conditions which have been applied to the data. As our aim is to implement the veto within a cascade analysis for our first comparison we used CORSIKA background simulation events which had been subjected to the same filter cuts as the sample that we would be applying the veto criteria to. We checked how correlated primary energy is with any reconstructed quantity that we could use. Our second comparison was using the EHE sample and gave us a best-case scenario' result. We did our study with the Credo energy quantity (see section 2.5) and MuEx.

Fig 3.8 shows the 2D histogram of the simulation results for the background sample which has been subjected to typical cascade filter constraints including removing coincident events and constraining the event vertex to be not too far outside the detector edge<sup>3</sup>. The vertical axis of the histogram is the primary cosmic ray energy and the horizontal axis is an estimate of the energy of the particles passing through the detector. The number given in each box shows the number of events falling within that box.

---

<sup>3</sup>The specific filter conditions are cascades with *acerenergy* > 10000, *CredoFitposition* < 500, *topoSplit* = 1, *I3XY scale* < 1.2 and extended icetopCut.

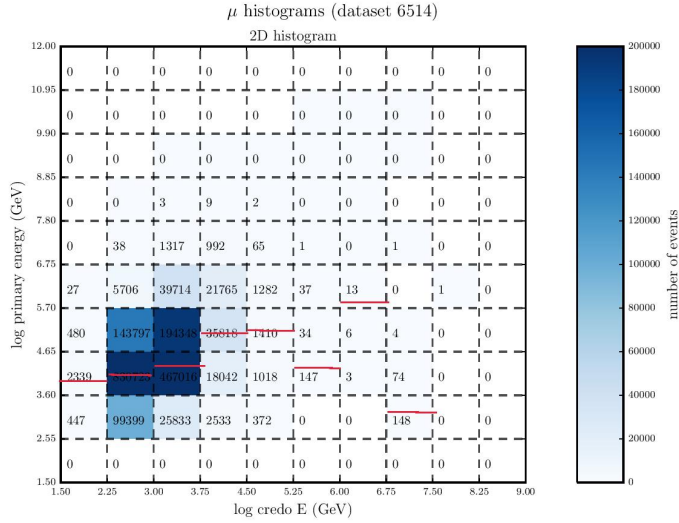


Figure 3.8: Two-dimensional histogram showing the distribution of primary cosmic ray energies against reconstructed credo energies. Numbers are the number of events falling in each bin. The red horizontal lines show median values of the primary cosmic ray energy for a given credo energy. This plot was produced from CORSIKA dataset 6514 with cascade filtering applied.

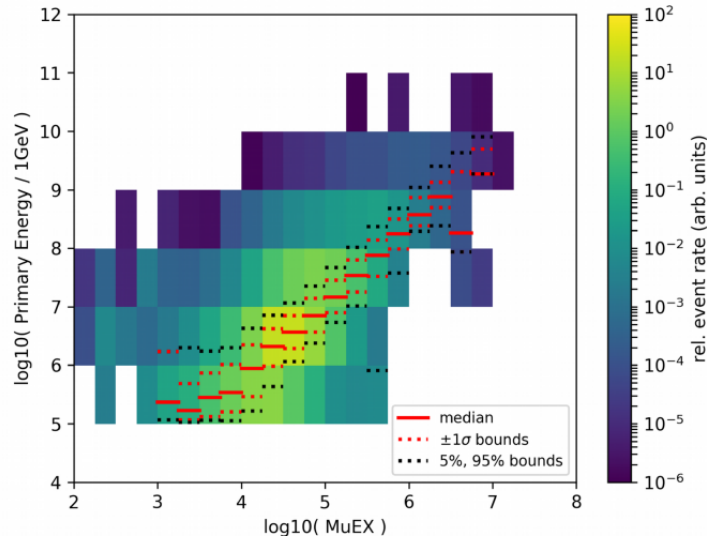


Figure 3.9: The relation between cosmic ray energy and MuEx. The median energy of the primary particle is represented by the red solid line.

A plot of MuEx versus primary particle energy is shown in fig. 3.9. This is produced using CORSIKA simulations. This CORSIKA simulation was subjected to the same filtering process as the EHE sample. As can be seen from the spread in blue shading a given MuEx value result from a spread of primary particle energies. The median primary energy is shown in red and the first and second standard deviations are shown by the dashed lines. It can be seen that for a given MuEx 90% of primary particle energies lies within a reasonably narrow range.

As expected both fig. 3.8 and fig. 3.9 show a spread in primary particle energies for a given reconstructed quantity. The distribution illustrated in the figures could be used within a likelihood veto method relating the number of hits predicted in a surface array with the number of events seen. However in this preliminary investigation we decided to take a simpler approach with a decision to veto events based on the number of IceTop hits seen within a time-window around the expected shower front time at each IceTop tank. The parameterisation code was not used in the veto criteria for the data applied in the remaining chapters of this thesis, but was used to estimate the veto performance on background simulation. The likelihood approach could be pursued in future implementations of the veto.

## Chapter 4

# Incorporating an IceTop veto into a Cascade Analysis

In previous chapters the air shower parametrization code was used to investigate the possible performance of an IceTop veto for removing cosmic ray events as a function of the cosmic ray angle, energy and surface intercepts. In this chapter the potential for the improvement from using an IceTop veto in a cascade analysis is studied. As explained in section 2.3 various different strategies are used to obtain neutrino samples and this thesis is particularly concerned with the cascade analysis strategy. We now investigate the performance of the IceTop veto on a sample of background events which has already been reduced by cuts aimed at selecting events with properties typical of neutrino induced cascade events.

We are interested in how much further background can be removed from the IceCube data stream after the data has already been filtered through the standard cascade criteria. In addition, we are interested in the feasibility of relaxing some of the standard cascade criteria and replacing them with the IceTop veto. The motivation for this is that neutrino signal events are also removed by some of the filter requirements and so relaxing some of the requirements may allow a higher proportion of signal events to be retained.

As explained in section 2.3 it is useful to separate cascade events which are completely in the detector and the ones which are partially within IceCube,

with the events belonging to either the contained or the uncontained sample. These two samples can be analysed separately. The contained sample still contains a large number of background events as the string spacing means that it is possible for muons to enter the inner part of IceCube without being detected on the outer strings. However it will have a lower proportion of background than the uncontained sample meaning that different filtering criteria are appropriate for the contained and uncontained samples. The performance of the IceTop veto is studied separately for the contained and uncontained samples. It is found that there is no additional gain in using the IceTop veto with the contained event selection but there is potential for gain with the uncontained cascade analysis.

We first briefly describe the standard cascade filtering steps before describing the effect of incorporating the IceTop veto. A detailed description of the relevant contained and uncontained cascade analysis steps can be found in Achim Stoessel's PhD thesis [56]. The studies performed on this chapter were applied to IC79 background samples as these were the samples used in the cascade analyses described in [56].

## 4.1 Initial Cascade Filtering Levels

IceCube data filtering is traditionally performed in stages which are referred to as levels. The first filtering levels are conservative and aimed to reduce the amount of background events so that it is feasible to run more computationally expensive algorithms.

As explained in chapter 2, before any filtering on the data transferred to the Northern Hemisphere is applied, a general processing called level 2 is run on all events. This is followed by level 3, where the data stream is split into sub-streams, and events which do not satisfy the relevant quality criteria are removed from the stream. Data at level 3 processing is reduced by about 2 orders of magnitude compared to the level 2 data stream. Cascade specific reconstruction algorithms are mainly part of L3 processing. There are 18 Cascade Variables calculated, like depth of the first hit (the  $z$  position in metres of the first hit DOM), maxDomChargeOM (the OM number of the DOM with the most charge) and earliest Layer (the horizontal layer with the earliest hit in it), which are used as statistics for discriminating signal and



background.

In the cascade samples used in this thesis, only single events are retained. By single events, it is meant events where there is no evidence of two or more coincident events as determined by the Topological Splitter module. The Topological Splitter module searches for sub-patterns which are causally connected in an event and splits the event into the sub-patterns. The number of splits is also stored for each event. Two pulses are causally connected, if their distance in time and space is compatible with the hypothesis that a particle moving with the speed of light could cause the pulses.

For consistency checks between the contained and uncontained samples, the two separate samples are optimized separately with different selection criteria. Both a low and a high-energy sample are obtained for the contained analysis and only a high-energy sample for the uncontained analysis. To define the high energy branch in the Cascade Level 3 filter a routine called Acer is used which was introduced in section 2.5.

### 4.1.1 Containment criterion

The various reconstruction routines mentioned in section 2.5 can be used to estimate the vertex for each event. Events for which the reconstructed CredoFit vertex is beyond the detector, or where the DOM with the largest charge is on one of the outer strings are classified as uncontained events and the rest are contained events. In fig. 4.1 the definitions of the  $x - y$  plane layers in IceCube are shown with the layers defined by the string number. The further in from the edge strings we are, the more contained the event, and the smaller the layer number. The defined horizontal layers go from 0 at the core to outermost strings. Layer 5 is the outer most layer which is the boundary used to define containment.

However this containment criteria can be inefficient in extremely dusty regions of the ice. For example consider a muon that enters the detector in a very dusty region so that the light by the muon as it enters the detector is absorbed before detection on any DOMs, and the first light which is seen is in the central part of the detector. Such a muon event would be included in the contained sample. A way to counter this is to include in the containment criteria conditions excluding events where the first light observed is close to

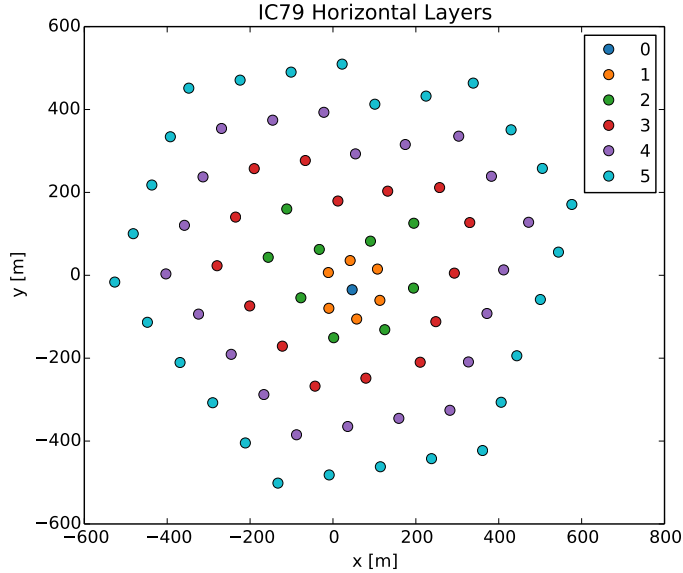


Figure 4.1: IceCube layers in Horizontal plane. This is used to define the events inside the detector or the ones partially contained.

the dust regions.

Further containment criteria were applied within the contained analysis with depth dependent  $z$  restriction for the event vertex only applied later in the filter sequence.

## 4.2 Contained Event Selection

The contained analysis criteria used in this study were optimised by Mariola Lesiak-Bzdak [57] for both atmospheric and astrophysical analyses of IC79. The first set of cuts are summarised in section 4.2. The first five variables used are collectively referred to as Preliminary Level 4. The subsequent three cuts were applied for the astrophysical branch with a cut on energy two further position-based cuts added in order to have a full containment at this cut level.

Events with vertices at the top and bottom of the detector are more likely to

Level	Cut Label	Cut Value	Description
Prel L4	TopoSplits	TopoSplits ==1	Select events with only one subevent found by Topological-Splitter
Prel L4	NString	NString $\geq$ 4	Select events seen by 4 or more strings (calculated from HLC pulses)
Prel L4	DepthFirstHit	-430 < DepthFirstHit < 430	Select events with the first hit (HLC+SLC) between -430 meters and 430 meters.
Prel L4	EarliestLayer	EarliestLayer $\leq$ 4	Retain only the events which have the first hit on inner or middle layer
Prel L4	MaxChargeOM	58 $\geq$ MaxChargeOM $\geq$ 8	Cut away events where the maximum charge was seen by 7 top most DOMs .
	log10(CredoEnergy)	log10(CredoEnergy) > 10 TeV	This analysis is aimed at searching for high-energy cascades (above $\sim$ 20 TeV) and with this cut we reject lower energy events dominated by atmospheric background
	CredoPosZ	-450 < CredoPosZ < 450	Select events with the reconstructed vertex between -450 m and 450 m
	PolygonCr1it	PolygonCr1it	Remove uncontained events for Credo 1it vertex .

Table 4.1: Summary of Level4 selection criteria applied in the contained analysis [57]

be background. Therefore we require that we reject events with credo position  $z$  above and below 450 meters. In addition it is found that background can be reduced if cuts based on the depth of the DOM which observed the most charge is applied. We find that there is a substantial reduction in the atmospheric muon background when considering events with an index corresponding to the top of the detector. In order to remove these background events, the DOM with maximum charge was required to have an index of 8 or below, which corresponds to requiring the DOM with maximum charge to be below 120 meters ( $7 \times 17$  m DOM spacing on a string) of the top of the In-Ice detector. In addition we also require that the maximum charge DOM is not one of the lowest two DOMs on a string.

### 4.3 Uncontained Event Selection

Here we discuss the uncontained event filtering, which differs from contained events. This filtering strategy was developed by Achim Stoessel [56].

An energy cut is applied as the Monte Carlo simulation shows a large drop in statistics for cosmic ray primaries with energies smaller than 30 TeV per nucleon. Therefore it is required that the reconstructed energy to be larger than 10 TeV given that the background modelling is inaccurate for lower energy events. A large suppression of background muons due to the steeply falling atmospheric muon spectrum is an effect of this condition.

The ice is less clear in the top region of the detector, and thus reconstruction performance is relatively poor, so the reconstructed  $z$ -position of the vertex, calculated by single iterative CREDO fit (1-fold iterative reconstructions) performed at level 3, is used to remove the region above the instrumented volume of IceCube. A fiducial volume and a very simple quality criterion is required because cascades which have their vertices outside the instrumented volume of IceCube can only be detected up to a certain distance. The individual DOMs need to register a certain amount of photoelectrons in order for reconstructions algorithms to effectively reconstruct the event. As the light intensity decreases with the distance from the event vertex for cascades, not taking into account scattering and absorption in the ice it prohibits to go further out than about 500 - 800 m.

Vertices which are large distances from the IceCube footprint are likely to have unreliable reconstructions. Two cuts on the scaling variable (I3XYScale) and on L3Credo vertex  $z$  are applied to remove these events. I3Scale is part of the project phys-services. The “I3Scale” parameter, is for a given vertex, the factor by which the original IceCube geometry (defined by its geometric volume) has to be scaled to such a size that the vertex lies on the edge of the scaled detector. This variable indicates if the reconstructed vertex of an event might be contained. Its value is less than 1 if the detector geometry needs to be shrunk to contain the reconstructed vertex and is greater than 1 if the detector geometry needs to be expanded to contain the reconstructed vertex. This variable can be split into its  $XY$  and  $Z$  components, however only its  $XY$  component is used here. So I3XYScale describes the factor by which the polygon spanned by the IceCube geometry in the  $XY$  plane has to be scaled so that the reconstructed vertex lies on the edge of that polygon.

Events which have triggered less than 120 optical modules are removed from the data. The reason for this is that the number of active channels or DOMs with observed pulses can be used as an energy proxy. The variable NChannel yields small values for low energy events, or for events which are outside the detector, or for muon tracks with only a few, dim catastrophic energy losses. Besides rejecting low energy background events this variable varies largely with the position of the interaction vertex and so it serves as an estimate of event quality. This is especially important, as for vertices at the edge of the instrumented volume the hit pattern might look different than the patterns some of the selection criteria algorithms were optimized for. Thus requiring a minimum of active channels ensures that the calculation of such variables yields these differences are getting smaller. After ensuring that events have a good enough quality for the reconstruction of hit-pattern characteristics at level 4, a massive suppression of background happens at the level 5 analysis filter by exploiting the reconstruction results with the aim to separate shower events from mis-reconstructed events. Variables and the motivation of these variables used at this level of cascade analysis are described as follows:

The ratio of Maximum charge to the total charge :  $Q_{Max}/Q_{TOT}$

$Q_{Max}$  is the dom max charge and  $Q_{TOT}$  is the total charge obtained in an event. There are events referred to as balloon events which are mainly tracks of atmospheric muons which pass very close or even through a single DOM and deposit a large amount of charge in that single DOM. Many of the

selection criteria variables might falsely classify these events as a high quality cascade like events and falsely attribute high reconstructed energies to such events especially if the incident muon has a catastrophic energy loss at that position and rest of the track is dim. A variable, which is sensitive to such events is the ratio of the maximum of the observed charges by all active DOMs and the sum of all observe charges. The reason that the total amount of collected charge of all active DOMs is chosen to look at is because it serves as an energy proxy too and enhance a measure of cascade event quality is provided as complementary to number of active channels (DOMs). What this means is if a little amount of light is deposited by an event total charge yields a small number, however NChannel might be large. This might be the case for a cascade far outside the instrumented volume where the registered light is scattered multiple times and thus many DOMs record only few photons, or alternatively for a muon track, which crosses over entire detector, leaving only a few hits in each optical module.

#### SPEFIT:

SPEFIT is the zenith angle obtained using the SPEFIT routine. We want SPEFIT to find things that reconstruct approximately as muons. The algorithm is implemented as a direction reconstruction for muon tracks without energy reconstruction. SPEFIT, short for single photo electron fit, only considers the very first pulse of each DOM. There are CORSIKA background events which might even pass the cascade cuts but have a SPEFIT that reconstructs a roughly right direction, so the events that pass other cuts but have down going tracks might be removed using SPEFIT cut. The CORSIKA events on the top reconstructed as down going are the best targets in this case as IceTop cut can also help to recover part of the signal flux. The distribution of the signal events against  $\cos\theta$  should be uniform, and therefore signal events can be kept by relaxing the SPEFIT cut.

#### TIME SPLIT:

Another topology variable used in analysis is TimeSplitPosition splitting the event in time or in space. Splitting the event in time, each event is split into two halves based on the charge-weighted mean time, and the cascade reconstruction is run on each half separately. The differences between the two sets of individual reconstruction results are calculated. Then, the difference TimeSplitPosition between reconstructed vertex positions for both halves is calculated. For the events consistent with a signal cascade hit pattern

this number has a smaller value than for track-like events and allows the separation of signal and background.

#### CORECORONASPLIT:

Corecoronasplit is a variable which is obtained by the split reconstruction algorithm. It is a split reconstruction algorithm that follows a parametrization based on an estimate of how far the emitted light from the vertex can travel without being scattered. A sphere is defined and pulses are attributed within the sphere and pulses attributed outside the sphere. The vertex displacement is calculated from the vertices found after applying a cascade reconstruction algorithm on the two split pulse series. The vertex is expected to be invariant switching between the two pulse series for the profile of a cascade hypothesis of isotropic light emission.

#### DTNEARLY:

Assuming a point-like light emitter at a given vertex with no scattering, light will travel isotropically with the local speed of light in the ice from this point to the individual sensors and be recorded. If the vertex assumption is correct, no sensor will register hits at times earlier than the direct travel time added to the vertex interaction time. The direct travel time is given by  $t_{geo} = d/C_{ice}$  with  $d$  being the distance between sensor and vertex and  $C_{ice}$  is the speed of light in ice. Calculating the time difference between the first recorded hit and  $t_{geo}$  allows one to identify deviations in the hit pattern from the hypothesis. If the calculated time difference is found to be negative, this indicates that the given vertex position is not accurate. The background rejection power of DTN EARLY is the largest among the variables used to suppress background in the uncontained analysis with no IceTop cut distribution. It is especially useful when large parts of the track remain undetected, e.g. when a muon flies by the instrumented volume, leaving only very few hits of the track in the detector, but a large catastrophic energy loss. In these cases, often times DTN EARLY is the only variable classifying these events correctly.

## 4.4 IceTop Veto and the Contained Sample

In order to investigate whether an IceTop veto can remove any of the background events remaining after the data has been filtered through the con-

Cut Label	Cut Value
TensorOfInertia Eigenvalueratio	> 0.1
SPEFit4 zenith	< 0.25
CoronasplitDT	> -400
TimeSplitDT	< 550
DTNearly with Credo Vertex	> -70
Qmax(DOM)/Qtot	< 0.3
TimeSplitDR	< 75
magnet	< 0.1
Monopod4FillratioRMS	> 0.5

Table 4.2: Summary of the Level 5 selection criteria applied in the uncontained analysis [56]

tained cascade selection criteria we started by applying the IceTop veto to CORSIKA simulation events (6514 set) which had been taken to the *preL4* stage. The *preL4* criteria are given in section 4.2. Three further variables of Credo energy, Credo position and PolygonCr1it are added to preL4 to give the full level 4 filtering sequence. For each cosmic-ray event in the simulation sample we assessed the number of hits expected on the IceTop array using the parameterisation code described in section 3.4. The parameterisation code requires the cosmic ray energy, zenith direction, and surface intercept for which we used the true values from the original CORSIKA simulation. Given the charge and muon density expected at each tank’s location, the Poisson fluctuation expression described in section 3.4 was used to determine whether a tank registered a hit or not. An event was deemed to be cut by the IceTop veto if two or more IceTop tanks received hits. In this study there was no timing requirement implemented on these hits.

From fig. 4.2 we can see the ratio of the number events before and after the application of the IceTop veto is close to one showing that there is little to be gained from applying the IceTop cut on top of the preL4 stage. We wanted to investigate whether there could be a gain in applying the IceTop veto at an earlier stage where it could possibly be used to compensate for relaxing one of the cascade filter criteria which might allow greater signal retention. To be conservative we started from the L3 stage with the containment condition (shown in fig. 4.3) and checked the influence of adding the IceTop cut after each of the cut variables was individually applied. For instance fig. 4.4 shows the level of background reduction when earliestLayer



cut is added to containment criteria and fig. 4.5 shows the effect of veto cut on simulated background after both containment and maxDomChargeOM cuts are applied to the L3 cut sample. Among those after adding the IceTop veto to MaxDomOmCharge we saw that a very small number of events were reduced which means that it might be possible to relax MaxDomOmCharge and add IceTop veto cut instead to get rid of the events that was previously removed by MaxDomOmCharge.

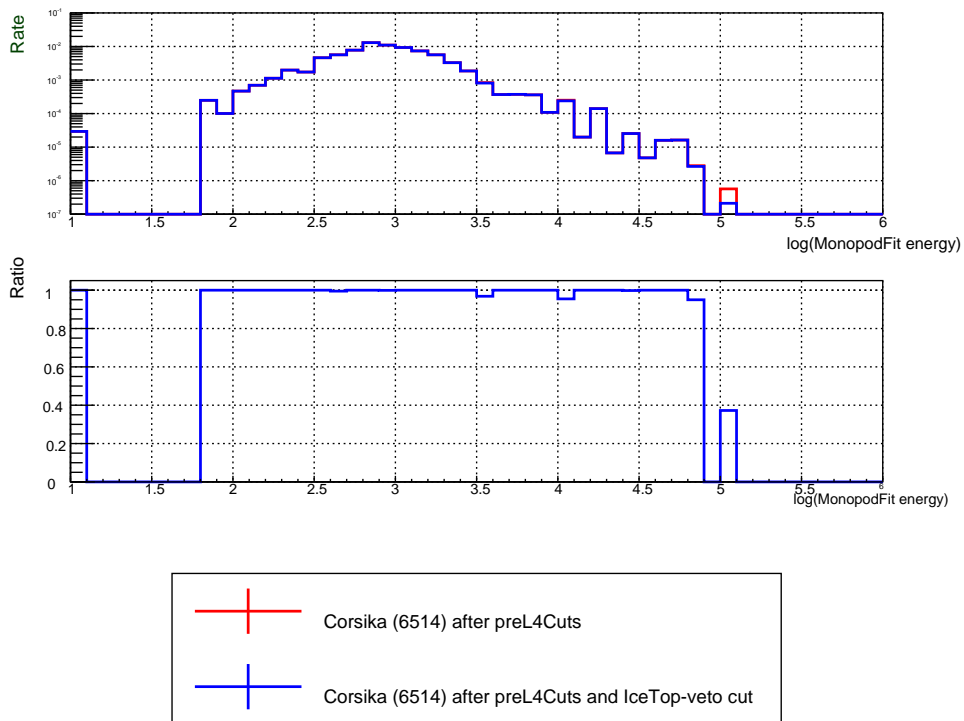


Figure 4.2: Rate of events as a function of energy. The veto cut has been made on simulated background at the level of preliminary\_L4 cut.

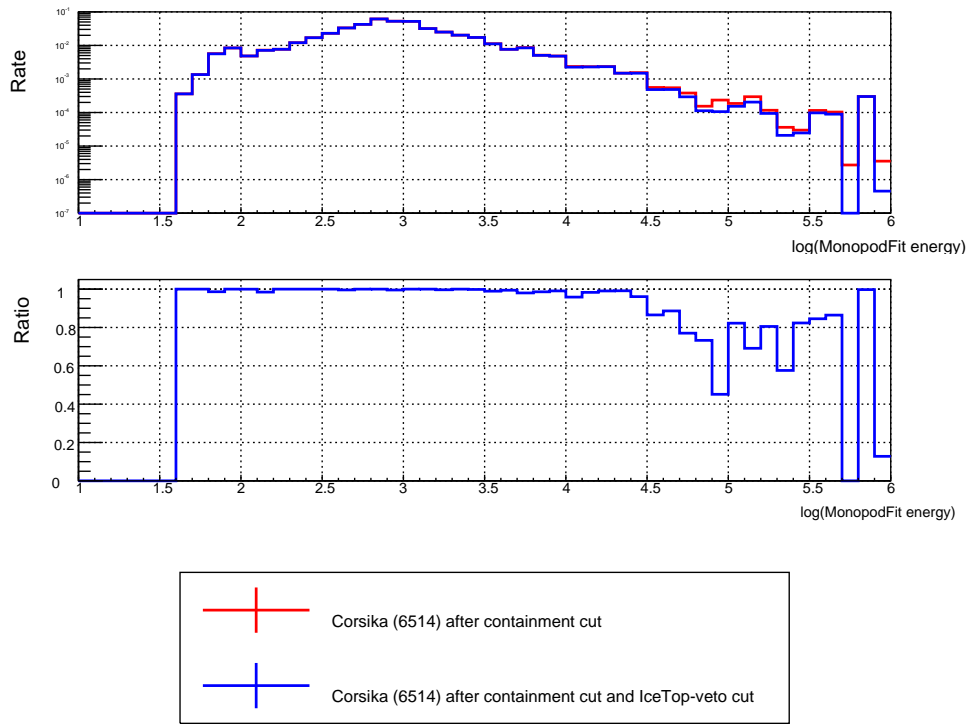


Figure 4.3: Rate of events as a function of energy. The veto cut has been made on simulated background after containment cut is applied to the L3 cut sample.

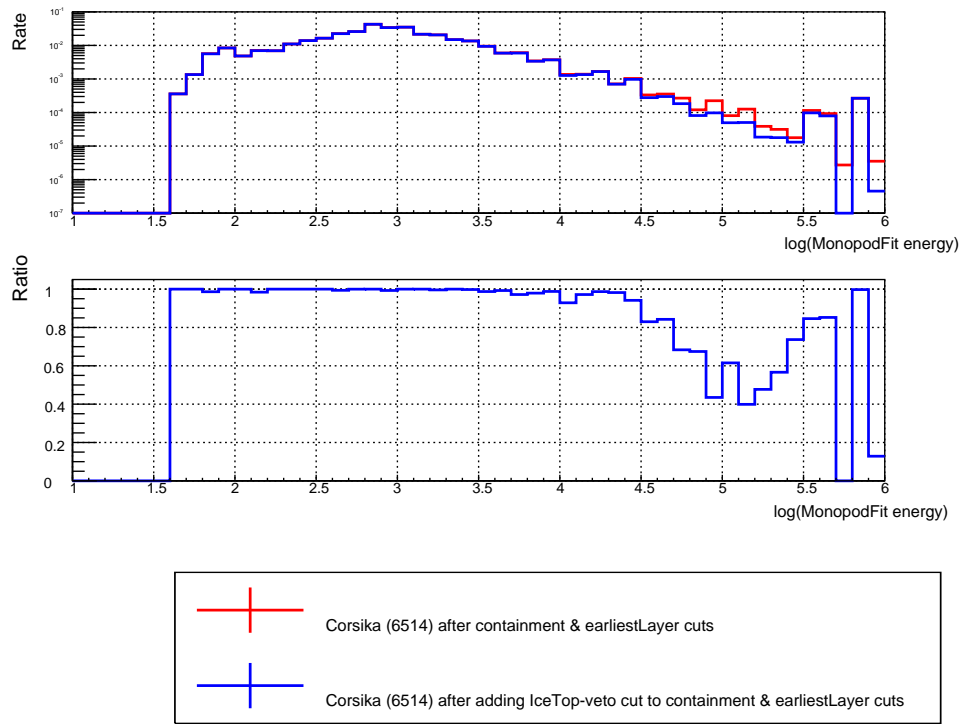


Figure 4.4: Rate of events as a function of energy. The veto cut has been made on simulated background after both containment and earliestLayer cuts are applied to the L3 cut sample.

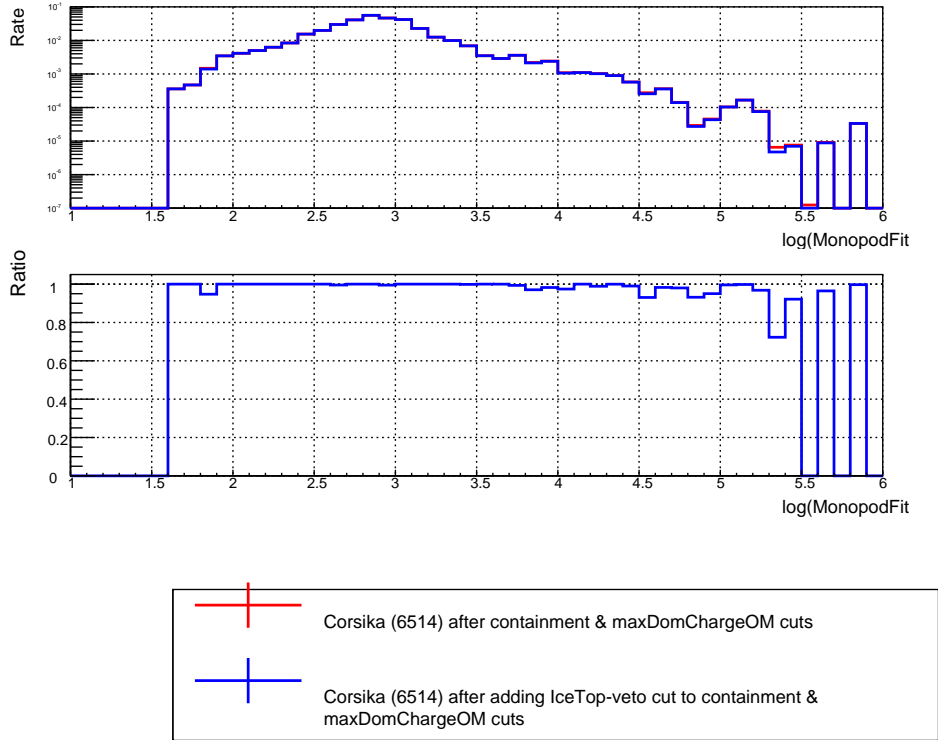


Figure 4.5: Rate of events as a function of energy. The veto cut has been made on simulated background after both containment and maxDomChargeOM cuts are applied to the L3 cut sample.

From this study we see that it might be possible to replace the MaxDomCharge cut with the IceTop veto cut. However before this decision can be made we also have to compare the amount of signal which is reduced by each of the possibilities. We used a nugen sample and compared the survival rate of signal event after all of the cascade cuts, except the MaxDomCharge cut, had been applied and then with the additional MaxDomCharge cut. The results of this study are shown in fig. 4.6.

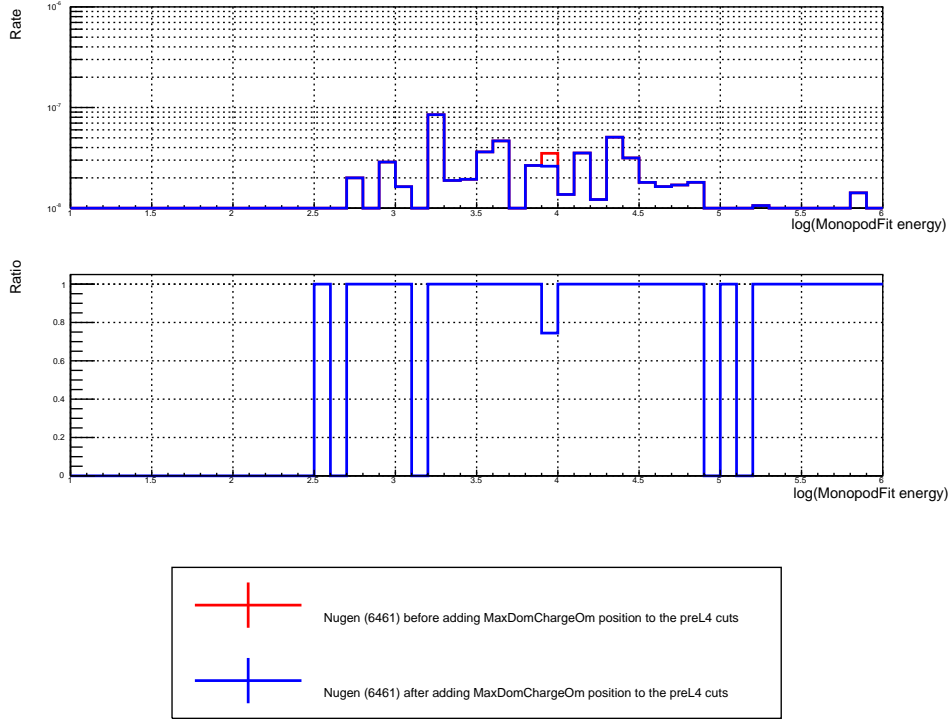


Figure 4.6: Signals before and after adding MaxDomChargeOm position to the preL4 cuts

It can be seen from fig. 4.6 that the MaxDomCharge cut removed very little additional signal which means that there is nothing to be gained with replacing this cut with the IceTop veto.

From the study of incorporating IceTop veto on the contained cascade sample, it was determined that there is nothing to be gained from applying the IceTop veto on contained sample because the cascade cuts remove all the same backgrounds that the veto could access with the remaining backgrounds outside of the range that IceTop veto can remove. Although the contained analysis doesn't benefit from the current surface veto, the extended array might catch the backgrounds which were not accessible by the current IceTop array.

Cut Level	Rate, no veto	+ IceTop cut	+ Extended surface array
L4_uncontained	0.014256	0.014106	0.012732
L4_uncon+Spe	0.000431	0.000428	0.000404
L4_uncon+qratio	0.013485	0.013342	0.012033
L4_uncon+magnet	0.011698	0.011593	0.010527
L4_uncon+ts(dr)	0.011492	0.011389	0.010620
L4_uncon+toi	0.014166	0.014017	0.012646
L4_uncon+fillratio	0.003609	0.003531	0.002882
L4_uncon+DTN	0.000284	0.000282	0.000239
L4_uncon+ tt	0.002545	0.002519	0.002132
L4_uncon + corona	0.003201	0.003146	0.002623
L5	0.000017	0.000017	0.000017

Table 4.3: Background reduction with IceTop and extended IceTop array.

## 4.5 IceTop Veto and the Uncontained Sample

In this section we investigate the potential for the IceTop veto to remove background for an uncontained cascade filter strategy. Again we examine the effect on reducing the background and also if there is utility in relaxing existing cuts values with aim of retaining more signal.

As for the contained sample we applied the IceTop veto to CORSIKA simulation events which had been processed to the Level 5 stage of the uncontained cascade analysis. For this study we determined the number of hits on the IceTop array using the Poisson fluctuation expression used with the shower particle density evaluated at each IceTop tank as described in section 3.4. We found that there was little change in the background rate if the IceTop filter was applied at level 5. The level 5 criteria are given in table 4.2. We investigated whether any of the Level 5 criteria could be replaced with the IceTop veto by taking the Level 4 processed data and examining the rate after applying each individual Level 5 cut, and also the background rate with each cut and also the IceTop veto cut. The results from this study are shown in table 4.3. The final line of the table gives the background rate at Level 5. In this table we also evaluate the potential of the extended surface array to remove background events in the third column. In addition we examined the removal of signal events by each of the Level 5 uncontained cut criteria and the results of this study are displayed in table 4.4.

Cut Level	Rate
L4_uncontained	79.878580
L4_uncon+Spe	54.427418
L4_uncon+qratio	74.965957
L4_uncon+magnet	76.999932
L4_uncon+ts(dr)	78.272953
L4_uncon+toi	79.805480
L4_uncon+fillratio	70.182136
L4_uncon+DTN	66.990518
L4_uncon+ tt	69.834602
L4_uncon + corona	73.577774
L5	32.257518

Table 4.4: In this table the reduction in signal rate is shown as a function of cut variable

It can be seen in table 4.4 that the SPE variable removes the most signal events. The SPE variable is the reconstructed incoming direction, or zenith angle, reconstructed with the SPEfit routine. The cut removes all events which have a cosine of this angle which is greater than 0.25. This motivates relaxing the SPE variable with the aim of replacing its background removal with that of the IceTop veto. As the IceTop veto should be most effective for cosmic ray events which are close to vertically down it was decided to trial keeping events with a zenith angle cosine of 0.9 or greater.

To understand the gain in signal expected with this change we plotted the distribution of signal events, at this level of the uncontained cascade analysis, as a function of zenith angle. We expect signal events to come from all directions equally and so to have a flat distribution as a function of zenith angle. However it can be seen that the signal distribution at Level 5 of the uncontained cascade analysis as shown in fig. 4.7 is not flat. This is presumably because signals coming from above are removed by other cuts already applied to the event sample. While the gain in signal is not as much as hoped for it was decided that it was still sufficient to warrant the change.

Figures 4.8, 4.9 and 4.10 display the results of the effect of applying the IceTop veto cut after the Level 5 uncontained cascade analysis cuts. For the results displayed in fig. 4.8 and fig. 4.10 the reduced zenith angle cut described above has been implemented. The red points show the background rate after

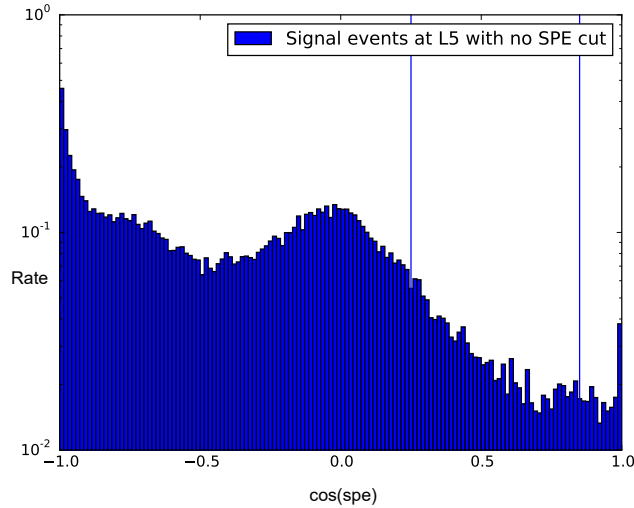


Figure 4.7: Signal distribution against SPE variable.

the uncontained cascade cuts, but before the IceTop veto is applied while the blue points are the background rate once the IceTop veto has been applied. The absence of a blue dot at higher energy levels in fig. 4.9 and fig. 4.10 is because there were no simulated events remaining after the IceTop veto cut had been applied. There is however low statistics available and this is indicated by the length of the blue vertical uncertainty bar. Figure 4.8 displays the event rate as a function of zenith angle, while fig. 4.9 and fig. 4.10 show the event rate as a function of energy. It can be seen from fig. 4.8 that the overall background rate is not diminished greatly with the IceTop veto but from fig. 4.9 and fig. 4.10 we can see that the IceTop veto is effective at higher energies. It appears that the extra background events which were able to pass due to the reduced zenith angle cut have not all been removed by IceTop veto cut. However the fact that the IceTop veto is more effective at higher energies motivates its implementation, and potentially to use the zenith angle cut in an energy dependent manner so only high-energy events from the vertical region are retained as these have a good probability to be removed by the IceTop veto.



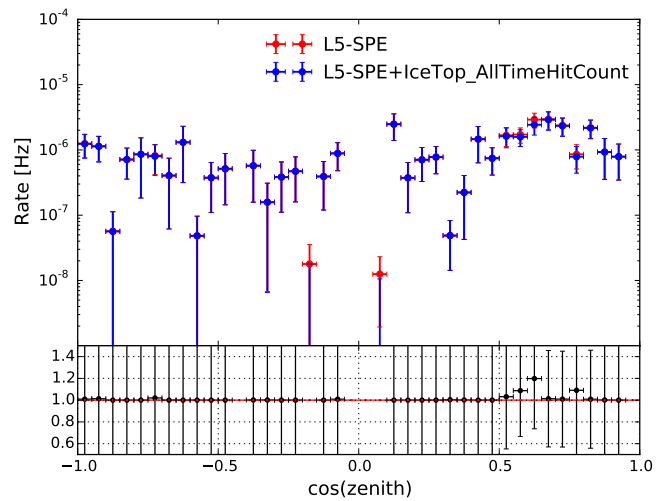


Figure 4.8: Event rate as a function of zenith angle. The red points show the event rate after the modified Level 5 contained cascade cuts. The modified Level 5 contained cuts are the standard contained cuts with the relaxed zenith angle cut as described in the text. The blue points show the event rate after the IceTop veto cut has been imposed (without any time restriction on the hits). The bottom panel is the ratio of the event rates before and after the IceTop veto is applied.

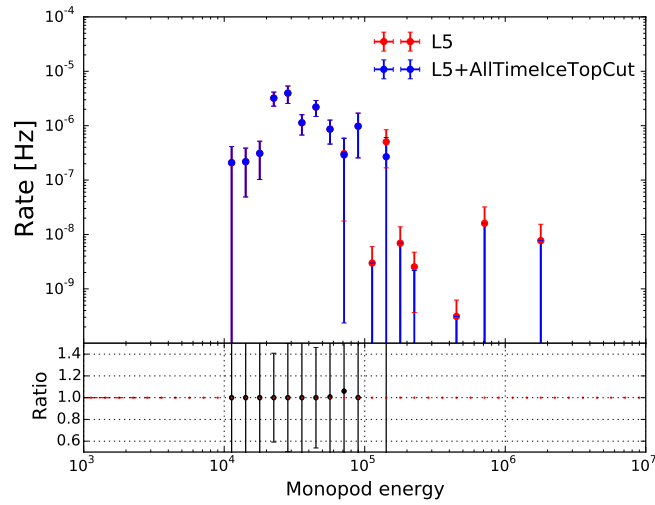


Figure 4.9: Event rate as a function of energy. The red points show the event rate after the uncontained cascade cuts. The blue points show the event rate after the IceTop veto cut has been imposed (without any time restriction on the hits). The bottom panel is the ratio of the event rates before and after the IceTop veto is applied.

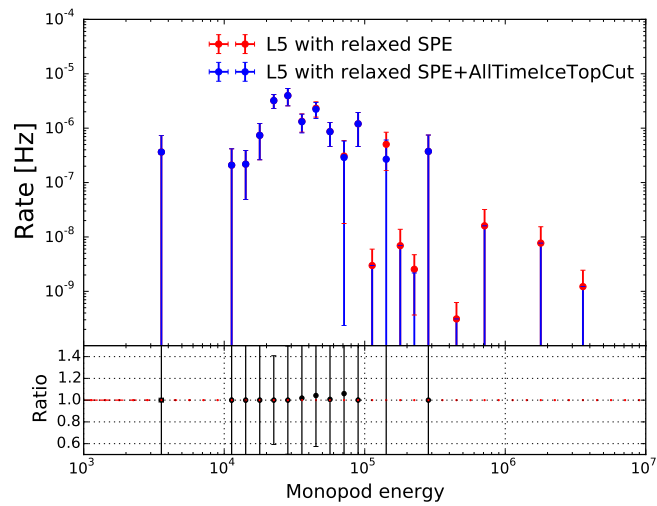


Figure 4.10: Event rate as a function of energy. The red points show the event rate after the modified Level 5 uncontained cascade cuts. The modified Level 5 uncontained cuts are the standard uncontained cuts with the relaxed zenith angle cut as described in the text. The blue points show the event rate after the IceTop veto cut has been imposed (without any time restriction on the hits). The bottom panel is the ratio of the event rates before and after the IceTop veto is applied.

## Chapter 5

# Investigations into a Suitable Time Interval to define Correlated Hits

In this chapter we present various studies performed in order to inform our decision on a suitable time-window to use to define correlated hits in the IceTop data. In the previous chapter we investigated the potential for further background reduction using an IceTop veto within a cascade analysis. Our investigations used simulations of the cosmic ray background. With simulated data there is no ambiguity over associating the IceTop hits with the IceCube-InIce event and the results we presented were based on all the associated IceTop hits being identified. In actual data however a defined time-window is needed to be able to associate the IceCube-InIce and IceTop detected signals. The optimum length of the time-window is a compromise between the risk of removing astrophysical neutrino events due to the time-window containing the chance coincidence of an unrelated air shower event, and the length of time needed to account for the spread in arrival times of associated IceTop hits. For the latter there is an inherent expected spread in times related to the width of the shower front and there are also uncertainties in relating the expected IceTop hit times to the IceCube-InIce hit times due to the uncertainties in the reconstruction direction of the IceCube event.

We start this chapter by describing how we estimate the expected time of hit IceTop tanks from the IceCube-InIce event time and direction. We then describe the studies we have performed to investigate the factors, discussed above, which inform the time-window choice. Included in this description are studies we have made to compare the various reconstruction routine options available for estimating the angular direction of the IceCube-InIce event.

## 5.1 Calculation of the front impact time on IceTop

The relationship between the IceCube-InIce event time and the hit times on IceTop tanks for air shower events is related to the geometry of the event and can be calculated from the IceCube-InIce event vertex coordinates and the reconstruction direction of the air shower. A schematic figure of an example coincident event is showed in fig. 5.1. The IceCube-InIce event in fig. 5.1 is assigned a vertex  $x_0$  and a time  $t_0$  by a reconstruction routine using the IceCube-InIce information. Under the assumption that the event is neutrino-induced, the vertex and time correspond to the estimate of the location and time of the neutrino interaction in the ice. In the case that the event is actually muon background the vertex and time do not actually correspond to any particular interaction but will represent an estimate for a location that the muon passed through at the time that it was at that location. In addition the reconstruction routine will estimate an angular direction for the event which is an estimate for the shower front axis direction when the event is a background event. In fig. 5.1 associated hits in the IceTop array are recorded on stations with coordinates  $x_1$  and  $x_2$  at times  $t_1$  and  $t_2$ . In the example shown in fig. 5.1  $t_1$  will be earlier than  $t_0$  while  $t_2$  will be after  $t_0$ . The relative time offset between  $t_0$  and  $t_1$  and  $t_2$  can be obtained by finding the distances  $d_1$  and  $d_2$  along the shower front axis and using the fact that the shower front moves at speed  $c$ . We define the time offset  $(t_0 - t_i) = d_i/c$ . The relative sign of  $t_0 - t_i$  will be related to the sign of the distance  $d_i$ . The distance  $d_i$ , including its sign can be determined from the dot product of the unit vector in the direction of wave front axis with the vector directed from the event vertex coordinate to the tank coordinate. The latter vectors are labelled as  $l_1$  and  $l_2$  in the diagram. Given  $x_0, t_0$  and the reconstructed

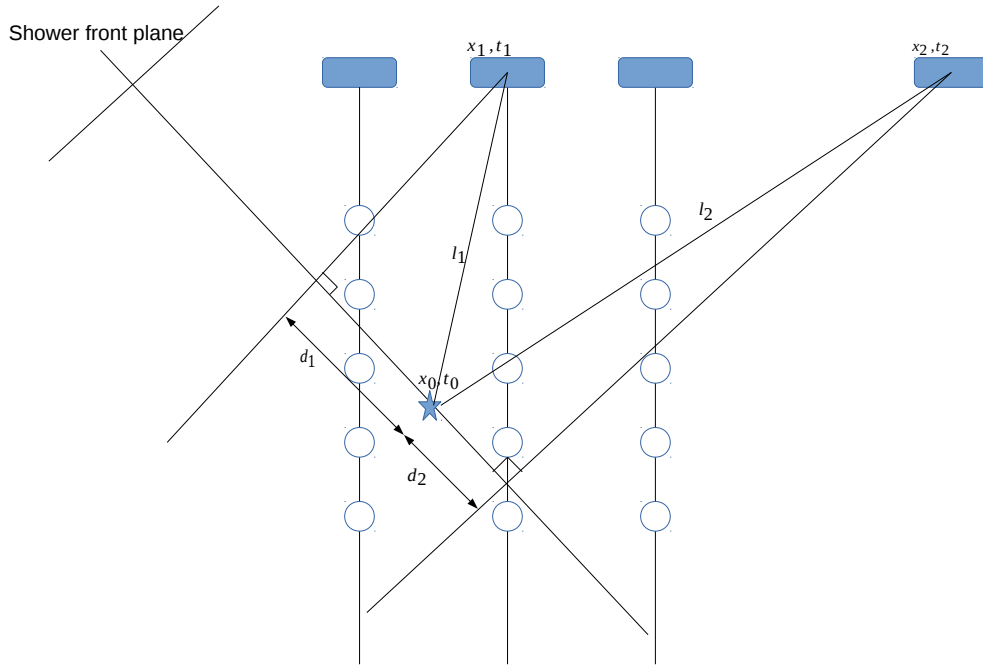


Figure 5.1: An example of an event detected coincidentally in IceCube-InIce and IceTop is displayed. The IceCube-InIce event is assigned a vertex coordinate and event time defining the time difference between an IceTop tank hit time and an event time in the IceCube-InIce array.

direction for an IceCube-InIce event the expected time for associated hits on each IceTop tank can be estimated. There will be some scatter in the recorded IceTop tank hit times so that the actual IceTop hit times will arrive in a time window around this expected time. This scatter is due to the fact that the shower front has some inherent width and also because any difference between the estimated shower front direction and the true shower front direction will result in an error in the estimated tank hit time. In the next section we investigate the expected scatter in tank hit times resulting from these effects.

## 5.2 Time window considerations

To help inform our decision on an appropriate time-window we investigated three factors. First we needed to consider the natural spread in the hit times that arrive. Second, we also needed to know what is the expected angular resolution for cascade-like background events and to find the resulting error in the expected tank hit-time due to the error in the reconstructed cosmic-ray direction. Because we are analysing cascade-like events the direction reconstruction is likely to be worse than unfiltered background. The third factor is to investigate the hit rate on IceTop tanks; the larger we make our time-window the greater the risk that an astrophysical neutrino event will be vetoed because of a chance coincidence of an unrelated air shower event with the neutrino event and we investigated this accidental veto probability as a function of time window size. Each of these factors were investigated with separate studies which are described below.

### 5.2.1 Natural spread

In our first study we investigated the spread in time that hits are seen on IceTop. We expect some spread due to the fact that we have assumed a flat shower front while actually the shower front will be curved and there will also be some longitudinal depth of particles in the air-shower front.

In order to study the correlated hits and time window the in-ice EHE data sample, described first in section 2.3 and also used in section 3.4.1, was used due to the better angular resolution of the track like events so that we can expect that the spread seen is due to the factors mentioned above rather than a misreconstruction of the shower direction. The impact time at each IceTop tank was calculated for an extrapolated shower front using the direction reconstructed from the IceCube-InIce information. For each hit detected on IceTop, the residual time, which is the time difference between the actual time of the hit and the predicted time at the hit tank, was calculated. From fig. 5.2 it can be seen that most of the hits were recorded at the predicted time, and within a few hundred nanoseconds after this time with the histogram is peaked around the zero residual time bin. As mentioned above some of the width of the distribution can be attributed to the curvature of the air shower

front which has been assumed to be flat in our time estimate. There will also be some width to the distribution due to the fact that the shower front is not a thin identity and it has some depth. It is also likely that some of the time residual will also be due to the reconstruction of the direction and vertex differing from their true values but given the EHE events will have better reconstructions for these quantities than the cascade-like events in our study we can take the spread of the distribution in fig. 5.2 as a lower floor for the time window size needed to capture associated hits in IceTop.

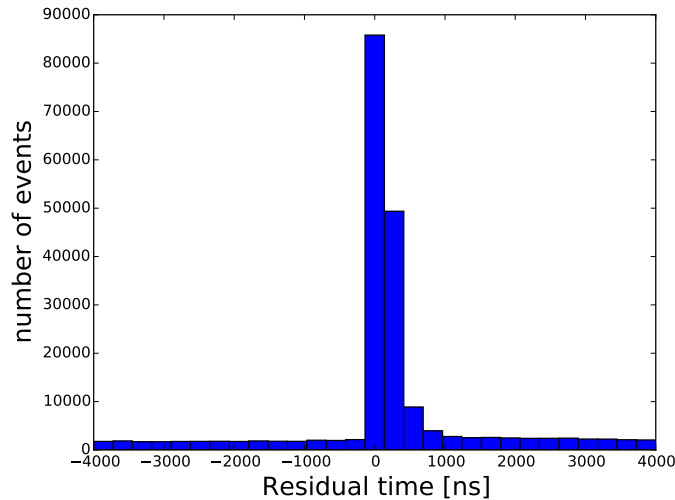


Figure 5.2: Time difference between the actual time of a hit on any IceTop tank and the predicted time at that tank.

### 5.2.2 Angular resolution of the cascades

In general cascade events suffer from poorer angular direction resolution than track events. This poorer angular resolution will impact on our ability to estimate the expected time of IceTop hits associated with IceCube-InIce events. In this section we investigate the angular resolution expected for the events in our sample and the corresponding time resolution in hit times on IceTop tanks.



## Angular resolution of reconstruction routines

There are two main reconstruction routines used for estimating the characteristics of IceCube-InIce events within cascade analyses; SPEFit and MonopodFit. These were introduced in section 2.5. SPEFit is tailored to track events while MonopodFit was developed to be used on cascade events.

We can evaluate the resolution of the routines using CORSIKA simulation data for which the true direction of the cosmic ray is known. We are interested in the resolution at the Level 5 filter stage as this is the sample of events that the IceTop veto will be applied. Figures 5.3 and 5.4 give an indication of the ability of the two routines to reconstruct the direction of the incoming particle. In each plot the horizontal axis is the reconstructed zenith angle while on the vertical axis is the cosine of the angle between the true direction of the cosmic ray primary and reconstructed direction. This angle is measured in the plane which contains both the true and reconstructed direction vectors and thus includes differences between the reconstructed and true values of both the zenith and azimuth angles. Figures 5.3 and 5.4 were produced using CORSIKA simulation data sets 6514 and 9030 datasets at Level 5 of processing with the cut on SPE zenith removed. The numbers in the boxes indicate the number of events falling in that box without any weighting included in the event numbers. fig. 5.3 is for the MonopodFit reconstruction routine while fig. 5.4 is for the SPEFit reconstruction routine. MonopodFit reconstructs 40% of events to fall in the upper, desired row of the histogram while SPEFit reconstructs 99 % of events to fall in the upper bin of resolution. It should be noted though that with the rather coarse binning the upper row can contain events which are mis-reconstructed by up to nearly  $40^\circ$ .

To study the resolution with a finer binning fig. 5.5 and fig. 5.6 were produced. In this case the upper row corresponds to a resolution of  $12^\circ$  which it will be seen from the studies presented in the next section and the remainder of this section corresponds to the time window which would lead to the false rejection of around 10 % of signal events. We find that 10% of the events are reconstructed within  $12^\circ$  by MonopodFit while 87% of the events are reconstructed within  $12^\circ$  by SPEFit.

It is clear from the studies presented in this subsection that SPEFit performs best for angular reconstruction of the remaining cosmic ray background

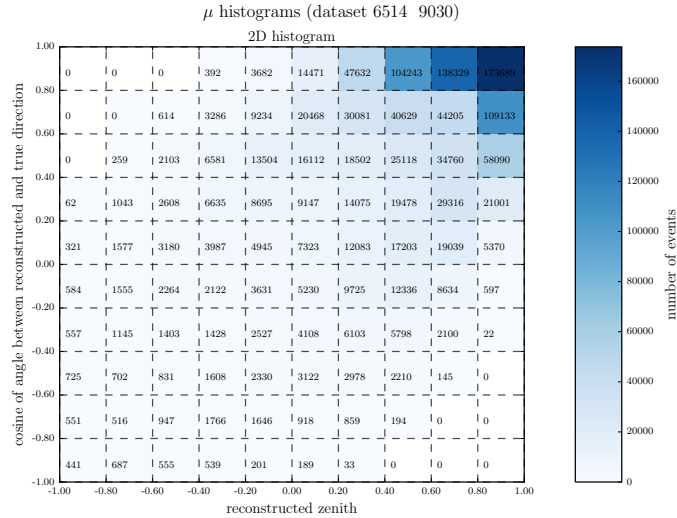


Figure 5.3: Cosine of the angular difference between the cosmic ray shower axis and the reconstructed direction found using MonopodFit. The data is CORSIKA simulations filtered to level 5 of the cascade filtering described in chapter 4.

events at level 5 of the cascade filter.

### Implication of angular resolution for timing

To study the time uncertainty for hit times on IceTop related to the uncertainty in the angular direction we examined the difference in predicted time for a range of directions chosen within a cone around a central incident direction. A cartoon showing the parcel of possible incident direction vectors for a zenith angle of  $15^\circ$  is shown in fig. 5.7.

In fig. 5.8 the resulting hit times from the parcel of incident directions is shown. The horizontal axis displays the tank number for the IceTop array, and each column of small horizontal dash marks shows the distribution of times related to the  $15^\circ$  uncertainty for each particular tank. Given the slight inclination of the central vertex angle, the central times on each tank are not the same and shows the necessity of considering a separate time window for each tank in which to search for associated hits. The vertical spread of time

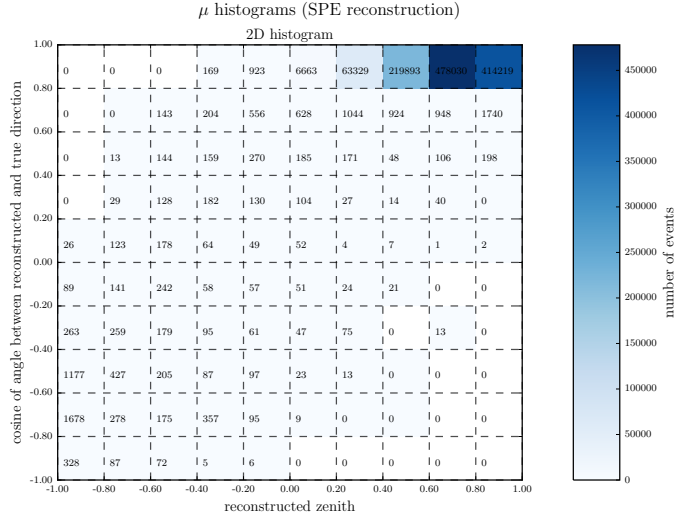


Figure 5.4: Cosine of the angular difference between the cosmic ray shower axis and the reconstructed direction found using SPEFit. The data is CORSIKA simulations filtered to level 5 of the cascade filtering described in chapter 4.

hits indicated the time window size needed to find all associated hits if the true incident direction is displaced by up to  $15^\circ$  from the reconstructed direction. In fig. 5.8 there is typically a spread of around 1000 ns. An uncertainty of  $15^\circ$  is actually quite optimistic as we saw in the previous section that this was only achieved in around 10 % of the event for MonopodFit but up to **87** % of the time for SPEFit.

The spread of the hit times for a given uncertainty depends on the zenith angle with the smallest spread occurring for vertical showers and the largest for horizontal showers. In section 5.2.2 and section 5.2.2 the spread in arrival times are listed for range of central zenith angles. As expected the time spread increases as the central angle as the central zenith angle becomes more horizontal. In these tables the time spread is the range from the earliest to latest hit times calculated with the average taken over all IceTop tanks.

From the tables section 5.2.2 and section 5.2.2 it can be seen that time windows of around 6000 ns would be needed to capture most of the associated hits. It should be noted that here we have been estimating the time spread

Central Zenith Angle	Average Time Spread (ns)
1	2440
5	2540
8	2670
10	2760
15	3010
21	3360
30	3910
40	4480
60	5450
80	5880

Table 5.1: The spread in arrival times arising from a parcel of incident directions distributed in a cone of width  $21^\circ$  around the central zenith angle given. The time spread for each tank is calculated by subtracting the earliest time from the latest time, and the value listed in the table is the average of this quantity over all IceTop tanks.

Central Zenith Angle	Average Time Spread (ns)
1	1410
5	1470
8	1550
10	1600
15	1740
21	1950
30	2270
40	2600
60	3160
80	3410

Table 5.2: Tabulated values are as in section 5.2.2 but with the parcel of incident directions distributed in a cone of width  $12^\circ$ .

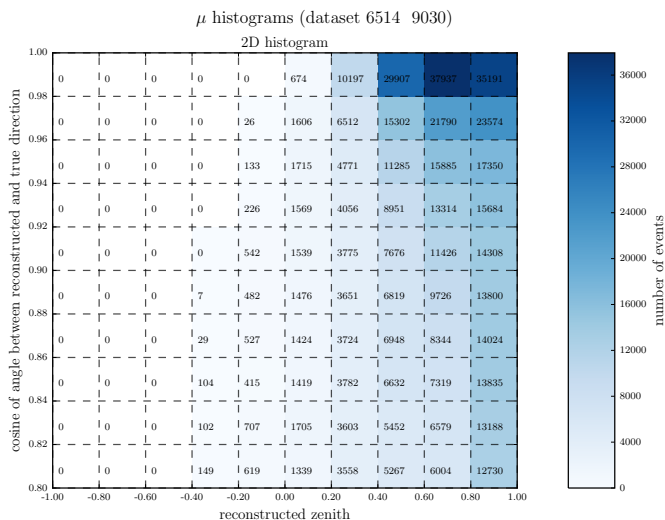


Figure 5.5: This figure shows the same comparison as in fig. 5.3, displaying the reconstruction resolution of MonopodFit, but limited to the best reconstructed events presented with a finer angular resolution binning than in fig. 5.3.

from the uncertainty in the incident angle but there will also be a time difference related to any offset in the vertex associated with the event. It has been assumed that the IceCube-InIce vertex lies on the shower axis but if this is not the case a further difference in the impact time on IceTop tanks will arise.

### 5.2.3 Unwanted removal of signals

In this section we examine the accidental veto rate as a function of time window size. An accidental veto will occur when a neutrino event is vetoed because, by chance, an air shower event resulted in hits on IceTop tanks in the time window around the neutrino event. To examine the accidental veto rate we used the Fixed Rate Trigger data capture. This is an unbiased IceTop hit sample where a stream of IceTop tanks hits are recorded with no specific trigger requirement. This allows us to study typical background rate in IceTop regardless of what is observed in IceCube with a random interval

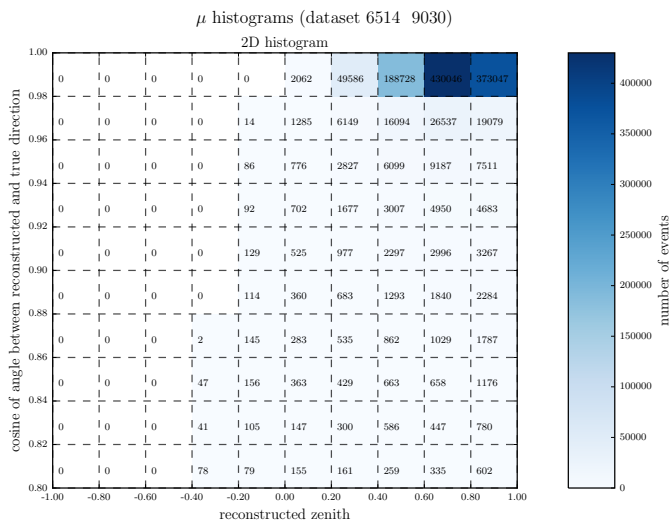


Figure 5.6: As for fig. 5.5 but for SPEFit.

extracted from the Fixed Rate Trigger datastream mimicking what would be detected in IceTop in association with an IceCube astrophysical neutrino event.

We studied the accidental veto rate as a function of time window size and also as a function of the number of hits recorded in IceTop in the time window. The fixed rate trigger data was split into intervals of a particular size and the proportion of such intervals with  $n$  hits was recorded. The results are displayed in tables 5.3 to 5.5. Table 5.3 and 5.4 are for run dates in May 2013 and December 2013 respectively while table 5.5 is for a run date in December 2014. It can be seen that proportion of time intervals with a given number of hits is reasonably stable across the seasons and years studied.

### 5.3 Chapter summary

In this chapter we examined the various factors which affect the decision on the optimal time window size. While a time window of 6000 ns seemed necessary to capture all associated hits given the angular resolution of cascade filtered events (as presented in section 5.2.2) such a large time window would

Nhits	2000 ns	3000 ns	4000 ns	5000 ns
0	0.606	0.473	0.369	0.288
1	0.301	0.350	0.363	0.353
2	0.077	0.133	0.183	0.222
3	0.013	0.035	0.063	0.093
4	0.002	0.007	0.017	0.031
5	0.0003	0.001	0.004	0.009
6	0.0001	0.0003	0.0009	0.002
7	$4.167e^{-05}$	$8.125e^{-05}$	0.0002	0.0005
8	$1.667e^{-05}$	$4.688e^{-05}$	$9.583e^{-05}$	0.0002
9	$1.0417e^{-05}$	$2.188e^{-05}$	$2.083e^{-05}$	$6.25e^{-05}$
10	$1.25e^{-05}$	$2.500e^{-05}$	$3.333e^{-05}$	$5.208e^{-05}$
$\geq 2$	0.09	0.17	0.26	0.35

Table 5.3: This table shows the percentage of time a randomly chosen time window of the given time length contained the number of hits given in the Nhits column. This table is for an unbiased data run taken on the 2013.05.05.

Nhits	2000 ns	3000 ns	4000 ns	5000 ns
0	0.648	0.523	0.422	0.339
1	0.280	0.337	0.361	0.367
2	0.061	0.109	0.156	0.195
3	0.009	0.025	0.047	0.072
4	0.001	0.004	0.011	0.019
5	0.0002	0.001	0.002	0.005
6	0.0001	0.0002	0.0004	0.001
7	$3.571e^{-05}$	$6.429e^{-05}$	0.0001	0.0003
8	$1.428e^{-05}$	$4.286e^{-05}$	$7.143e^{-05}$	0.0001
9	$1.428e^{-05}$	$3.215e^{-05}$	$4.286e^{-05}$	$5.357e^{-05}$
10	$1.428e^{-05}$	$4.286e^{-05}$	$2.857e^{-05}$	$1.786e^{-05}$
$\geq 2$	0.07	0.13	0.21	0.29

Table 5.4: Same as table 5.3 for an unbiased data run taken on the 2013.05.05.

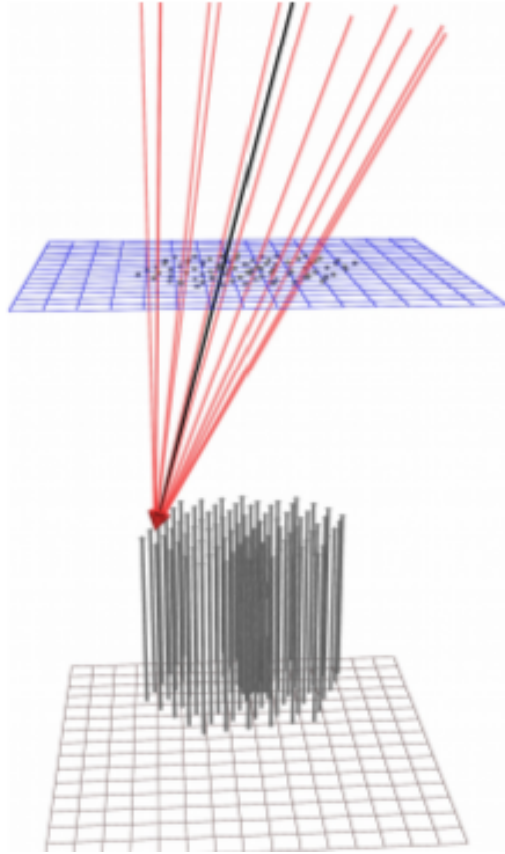


Figure 5.7: This plot is an example of different possible shower planes on the surface array.

remove around 20 % of signal events. The decision on time window size depends on the tolerance for removing signal events versus that of passing background events, and on the specific veto strategy in terms of the number of hits used in the veto criteria. A full optimisation study is needed to determine the optimal time window size and number of hits to use. Due to time constraints this was not undertaken in the preliminary investigation presented in this thesis. Instead we decided to use a time window of 2000 ns guided by our interest in retaining signal. A time window of 2000 ns is expected to remove less than 10 % of signal events. In the next chapter we examine the background rejection which can be achieved using a 2000 ns time window to associate hits in IceTop with in IceCube-InIce. We revisit



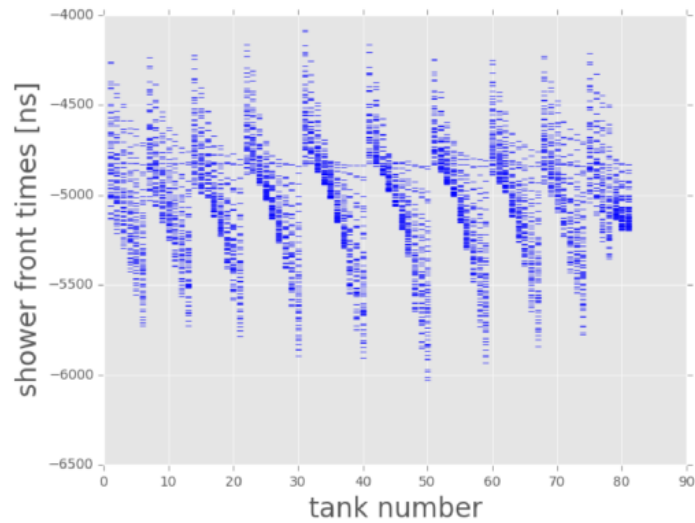


Figure 5.8: The distribution of tank times that could be seen as a result of uncertainty in the reconstructed direction of the cosmic-ray incident direction. The horizontal axis displays the tank number for the IceTop array. Each small horizontal dash marks shows a hit time for one of the possible incident directions tested. incident directions were chosen in a  $15^\circ$  cone around the  $15^\circ$  zenith angle.

the Corsika background data used in chapter 4 and also present results from applying the filtering criteria on a small sample of actual data.

Nhits	2000 ns	3000 ns	4000 ns	5000 ns
0	0.668	0.544	0.446	0.364
1	0.266825	0.331608	0.3577	0.366
2	0.055	0.098	0.144	0.185
3	0.008	0.022	0.0417	0.062
4	0.001	0.001	0.008	0.018
5	0.001	0.0006	0.001	0.004
6	$3.75e^{-05}$	0.0001	0.00055	0.0006
7	$3.75e^{-05}$	$3.75e^{-05}$	0.0001	0.0003
8	$1.25e^{-05}$	$1.875e^{-05}$	$2.5e^{-05}$	$3.125e^{-05}$
9	$2.5e^{-05}$	$1.875e^{-05}$	$7.5e^{-05}$	$6.25e^{-05}$
10	0.0	0.0	0.0	0.0
$\geq 2$	0.06	0.12	0.19	0.26

Table 5.5: Same as table 5.3 for an unbiased data run taken on the 2014.12.31.

## Chapter 6

# Incorporating the time dependent IceTop veto on the uncontained cascade sample

In Chapter 4 the potential for an IceTop veto to identify any remaining background events in a cascade event sample was investigated. It was seen that there was limited potential for further improvement in the contained cascade filtered sample but there was possibility for further background reduction in the uncontained cascade sample. The study in Chapter 4 did not apply any timing constraints on the IceTop hits used in the veto criteria. In this chapter we return to the uncontained cascade event sample and apply the time dependent veto criteria developed in Chapter 5. We apply the time-dependent veto to both a simulated background sample and also to a subset of experimental data. While we find that there is some background rejection potential the limitations of the direction reconstruction mean that the rejection is not as effective as seen in Chapter 4.

## 6.1 IceTop veto with a time window on simulated background

In section 4.5 an IceTop veto cut was applied to simulated background events which had been filtered through the uncontained cascade filter steps up to Level 5. The CORSIKA sets of 6514 and 9030 were used in the study. In addition to applying the IceTop veto on the simulated data, filtered through the standard uncontained cascade steps, we also investigated relaxing the vertex direction cut usually applied, in combination with the IceTop veto cut. The rationale was that the relaxation of the vertex angle cut would allow more signal to be retained and any additional background would be removed by the IceTop veto cut.

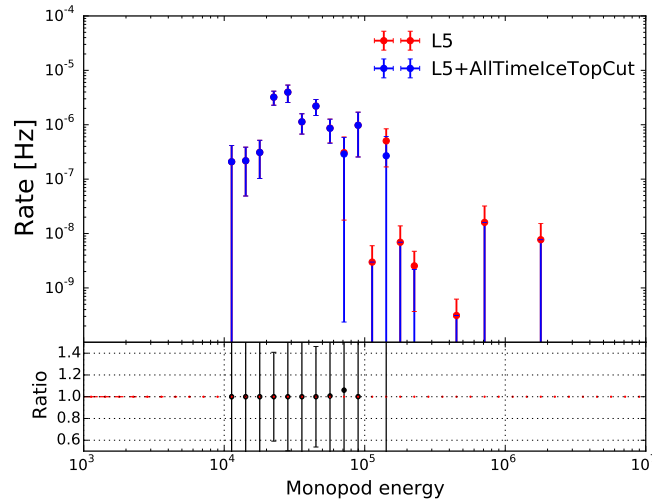


Figure 6.1: Veto potential on CORSIKA level 5 events. This has a lack of statistics due to the limits of the simulation datasets and the effectiveness of the cuts at level 5. The bottom panel is the ratio of the before and after rates. The unit for the Monopod energy is GeV.

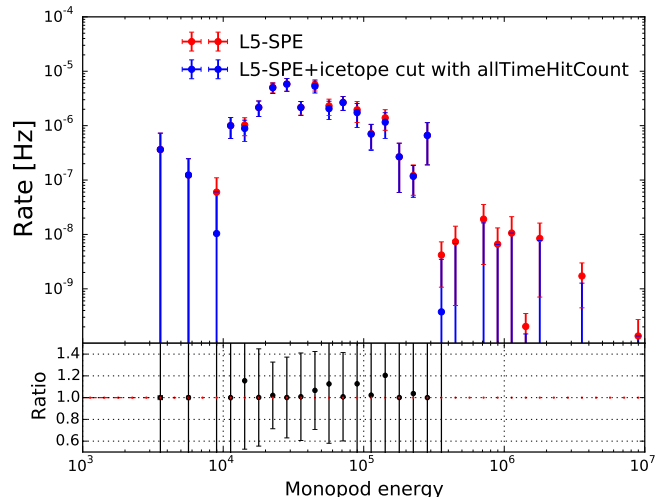


Figure 6.2: Veto potential on CORSIKA level 5 events after relaxing SPE criteria. This has lack of statistics due to the effectiveness of the uncontained cascade cuts. The statistics are increased with the removal/change of the SPE cut criteria. The bottom panel is the ratio of the before and after rates. The unit for the Monopod energy is GeV.

The figures showing how the simulated background was reduced through the IceTop veto cut were given in fig. 4.9 and fig. 4.10 and are repeated here as fig. 6.1 and fig. 6.2 to allow easy comparison. The figures show the background rate as a function of energy. The energy displayed is that found by the Monopod reconstruction routine. The red points show the background rate after the uncontained cascade cuts, but before the IceTop veto is applied while the blue points are the background rate once the IceTop veto has been applied. The absence of a blue dot at higher energy levels is because there were no simulated events remaining after the IceTop veto cut had been applied. There is however low statistics available and this is indicated by the length of the blue vertical uncertainty bar. It can be seen that above 100 TeV the IceTop veto is providing a reduction in background events while there is little reduction in the rate of events with lower energies.

The bottom panel of fig. 6.1 and fig. 6.2, and other figures in this chapter, shows the ratio of unvetoes events to IceTop vetoed events, such that a ratio greater than 1 indicates there has been a reduction in background events

and in the case when there is no events remaining after the IceTop veto application, there is no point showing (as the ratio is infinite)<sup>1</sup>.

The studies described in section 4.5 had no timing restriction applied to the IceTop hits as these were studies on simulated data. However in the experimental context we need to have a time window in order to assess the number of IceTop hits as discussed in the previous chapter. In this section we apply the method for determining a unique time window for each IceTop tank described in chapter 5. As described there, in order to determine the time window, the incoming direction of the cosmic ray is needed. We use three different hypotheses for the incoming direction: the reconstructed direction found by the SPEFit routine and that found by the Monopod routine, and also a vertical proxy, for which we assume the cosmic ray was vertically incident.

The results obtained from applying a 2000 ns time window on simulated background events, for the three hypotheses for the incoming cosmic ray direction, are shown in figures 6.3 to 6.5. Fig. 6.3 displays the results found using the SPEFit reconstruction for the cosmic ray direction, fig. 6.5 using the Monopod reconstruction and fig. 6.4 using the vertical proxy of a vertically incident cosmic ray.

It can be seen through comparison of fig. 6.2 with figures 6.3 to 6.5 that applying the time window results in a reduced veto capability. This is to be expected as the case with no time window was a best case scenario. The difference is due to the error in the reconstructed direction. We can see from the blue points being lower than the red points in the upper plots, and the lower panels displaying some ratios greater than 1 that using the SPEFit reconstruction (figure 6.3) and the Monopod reconstruction (figure 6.5) there is still some level of veto capability, particularly above 100 TeV.

Of the different cases, using the vertical proxy (figure 6.4) vetoes the fewest events. A contributing factor for this is due to the fact that for small zenith angle, the time window is smallest due to the way the time window is constructed.

In section 6.3 we study further the events which had potential to be vetoed

---

<sup>1</sup>It was realised that it would be preferable to plot the inverted ratio of vetoed event rate divided by unvetoed event rate but this was too late for the timescale of the thesis deadlines

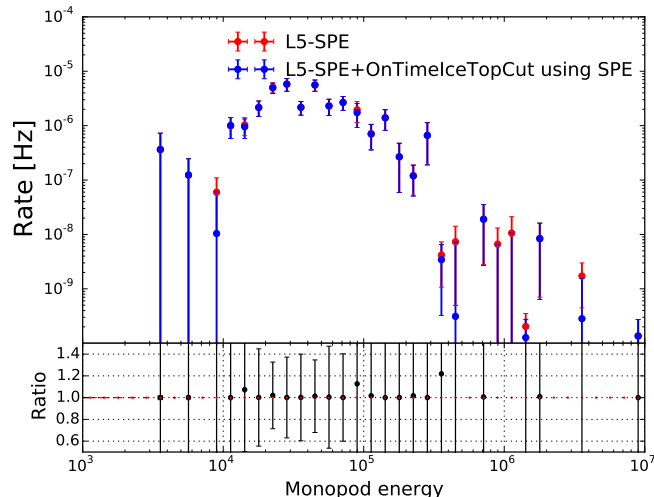


Figure 6.3: Rate of CORSIKA events as a function of energy before and after a cut on IceTop hits within a specific time window. Here, the time window was based on the angle from the SPEFit reconstruction. The bottom panel is the ratio of the before and after rates. The unit for the Monopod energy is GeV.

but were not caught in the time window to see how much in error the reconstruction for the incident cosmic ray direction was from the true simulated incoming direction, and to consider how the veto might be improved.

## 6.2 IceTop veto with a time window on a subset of experimental data

In this section we apply the IceTop veto, as used in the previous section, on a sample of experimental data. We use the burn sample which is a fraction of around 10% of experimental data. The burn sample is used in most IceCube analyses to allow comparison between simulation and experimental data without compromising the analysis procedure which is only applied to the remaining 80 % of the data. We used the subset of experimental data from 2010 which has a livetime of 33.3 days. We used a merged series of re-

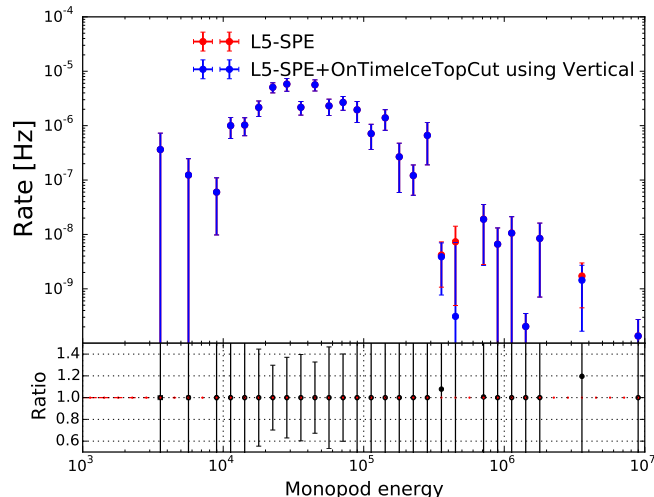


Figure 6.4: Rate of CORSIKA events as a function of energy at L5 and after taking out cuts when timewindow was obtained around the vertex based on vertical proxy for the shower. The bottom panel is the ratio of two quantities. The unit for the Monopod energy is GeV.

constructed pulses for each IceTop tank, merging the series of the two DOMs in the tank. Specifically, the merged series combines the pulses recorded both by a single DOM called Soft Local Coincidence (SLC) pulses, usually the low-gain DOM which records small signals (and therefore more pulses), and the series of both DOMS called Hard Local Coincidence (HLC) pulses, which by definition includes the high-gain DOM which records large signals.

The results obtained from applying a 2000 ns time window on a sample of experimental data, for the three hypotheses for the incoming cosmic ray direction, are shown in figures 6.6, 6.7 and 6.8. Although there could be neutrino signal events present in this sample it is expected that the majority of events in this experimental sample are background events. As in the previous section the red points show the rate after the uncontained Level 5 cuts have been applied and the blue points once the IceTop veto has been applied.

It can be seen from figures 6.6, 6.7 and 6.8 that there was some event reduction in all cases with the most reduction being achieved with the Monopod



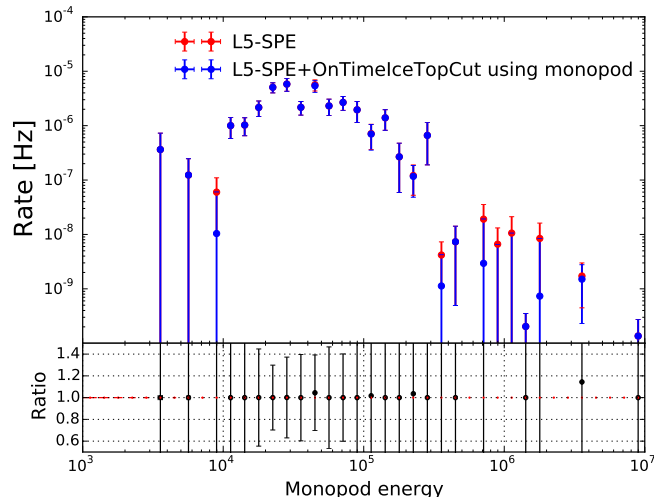


Figure 6.5: Rate of CORSIKA events as a function of energy that remained after taking out cuts when timewindow based on monopod reconstruction was used. The bottom panel is the ratio of the before and after rates.

reconstruction routine but the overall reduction wasn't very good, especially when considering that there each event has a 8% probability of being removed because of the random chance of coincident IceTop hits. It should also be noted that the simulation studies showed that the best potential for the IceTop veto were for energies above 100 TeV but due to the low statistics in the experimental data subset there were very few events in this energy bracket.

Figures 6.6, 6.7 and 6.8 are consistent with the expectation from the previous section where it was recognized that the errors in the direction reconstruction reduced the potential for background reduction. To investigate if any of the experimental data events might have been vetoed with an alternative direction reconstruction we examined individual events from the sample and looked for a clustering of IceTop events offset from the time which was used. Examples of these plots are displayed in fig. 6.9 and fig. 6.10. The black dashed vertical line indicates the time stamp for the InIce event. The red dashed line indicates the time which a vertical shower front would have impacted IceTop relative to this InIce event timestamp. The various IceTop hits are represented by the blue vertical lines. Although it was useful to see

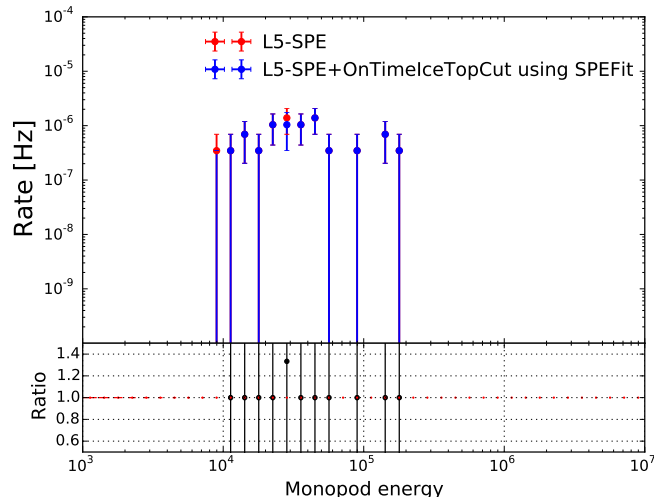


Figure 6.6: Event rate for experimental data, as a function of energy, at Level 5 and after applying an IceTop veto with a time window based on the SPEFit reconstruction for the shower direction. The bottom panel is the ratio of the rates before and after the IceTop veto is applied.

this visualisation, a deeper study is needed to derive any conclusions. For example a study which incorporated the position of the IceTop tanks which received hits comparing the direction of a shower derived from the IceTop hit times with the InIce derived direction could indicate whether the InIce and IceTop hits were related. The number of IceTop hits in an enlarged time window around the InIce event time could be examined and compared with the average number of IceTop hits expected in this time window size.

### 6.3 Potential Improvement of the IceTop Veto

In this section we investigate the reduction in the veto capability between the IceTop veto applied without any time constraint and that with the time window condition applied. As discussed previously the difference in the blue points on fig. 6.2 and those in figures 6.3 to 6.5 is due to the error in the reconstructed direction for the incoming cosmic ray direction.

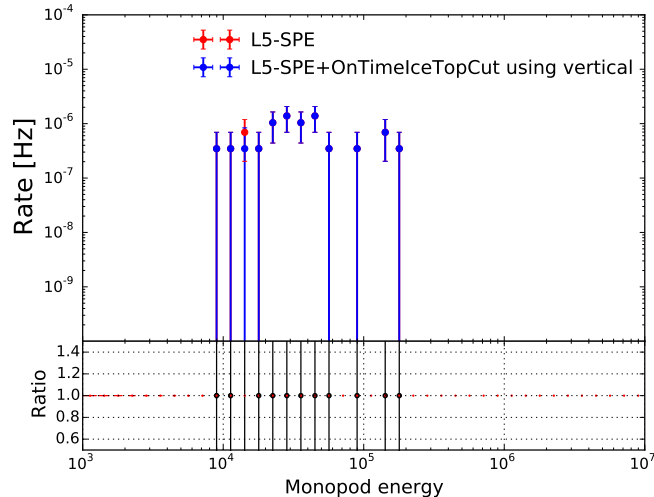


Figure 6.7: Event rate for experimental data, as a function of energy, at Level 5 and after applying an IceTop veto with a time window based on the vertical proxy for the shower direction. The bottom panel is the ratio of the rates before and after the IceTop veto is applied.

Figure 6.11 is a scatter plot showing the events remaining at the relevant filtering stage. The vertical axis is the Cosine of the true zenith angle while the horizontal axis is the Cosine of the solid angle difference between the true and reconstructed zenith angles. Events which are well reconstructed are to the right of the plot with a Cosine value of 1 arising when there is no difference between the reconstructed and veto direction. The scale on the horizontal axis should be noted; 0.9 is the starting value on the axis which corresponds to a reconstruction error of  $25^\circ$ . It is encouraging that the majority of events are clustered on the right-hand side. The green crosses are events which produced less than two hits on IceTop and so cannot be vetoed with any length time window for a two hit condition. The red triangles are events which were rejected by the IceTop veto with two hits within the required 2000 ns time window. The blue circles are events which do have two or more hits but were not vetoed due there not being sufficient hits in the calculated time window. These are the events where there could be improvement in veto capability with improved reconstruction. It is interesting to see that there are red triangles appearing in the left part of fig. 6.11. These are

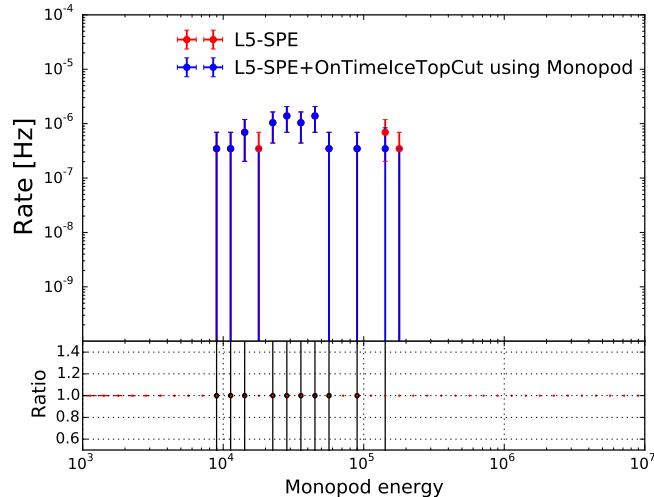


Figure 6.8: Event rate for experimental data, as a function of energy, at Level 5 and after applying an IceTop veto with a time window based on the Monopod reconstruction for the shower direction. The bottom panel is the ratio of the rates before and after the IceTop veto is applied.

events which have rather poor reconstruction but are still able to be vetoed. Given the similar distributions of red triangles and blue circles there doesn't appear to be a particular correlation between the reconstruction error and the probability for the event to be vetoed by the IceTop veto with a time window.

One possibility for countering the reconstruction uncertainty is to increase the size of the time-window and the number of hits required from two to three. In fig. 6.12 we investigate the amount of background which could be rejected if three or more hits were required to be registered on IceTop. There is no time window restriction applied in fig. 6.12.

It can be seen by the presence of blue points lying below red points in fig. 6.12 that there are events that have three or more hits. In section 5.2 it was found that the chance coincidence rate for three hits was 8% for a time window of 4000 ns. Thus a three hit requirement in 4000 ns could be used without breaking the threshold of 8% signal reduction by chance coincidence. The difference in the veto efficiency is difficult to determine with the limited

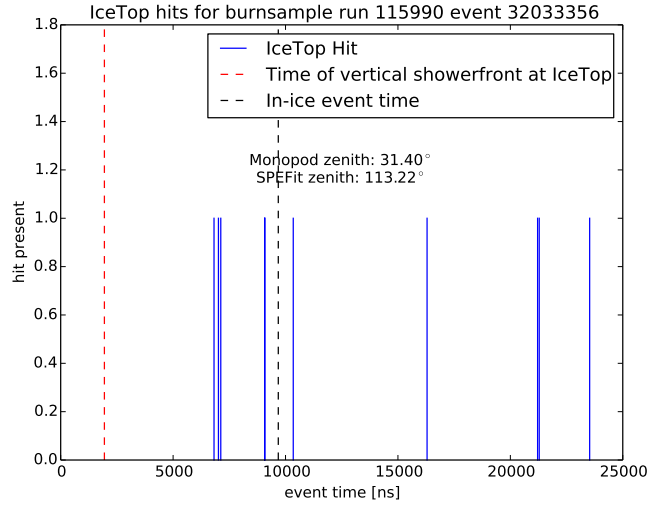


Figure 6.9: Hits on IceTop with their original times.

number of CORSIKA event statistics at Level 5. There is obviously a trade-off between the larger number of events which have two hits on IceTop and the greater success rate of the IceTop veto with a larger time window. Further studies are required to determine which of these two strategies would be best. Unfortunately the time-frame of this thesis did not allow for these studies but these are suggested as a future direction for developing an IceTop veto.

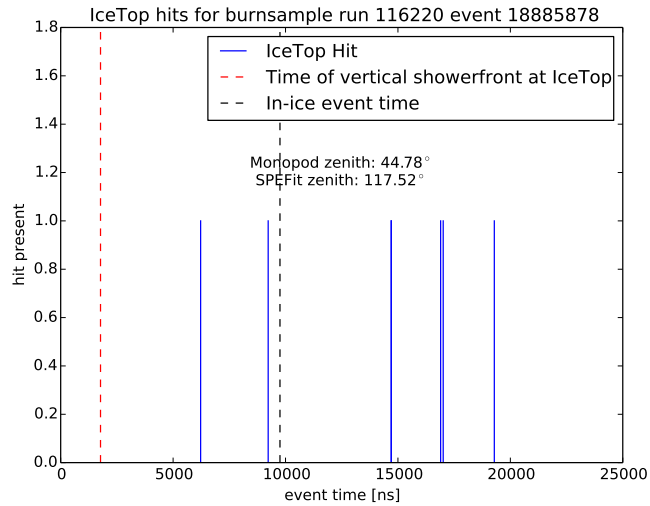


Figure 6.10: Hits on IceTop with their original times.

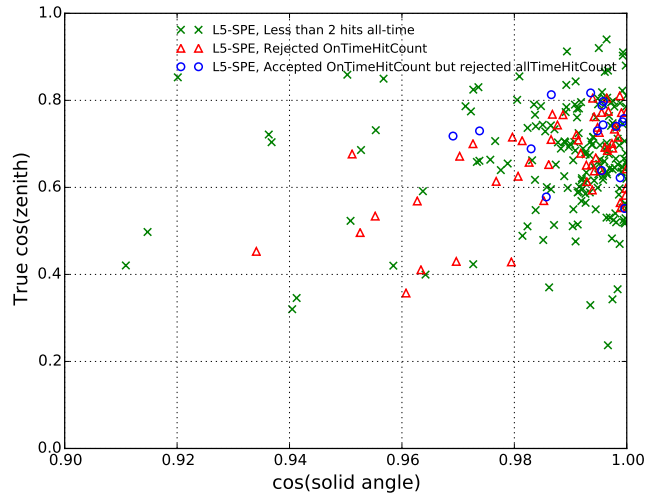


Figure 6.11: Scatter plot of zenith versus angle between true and reconstructed directions for simulated cosmic ray events at L5 (without the incident vertex direction cut). Points in blue are events which could be vetoed due to the total number of hits but are not removed by the time-dependent IceTop veto.

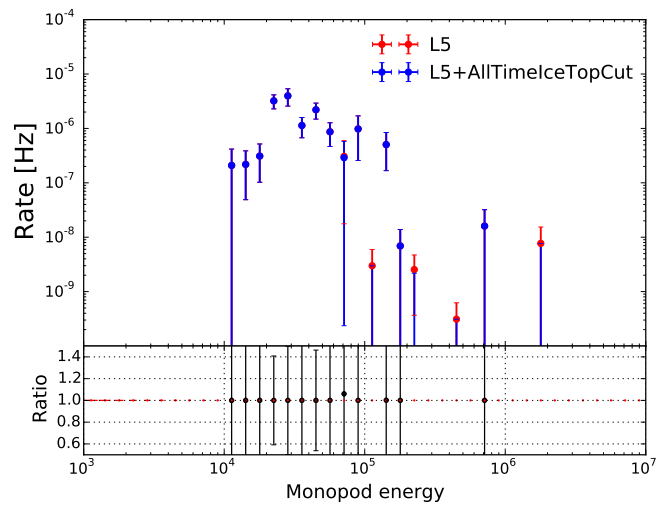


Figure 6.12: Event rate as a function of energy. The red points show the event rate after the Level 5 uncontained cascade cuts. The blue points show the event rate after an IceTop veto cut which requires three hit tanks, rather than two, has been imposed (without any time restriction on the hits). The bottom panel is the ratio of the event rates before and after the IceTop veto is applied.

# Chapter 7

## Discussion and Conclusion

The IceCube neutrino observatory aims to detect astrophysical neutrinos. The astrophysical neutrino signal is small and is hidden in the large background of atmospheric muons created in the interactions of cosmic rays with the atmosphere. Searches for neutrino induced particle showers, so called cascades, are one of the analysis techniques used in IceCube to isolate neutrino events from the muon background. The work presented in this thesis is focused on the use of the IceTop surface array to further identify and veto the muon background within a cascade analysis.

To assess the number of hits expected on the IceTop array for any given cosmic-ray event we used a code developed originally by Sebastian Euler [50]. This code parameterises the particle density of a cosmic ray air shower as a function of lateral and longitudinal distance from the air shower axis. In Chapter 3 we presented studies benchmarking the predictions of this code against the hit rate observed in IceTop and investigations into the scope over which an IceTop veto could be efficient. The predictions of the code were seen to compare well with the IceTop data and IceTop's feasibility as a veto was confirmed although limited by the extent in area that IceTop covers being only directly above the IceCube-InIce array.

In Chapter 4 we explored the possible gains from integrating an IceTop veto into the established cascade analysis criteria. We studied separately the potential of further background removal in the uncontained and contained cascade samples at Level 5 of the analysis. Our study was made using COR-



SIKA background simulation with the parameterisation code used to simulate air-shower hits on IceTop. In these studies, a background event was deemed to be caught by the IceTop veto if there were two or more IceTop simulated hits, with no timing constraint on these hits. Investigation was made into whether any of the cascade analysis criteria could be relaxed allowing more signal to be retained, with the extra background being removed instead by the IceTop veto. The variables which remove significant numbers of signal events, and have an overlap into a region in which the IceTop veto may be more efficient are the best variables to relax. It was found that the contained cascade analysis was already efficient at removing background in the range where the IceTop veto could be effective. However it was found there was potential in the uncontained cascade analysis to remove additional signal and to relax the cascade cuts based on zenith angle. Events which were reconstructed as being close to vertical were had the best potential for removal by the IceTop veto.

For the implementation of IceTop as a veto it is necessary to choose a time window, related to the IceCube-InIce event time, within which IceTop hits are deemed to be correlated. The optimum length of the time-window is a compromise between the risk of removing astrophysical neutrino events due to the time-window containing the chance coincidence of an unrelated air shower event and the length of time needed to account for the spread in arrival times of associated IceTop hits. For the latter there is an inherent expected spread in times related to the width of the shower front and there are also uncertainties in relating the expected IceTop hit times to the IceCube-InIce hit times due to the uncertainties in the reconstruction direction of the IceCube event. Each of these factors was examined in Chapter 5. It was seen that the poor angular resolution of the cascade type events motivates a time window as large as a few thousand nanoseconds. It was decided that for the preliminary studies made in this thesis to take, however a time window of 2000 ns which was motivated by wanting to restrict the signal removal to a level of 10 %.

In Chapter 6 the 2000 ns time window was used to associate IceTop hits with IceCube-InIce events. Simulated background events which had been filtered by the uncontained cascade criteria up to Level 5 were also subjected to an IceTop veto. The IceCube-InIce events were reconstructed with two possible reconstructed routines, SPEFit and MonopodFit, to obtain the hypothesis for the primary cosmic-direction. This direction was used to predict the

shower impact time at each IceTop tank. The IceTop veto requirement was two on-time hits, that is two hits 1000 ns before or after the tank shower impact time. In addition to the reconstructed directions from the SPEFit and MonopodFit routines a third impact tank impact time was tested where the direction of the primary was assumed to be vertical. From fig. 6.12 we saw that increasing the threshold for hits and increasing the time window duration is a potential different approach to address this problem, but with a compromise to the ability to veto lower energy events. However, with the current reconstructions chosen which determine the time window, we find that the reduction of events on simulation is limited due to the corresponding time window, and this is confirmed by the same study on the burn sample. Some events are expected to get vetoed are being vetoed (red triangles as shown in fig. 6.11 using spe reconstruction) for the time window. Although there are events which are not removed at all due to not having enough hits the most concern goes for the events which were supposed to get removed but were accepted due to timewindow ( blue circles) due to the reconstruction. These events are False for alltimehitcount  $< 2$  but True for ontimehitcount  $< 2$  . So the blue circles are all events which might have enough hits but they don't fall in the time window. So constructing the time window that can capture these events with a better reconstruction is the future plan.

In principle, high energy ( $>100\text{TeV}$ ) uncontained cascade events of a cosmic ray origin have the potential to be vetoed but in practice, events are being vetoed, but not as much as the potential in fig. 6.2, and the difference must be due to misreconstructions so a reconstruction that identifies the shower axis is needed to more reliably veto events.

Due to the poor direction resolution of cascade events a time window larger than 2000 ns is motivated. With the requirement of two hits, in this thesis work it was decided that a larger time window would remove too many signal events. We briefly investigated the requirement of three or more hits for the IceTop veto. This allows a larger time window to be used, but the three hit condition does mean that the energy threshold for the IceTop veto to be useful is higher, and a smaller number of events in the sample can be vetoed.

Future work is also adding IceVeto extended array to IceTop veto under the condition of two hits in surface array, this can give us a better possibilities of veto efficiency. the extended array is inherently less dense, but may still be a good veto for the highest energy events. To use such an extended

veto array, we would therefore have to not only apply a time window but select where on the array we want to test for hits, otherwise the number of irreducible background hits across the full array would be too high. This may again require the use of better directional reconstructions for the muon backgrounds that pass our cascade criteria. With the proposed IceCube Gen-2 detector which has increased distances between In-Ice strings, such surface veto techniques may be vital to remove muon background from both contained and uncontained cascade events.

# Bibliography

- [1] T. K. Gaisser, R. Engel, and E. Resconi, *Cosmic Rays and Particle Physics*. Cambridge University Press, 2 ed., 2016.
- [2] S. V. Hickford, *A Cascade Analysis for the IceCube Neutrino Telescope*. PhD thesis, 2012.
- [3] A. Gazizov and M. P. Kowalski, *ANIS: High energy neutrino generator for neutrino telescopes*, *Comput. Phys. Commun.* **172** (2005) 203–213, [astro-ph/0406439].
- [4] M. Aartsen, R. Abbasi, *et. al.*, *Measurement of south pole ice transparency with the icecube led calibration system*, *Nuclear Instruments and Methods in Physics Research Section A: Accelerators, Spectrometers, Detectors and Associated Equipment* **711** (2013) 73 – 89.
- [5] J. Abraham, P. Abreu, *et. al.*, *Measurement of the Depth of Maximum of Extensive Air Showers above  $10^{18}$  eV*, *Physical Review Letters* **104** (2010) 091101, [arXiv:1002.0699].
- [6] A. M. Hillas, *Cosmic Rays: Recent Progress and some Current Questions*, in *Conference on Cosmology, Galaxy Formation and Astro-Particle Physics on the Pathway to the SKA Oxford, England, April 10-12, 2006* (2006) [astro-ph/0607109].
- [7] T. K. Gaisser, *Spectrum of cosmic-ray nucleons, kaon production, and the atmospheric muon charge ratio*, *Astroparticle Physics* **35** (2012) 801806.

- [8] H. S. Ahn *et. al.*, *Discrepant hardening observed in cosmic-ray elemental spectra*, *Astrophys. J.* **714** (2010) L89–L93, [arXiv:1004.1123].
- [9] A. D. Panov *et. al.*, *Energy Spectra of Abundant Nuclei of Primary Cosmic Rays from the Data of ATIC-2 Experiment: Final Results*, *Bull. Russ. Acad. Sci. Phys.* **73** (2009) 564–567, [arXiv:1101.3246].
- [10] **Particle Data Group** Collaboration, K. A. Olive *et. al.*, *Review of Particle Physics*, *Chin. Phys.* **C38** (2014) 090001.
- [11] E. Fermi, *On the origin of the cosmic radiation*, *Phys. Rev.* **75** (1949) 1169–1174.
- [12] A. M. Hillas, *The origin of ultra-high-energy cosmic rays*, *Annual Review of Astronomy and Astrophysics* **22** (1984) 425–444, [<https://doi.org/10.1146/annurev.aa.22.090184.002233>].
- [13] K. Kotera and A. V. Olinto, *The Astrophysics of Ultrahigh-Energy Cosmic Rays*, *ARA&A* **49** (2011) 119–153, [arXiv:1101.4256].
- [14] **Fermi-LAT** Collaboration, M. Ackermann *et. al.*, *Detection of the Characteristic Pion-Decay Signature in Supernova Remnants*, *Science* **339** (2013) 807, [arXiv:1302.3307].
- [15] L. A. Anchordoqui, *Acceleration of ultrahigh-energy cosmic rays in starburst superwinds*, *Phys. Rev.* **D97** (2018) 063010, [arXiv:1801.0717].
- [16] A. Loeb and E. Waxman, *The Cumulative background of high energy neutrinos from starburst galaxies*, *JCAP* **0605** (2006) 003, [astro-ph/0601695].
- [17] W. Pauli., *Open letter to the group of radioactive people at the Gauverein meeting in tuingen*, .
- [18] S. M. Bilenky, *Neutrino. History of a unique particle*, *Eur. Phys. J.* **H38** (2013) 345–404, [arXiv:1210.3065].
- [19] F. Reines, C. L. Cowan, F. B. Harrison, A. D. McGuire, and H. W. Kruse, *Detection of the free antineutrino*, *Phys. Rev.* **117** (1960) 159–173.

- [20] J. A. Formaggio and G. P. Zeller, *From  $\nu_e$  to  $\bar{\nu}\nu$ : Neutrino cross sections across energy scales*, *Rev. Mod. Phys.* **84** (2012) 1307–1341.
- [21] J. G. Learned and K. Mannheim, *High-energy neutrino astrophysics*, *Annual Review of Nuclear and Particle Science* **50** (2000) 679.  
Copyright - Copyright Annual Reviews, Inc. 2000; Last updated - 2014-05-21.
- [22] T. K. Gaisser and T. Stanev, *Neutrinos and cosmic rays*, *Astroparticle Physics* **39** (2012) 120–128, [arXiv:1202.0310].
- [23] U. F. Katz and C. Spiering, *High-Energy Neutrino Astrophysics: Status and Perspectives*, *Prog. Part. Nucl. Phys.* **67** (2012) 651–704, [arXiv:1111.0507].
- [24] L. A. Anchordoqui, H. Goldberg, F. Halzen, and T. J. Weiler, *Neutrinos as a diagnostic of high energy astrophysical processes*, *Physics Letters B* **621** (2005) 18 – 21.
- [25] **IceCube** Collaboration, M. G. Aartsen *et. al.*, *Flavor Ratio of Astrophysical Neutrinos above 35 TeV in IceCube*, *Phys. Rev. Lett.* **114** (2015) 171102, [arXiv:1502.0337].
- [26] F. W. Stecker, C. Done, M. H. Salamon, and P. Sommers, *High-energy neutrinos from active galactic nuclei*, *Phys. Rev. Lett.* **66** (1991) 2697–2700.
- [27] **IceCube** Collaboration, M. G. Aartsen *et. al.*, *Search for neutrino-induced particle showers with IceCube-40*, *Phys. Rev.* **D89** (2014) 102001, [arXiv:1312.0104].
- [28] **IceCube** Collaboration, R. Abbasi *et. al.*, *The Design and Performance of IceCube DeepCore*, *Astropart. Phys.* **35** (2012) 615–624, [arXiv:1109.6096].
- [29] A. Dziewonski, *The Encyclopedia of Solid Earth Geophysics*. 1989.
- [30] J. H. Koehne, K. Frantzen, *et. al.*, *PROPOSAL: A tool for propagation of charged leptons*, *Computer Physics Communications* **184** (2013) 2070–2090.

- [31] D. Heck, J. Knapp, J. N. Capdevielle, G. Schatz, and T. Thouw, *CORSIKA: a Monte Carlo code to simulate extensive air showers*. 1998.
- [32] A. Saa, *Proceedings, 33rd International Cosmic Ray Conference (ICRC2013)*, *Braz. J. Phys.* **44** (2014) pp.415–608.
- [33] **IceCube** Collaboration, M. G. Aartsen *et. al.*, *Evidence for High-Energy Extraterrestrial Neutrinos at the IceCube Detector*, *Science* **342** (2013) 1242856, [arXiv:1311.5238].
- [34] **IceCube** Collaboration, M. G. Aartsen *et. al.*, *Observation of High-Energy Astrophysical Neutrinos in Three Years of IceCube Data*, *Phys. Rev. Lett.* **113** (2014) 101101, [arXiv:1405.5303].
- [35] Taboada, *A view of the Universe with the IceCube and ANTARES neutrino telescopes*, 2018.
- [36] **IceCube** Collaboration, M. A. et al., *Evidence for High-Energy Extraterrestrial Neutrinos at the IceCube Detector*, arXiv:1710.0119.
- [37] **Liverpool Telescope, MAGIC, H.E.S.S., AGILE, Kiso, VLA/17B-403, INTEGRAL, Kapteyn, Subaru, HAWC, Fermi-LAT, ASAS-SN, VERITAS, Kanata, IceCube, Swift NuSTAR** Collaboration, M. G. Aartsen *et. al.*, *Multimessenger observations of a flaring blazar coincident with high-energy neutrino IceCube-170922A*, *Science* **361** (2018) eaat1378, [arXiv:1807.0881].
- [38] **IceCube** Collaboration, M. G. Aartsen *et. al.*, *The IceCube Realtime Alert System*, *Astropart. Phys.* **92** (2017) 30–41, [arXiv:1612.0602].
- [39] G. Notices (2018)
- [40] **IceCube** Collaboration, M. G. Aartsen *et. al.*, *Neutrino emission from the direction of the blazar TXS 0506+056 prior to the IceCube-170922A alert*, *Science* **361** (2018) 147–151, [arXiv:1807.0879].
- [41] **IceCube** Collaboration, M. G. Aartsen *et. al.*, *IceCube-Gen2 - The Next Generation Neutrino Observatory at the South Pole: Contributions to ICRC 2015*, arXiv:1510.0522.

- [42] R. Abbasi, Y. Abdou, *et. al.*, *IceTop: The surface component of icecube, Nuclear Instruments and Methods in Physics Research Section A: Accelerators, Spectrometers, Detectors and Associated Equipment* **700** (2013) 188 – 220.
- [43] **IceCube** Collaboration, M. G. Aartsen *et. al.*, *Astrophysical neutrinos and cosmic rays observed by IceCube*, *Adv. Space Res.* **62** (2018) 2902–2930, [[arXiv:1701.0373](#)].
- [44] **IceCube** Collaboration, M. G. Aartsen *et. al.*, *The IceCube Neutrino Observatory Part VI: Ice Properties, Reconstruction and Future Developments*, in *Proceedings, 33rd International Cosmic Ray Conference (ICRC2013): Rio de Janeiro, Brazil, July 2-9, 2013* (2013) [[arXiv:1309.7010](#)].
- [45] S. Schonert, T. K. Gaisser, E. Resconi, and O. Schulz, *Vetoing atmospheric neutrinos in a high energy neutrino telescope*, *Phys. Rev.* **D79** (2009) 043009, [[arXiv:0812.4308](#)].
- [46] T. K. Gaisser, K. Jero, A. Karle, and J. van Santen, *Generalized self-veto probability for atmospheric neutrinos*, *Phys. Rev.* **D90** (2014) 023009, [[arXiv:1405.0525](#)].
- [47] C. A. Argelles, S. Palomares-Ruiz, A. Schneider, L. Wille, and T. Yuan, *Unified atmospheric neutrino passing fractions for large-scale neutrino telescopes*, *JCAP* **1807** (2018) 047, [[arXiv:1805.1100](#)].
- [48] **IceCube** Collaboration, D. Tosi and H. Pandya, *Performance of IceTop as a veto for IceCube*, *PoS ICRC2017* (2018) 967.
- [49] B. Roberts, *University of Canterbury MAPH480 Project*, .
- [50] S. Euler, *Talk at icecube collaboration meeting, copenhagen, october, 2015*, .
- [51] T. Abu-Zayyad, K. Belov, *et. al.*, *Evidence for changing of cosmic ray composition between  $10^{17}$  and  $10^{18}$  ev from multicomponent measurements*, *Phys. Rev. Lett.* **84** (2000) 4276–4279.
- [52] **Pierre Auger Collaboration** Collaboration, A. Aab, P. Abreu, *et. al.*, *Muons in air showers at the pierre auger observatory: Measurement of atmospheric production depth*, *Phys. Rev. D* **90** (2014) 012012.



- [53] R. P. Kokoulin, A. G. Bogdanov, *et. al.*, *Local muon density spectra at large zenith angles as a probe of high-energy hadronic interaction models*, *Nucl. Phys. Proc. Suppl.* **196** (2009) 106–109.
- [54] **IceCube** Collaboration, H. Dembinski, *Investigating cosmic rays and air shower physics with IceCube/IceTop*, *EPJ Web Conf.* **145** (2017) 01003.
- [55] K. Munawar, *Identifying cosmic ray induced cascade events with IceTop*, 2017.
- [56] A. Stoessel, *A search for particle showers at the edge of IceCubes instrumental volume*. PhD thesis, 2016.
- [57] M. Lesiak-Bzdak, “Ic79 high energy cascade analysis.”